UNIVERSITAT DE LES ILLES BALEARS
DEPARTAMENT DE FÍSICA

Tesi Doctoral

Synchronisation and Collective Effects in Extended Stochastic Systems

Tesi presentada per Claudio Juan Tessone, *al Departament de Física de la Universitat de les Illes Balears, per optar al grau de Doctor en Física.*

Palma, novembre de 2006

El director de tesi Raúl Toral Garcés, Catedràtic de la Universitat de les Illes Balears, certifica que aquesta tesi doctoral ha estat realitzada pel Sr. Claudio Juan Tessone, i perquè quedi constància escrita firma

a Palma 7 de novembre de 2006.

Raúl Toral Garcés

Para vos.

Acknowledgements

This is definitively the toughest section to write in a thesis. I will, nevertheless, do my best to condense my thoughts about this. I will avoid mentioning specific names, unless strictly necessary. I know that only the people to whom these acknowledgements are directed will take them personally.

I can not mention Alejandra without remembering her grandparents, who made me feel part of their family and left an indelible memory on me. I want to thank her for letting me enjoying being with her. Sadly enough, I can only express my eternal gratitude for the many things she resigned, only to allow me to do what I like, without questioning. I wish I could say more than just a few words about Alejandra, the dedication of this thesis is just a minuscule tribute to her.

Also, I would like to mention the few friends that are far from me, but I still fill as close as ever.

From the academic point of view, this period at IMEDEA's Cross-Disciplinary Physics Group was plainly excellent. This is not only a real good place to live, but also to do research.

I will be always thankful to Raúl, for how much he trusted on me. First of all, for bringing me the possibility to do something really interesting, in a moment that was somehow critical for me, from an academic prospective. Later, for the freedom I had for working on the topics I wanted. And for the interesting, and always enlightening, discussions we had and I hope will continue having.

I am grateful to all the friends I made in this group. Talking with you all about work, programming, Boca Juniors, languages, idiosyncracies, leisure, cooking, people, the never ending discussions on operating systems... I thank all the colleagues coming from the other end of the *puddle* for making me remember the best things of home. For those coming from this end, for making me feel at home.

I am specially thankful to Prof. Jürgen Kurths, for allowing me to spend such profitable, but mainly joyful periods in Potsdam's Arbeitsgruppe Nichtlineare Dynamik. And obviously Dott. Alessandro Torcini, for such a wonderful period of rediscovery in the Istituto dei Sistemi Complessi, at Firenze. And also to Horacio Wio, who gave me the opportunity to learn once again.

Contents

Preface

In the last century, first due to the unveiling of the origin of *Brownian motion* and later with the advent of electronic devices, the study of noise effects on dynamical systems attracted large interest. Noise represents the reduction of that part of the degrees of freedom in a dynamical system that can not be modeled in a simple way. The typical image of its effect is that of perturbing in an unpredictable way the evolution of the system. Partly because of this, it was initially of interest how to reduce its effect, as considering it a nuisance that should be avoided.

In the last two decades, however, it was discovered that noise can have a constructive role in non-linear dynamical systems. Significant examples are *stochastic resonance* and *noise-induced phase transitions*. An optimal amount of noise induces, in the former, a large amplification of a weak signal acting on a dynamical system and, in the latter, a drastic change in its macroscopic properties.

Among dynamical systems, one class of broad interest are those named as *excitable*. These systems remain in an equilibrium state until a strong enough external perturbation drives the system away from it. After this temporal change in its configuration, it returns back to the original resting state. This excursion is called *firing* or *pulse*. A typical source of perturbation is noise acting on the system. Perhaps the most prominent example of excitable systems are the models describing the time-evolution of the action potentials in neurons and other types of cells. The first mathematical models for these systems date back to the 1940 decade. Excitable systems are, nevertheless, quite general, and can be found in optical, and other models of physical systems, in models of disease spreading, forrest fires, etc. A counter-intuitive role of noise acting on excitable systems was found in the last decade, and is signalled by an improvement in the regularity of the firings when the perturbation is noise of a given intensity, a phenomenon called *coherence resonance* or *stochastic coherence*.

A natural framework to analyse the above mentioned results is the study of interacting dynamical systems in the presence of noise. How dynamical systems interact, and which effects arise from this interaction is a very interesting question. In particular, synchronised collective behaviour being one of the most notorious possible aspect of this, as well as a very good example

of the minimalistic physical approach in modelling. A striking phenomenon not understood until the second half of the last century was that of the flashing fireflies, in South-eastern Asia. It was known that a large amount of these insects would start flashing in synchrony at dusk after some transient period. The full biological mechanism is not still well understood, but very simplistic models proved that the weak interaction provided by the visual signals originate the emergence of this collective phenomenon. This example clearly shows that the interacting units are not necessarily identical, but *diverse*. The effect of diversity resembles to what is conceived as the typical effect of noise: If the units are interacting, but very different to each other they would evolve in very different ways. This is a very important subject, as diversity is a common ingredient in many natural systems.

The aim of this thesis is to delve into the constructive role that *disordering elements* can play on dynamical systems. For systems composed by many units, by *disordering elements*, we mean ingredients that cause each unit to evolve in a different way. For example, uncorrelated noise sources acting independently on the system constituents. Also, we consider *diversity*: in many systems of interest not all the interacting units are equal. Strikingly, it is the loss of degree order what causes the systems to exhibit a more coherent behaviour. We further consider the effect of different kinds of interaction, and we also show that they can generate a rich variety of phenomena: from leading towards a more coherent behaviour to causing interesting effects in chains of diverse elements.

We will now describe the different parts of this thesis, together with the main results in more detail:

Part I: Introduction

The first part is devoted to introduce the main concepts used throughout the remaining chapters, as we intend this thesis to be as much self-contained as possible.

In the first chapter of this part, we focus on general definitions regarding dynamical systems. We then go into a basic introduction to bifurcation theory, defining those that later appear in the chapters with the results. We finally define the concept of dynamical systems in a circle.

The second chapter describes the effect that noise has on dynamical systems. After an (conceptual and historical) introductory section, we define the mathematical tools used to study these kind of systems. We then describe the constructive effect that noise can have on dynamical systems, introducing the *stochastic resonance* phenomenon; we explain it and describe the theory involved in its understanding.

Excitable systems are widespread in many branches of science. Along the third chapter, we define them, and describe according to their dynamical properties. Two prototypical models of excitability are the *FitzHugh–*

Nagumo and *active-rotator* models: we define them and explain some of their properties in this section. Excitable dynamical systems exhibit the phenomenon of *coherence resonance*, briefly described in this chapter.

The last chapter of this part is devoted to present the *synchronisation* phenomenon. We show a paradigm of synchronisation: *the Kuramoto model* and the similar (disordering) roles that noise and diversity play in this system.

Part II: Results

Diversity, which has typically been thought as an empovering factor, can also play a constructive role in many dynamical systems. Namely, we show in this part that diversity can be, counterintuitively, a source of a more regular behaviour. We find that these results are very general, and as such, we expect this part to be of broad applicability and many extensions can be foreseen.

In chapter 5 of the thesis we study a set of active-rotator excitable systems. The main finding of this chapter is a simple, yet insightful, theory that unveils the mechanism behind the emergence of collective firing of the excitable units. We find that this behaviour occurs whenever the positions position of the units are disordered enough. This mechanism is very general, and happens regardless the exact source of disorder. This is further studied in chapter 6, where we study a set of coupled FitzHugh–Nagumo units. We find that the same phenomenon holds, and conclude that it is independent of the type of excitability exhibited by the system. Once again, we compare the results of noise and diversity, finding qualitatively the same results.

In the following chapter 7, we focus in another source of disorder: the effect of repulsive links acting on a set of identical active-rotator units. We find that, under the proper conditions, the presence of some repulsive interactions can also trigger a coherent, global firing of excitable media. We analyse also the properties of the topology of repulsive connections for this global phenomenon to occur. We find that some degree of *heterogeneity* in the network of repulsive links is needed in order to observe this coherent behaviour: repulsion must be stronger in some units that in others in order for this collective phenomenon to happen.

In the next chapter 8, we report an analogous phenomenon to that of stochastic resonance but induced by diversity instead of noise: the *diversity-induced resonance*. Specifically, we show that a system composed by many interacting *diverse* units, can respond better to a *weak* external signal if the units are not all identical, but some intermediate degree of diversity is present. The degree of the global response degrades if diversity is too large or too small. We develop a mean-field theory that convincingly explains the origin of the phenomenon and quantitatively agrees with extensive numerical simulations. We show that the same phenomenon appears in excitable

systems. This opens a new scenario for a collective large response to external signals in excitable systems composed by diverse units as, for example, in ensembles of neurons.

In chapter 9, we study a model for opinion formation which incorporates three basic ingredients for the evolution of the opinion held by an individual: imitation, influence of fashion and randomness. We show that in the absence of fashion, the model behaves as a bistable system with random jumps between the two stable states with a distribution of times following Kramers' law. We also demonstrate the existence of system size stochastic resonance, by which there is an optimal value for the number of individuals N for which the average opinion follows better the fashion. And finally, we also study the role played by diversity in this system, finding that it can have the same constructive role than randomness. We propose an extension for this model that allows to study this phenomenon.

We later study chains of excitable units. In chapter 10, we show the effect that coupling through the inhibitory variable in small chains of excitable and oscillatory units. Inhibitory coupling is present in many neuronal systems, and we pay attention to its effect in a system subjected to noise and a periodic forcing acting on one ends of the chain. We show that there is a regime in which the units located at the end of the chain can respond to the external stimuli, while the intermediate units remain silent. This occurs even if the intermediate units are oscillatory when uncoupled from the others. The mechanism is a resonant interplay of noise and the transmission signal provided by certain value of inhibitory coupling.

We then focus our attention on spatially extended systems. Here we present a study of *stochastic resonance* in an extended FitzHugh–Nagumo system with a field dependent activator diffusion. The fields are coupled through both activator and inhibitor variables. We show that the system response is enhanced due to the particular form of the non-homogeneous coupling. We show that this can be understood using the non-equilibrium potentials, that allow a potential description of far from equilibrium systems.

Finally, in the closing chapter we present the main conclusions that can be extracted from the results of this thesis. We also present some possible extensions of our work.

We believe that the results presented here are of broad interest, and will also trigger new research that can take profit of them. In this section, besides making a throughout description of the main results of this thesis, we also describe the open prospectives, and possible future research lines open by this thesis.

Prefacio

En el último siglo, debido inicialmente al descubrimiento del origen del *movimiento Browniano* y luego, con la proliferación de los aparatos electrónicos, el estudio de los efectos del ruido en sistemas dinámicos atrajo gran interés. El ruido representa la reducción de aquellos grados de libertad de un sistema dinámico que no pueden ser modelados de una manera simple. La imagen típica de su efecto es la de una perturbación en la evolución del sistema de una forma errática y de carácter impredecible. En parte debido a esto, la investigación se centró inicialmente en maneras de reducir sus efectos, al ser considerado como una molestia que debía ser evitada.

En las últimas décadas, no obstante, se ha descubierto que el ruido puede desempeñar un papel constructivo en sistemas dinámicos no lineales. Entre los ejemplos más significativos, están la *resonancia estocástica* y las *transiciones de fase inducidas por ruido*. En el primero, una intensidad de ruido óptima produce una gran amplificación de una señal débil que actúa sobre el sistema en cuestión. En el segundo fenómeno, se observa un drástico cambio en las propiedades macroscópicas del sistema.

Entre los sistemas dinámicos, un ejemplo que ha suscitado gran interés es el de los *sistemas excitables*. Estos permanecen en un estado de equilibrio hasta que una perturbación externa suficientemente fuerte los aparta del mismo. Luego de este cambio temporal en su configuración, el sistema regresa a su estado de equilibrio original. Esta excursión es llamada *pulso* o *disparo*. Una fuente de perturbación que se halla de manera corriente es precisamente el ruido. Tal vez el ejemplo más prominente de los sistemas excitables se encuentra en los modelos matemáticos que describen la evolución temporal de los potenciales de acción en neuronas y otros tipos de células. Los primeros modelos de este tipo datan de la década de 1940. Los sistemas excitables son, no obstante, muy generales, y pueden ser encontrados en sistemas físicos y ópticos, modelos de propagación de enfermedades, incendios de bosques, etc.

Una extensión natural para analizar los resultados mencionados previamente, es el estudio de sistemas dinámicos interactuantes en presencia de ruido. Cómo interactúan los sistemas dinámicos, y qué efectos emergen de esta interacción es un campo muy interesante, encontrando entre sus más notables ejemplos el del *comportamiento colectivo sincronizado*, siendo

también un muy buen ejemplo del enfoque minimalista, típico en la física a la hora de modelar. Un sorprendente fenómeno, que no fue comprendido hasta la segunda mitad del siglo pasado, es el de los destellos de las luciérnagas, en el sudeste asiático. Se conocía que al atardecer, grandes cantidades de estos coleópteros centellean al unísono luego de un período transitorio inicial. El mecanismo biológico completo no está aún totalmente comprendido, pero modelos muy simplificados demostraron que la débil interacción dada por las señales visuales originan este fenómeno colectivo. Este ejemplo muestra claramente que las unidades interactuantes no deben ser necesariamente idénticas, pero pueden ser asimismo *diversas*. El efecto de la diversidad se asemeja en este contexto a lo que se concibe habitualmente como el típico efecto del ruido: si las unidades interactúan, pero son muy diferentes entre sí, evolucionarán de manera muy distinta. Este problema es muy importante, ya que la diversidad es un ingrediente habitual en muchos sistemas naturales.

El propósito de esta tesis es profundizar en el papel constructivo que *elementos que generan desorden* pueden desempeñar en sistemas dinámicos. Para sistemas constituidos por muchos componentes, con esto hacemos referencia a ingredientes que causan que cada unidad evolucione de manera distinta. Por ejemplo, se puede citar fuentes de ruido descorrelacionadas actuando sobre los componentes del sistema. También, consideramos *diversidad*: en muchos casos las unidades que componen los sistemas no son idénticas. Sorprendentemente, hallamos que es precisamente la pérdida de orden lo que causa que los sistemas exhiban un comportamiento más coherente. También consideramos el efecto de diferentes clases de interacción, y mostramos que a través de las mismas se puede generar una amplia variedad de fenómenos: desde llevar a un comportamiento más coherente a todo el sistema, a causar fenómenos dinámicos muy interesantes en cadenas de elementos diversos.

Vamos ahora a describir todas las partes de esta tesis en más detalle, junto con los principales resultados.

Parte I: Introducción

La primera parte de esta tesis está dedicada a introducir los conceptos más importantes empleados durante los capítulos siguientes, ya que se pretende que esta tesis sea tan más auto-contenida como sea posible.

El primer capítulo de esta parte se concentra en las definiciones generales que atañen a los sistemas dinámicos. Después se realiza una breve introducción a la teoría de bifurcaciones, definiendo aquellas que aparecen luego en los capítulos de resultados. Finalmente, definimos un caso particular de sistemas dinámicos: aquellos que están definidos en un círculo.

En el segundo capítulo, se describe el efecto que el ruido tiene cuando actúa sobre sistemas dinámicos. Luego de una sección de introducción (tanto conceptual como histórica), definimos las herramientas matemáticas que se

emplean al estudiar esta clase de sistemas. Luego se describe el efecto constructivo que el ruido puede tener sobre sistemas dinámicos, mencionando el fenómeno de *resonancia estocástica*; después de explicar cualitativamente el fenómeno, se detalla el marco teórico que ayuda en su comprensión.

Existe una amplia variedad de ejemplos de *sistemas excitables* en la naturaleza. A lo largo del tercer capítulo, los mismos son definidos y se presenta una clasificación de acuerdo a sus propiedades dinámicas. Dos ejemplos prototípicos de excitabilidad son los modelos de *FitzHugh–Nagumo* y el de *rotores activos*. A ellos se dedican sendas secciones, donde se mencionan brevemente algunas de sus propiedades. El ruido actuando sobre sistemas excitables produce el fenómeno de *resonancia de coherencia*, que es brevemente descrita en la sección final de este capítulo.

El último capítulo de esta parte de la tesis está dedicado a reseñar el fenómeno de *sincronización*. En particular, se muestra en ejemplo paradigmático de este fenómenos: *el modelo de Kuramoto* y se hace hincapié en el papel similar que ruido y diversidad generan sobre este sistema.

Parte II: Resultados

La diversidad, que ha sido típicamente considerada como un factor de degradamiento en las características globales de sistemas acoplados, puede desempeñar un papel constructivo en muchos sistemas dinámicos. En particular, mostramos en esta parte que la diversidad puede ser, de forma contraintuitiva, una fuente de un comportamiento más regular. Encontramos que estos resultados son muy generales, y como tales esperamos que los mismos sean aplicables en una amplia variedad de fenómenos, ya que pueden preveerse muchas extensiones posibles.

En el capítulo 5 de esta tesis, se estudia un conjunto de sistemas excitables extendido de rotores activos. El principal hallazgo de este capítulo es una teoría simple, pero que permite tener un entendimiento completo de cuál es el mecanismo que subyace a la aparición de pulsos colectivos por parte de las unidades que componen el sistema. Se ha encontrado que este comportamiento ocurre cuando las posiciones de las unidades están lo suficientemente desordenadas. Este mecanismo es muy general, y es independiente de la fuente exacta de desorden. Esto es estudiado en detalle, asimismo, en el capítulo 6, donde se considera un conjunto de unidades de FitzHugh–Nagumo acopladas. Se encuentra que el mismo fenómeno aparece. A partir de estos resultados se concluye que este fenómeno es independiente del tipo de excitabilidad que el sistema exhiba. Asimismo se comparan los resultados que se obtienen con ruido y diversidad, encontrando cualitativamente el mismo comportamiento.

El siguiente capítulo 7, se focaliza en otra fuente de desorden: el efecto de enlaces repulsivos actuando sobre un conjunto de rotores activos idénticos. El resultado que se encuentra es que, bajo determinadas condiciones, la

presencia de algunos enlaces repulsivos puede asimismo provocar un estado en el que todas las unidades pulsan al unísono. Se analizan, asimismo, las propiedades que ha de tener la red subyacente de conexiones repulsivas para que este fenómeno global ocurra. Se encuentra que cierto grado de *heterogeneidad* en la red de enlaces repulsivos es necesaria para que se observe este comportamiento coherente: la intensidad de repulsión debe ser más importante en unas unidades que en otras para que esto ocurra.

En el siguiente capítulo, el número 8, se presenta un fenómeno análogo al de resonancia estocástica, pero inducido por diversidad en lugar de ruido: la *resonancia inducida por diversidad*. Especificamente, se muestra que un sistema compuesto por muchas unidades interactuantes *diversas*, puede responder mejor a una señal externa *débil* si las unidades no son todas idénticas, pero hay un grado intermedio de diversidad. La calidad de la respuesta global se degrada si la diversidad es demasiado grande o demasiado pequeña. Asimismo, se desarrolla una teoría de campo medio que explica de forma convincente el origen del fenómeno y ajusta cuantitativamente con simulaciones numéricas intensivas. Mostramos que, además, el fenómeno aparece en sistemas excitables. Estos resultados abren un nuevo escenario para la aparición de una respuesta elevada a señales externas, en sistemas compuestos por muchas unidades diversas, tal y como sucede en conjuntos de neuronas.

En el capítulo 9, se estudia un modelo para formación de opinión que incorpora tres ingredientes básicos para la evolución en la opinión mantenida por un individuo: imitación, influencia de la moda y aleatoreidad. Se muestra que, en ausencia de moda, el modelo se comporta como un sistema biestable, con saltos aleatorios entre los dos estados estables con una distribución de tiempos de acuerdo a la ley de Kramers. También se demuestra la existencia de resonancia estocástica dependiente del tamaño, por la cual existe un número óptimo de individuos tal que la opinión promedio sigue mejor los cambios de la moda. Finalmente, se propone una extensión del modelo que permite estudiar el efecto de diversidad, encontrándose que este ingrediente puede tener el mismo rol constructivo que la aleatoreidad.

Los resultados siguientes se adentran en el estudio de cadenas de unidades excitables. En el capítulo 10, se muestra el efecto que el acoplamiento a través de la variable inhibitoria tiene en pequeñas cadenas de elementos excitables y oscilatorios. El acoplamiento inhibitorio está presente en muchos sistemas neuronales, y en este capítulo se presta particular atención a sus efectos en un sistema sujeto a ruido y a un forzamiento periódico que actúa sobre uno de los finales de la cadena. Se muestra que existe un régimen dinámico en el cual las unidades ubicadas a ambos finales de la cadena pueden responder al estímulo externo, mientras que las interiores permanecen realizando oscilaciones sub-umbrales. Esto ocurre aun si las unidades intermedias, en ausencia de acoplamiento, son oscilatorias. El mecanismo de este fenómeno es dado por una interrelación entre ruido y la

transmisión de la señal, para ciertos valores del acoplamiento inhibitorio.

El último capítulo de los resultados muestra un estudio del fenómeno de resonancia estocástica en sistemas espacialmente extendidos. En particular, se estudia una versión simplificada del modelo de FitzHugh–Nagumo, donde la difusión de la variable activadora depende del valor del campo. Los campos se encuentran acoplados a través de ambas variables: la inhibidora y la activadora. Se muestra que la respuesta global del sistema es mejorada debido a esta forma particular de difusión, y que esto puede ser entendido a través de los *potenciales de no-equilibrio*, que permiten una descripción potencial de sistemas lejos del equilibrio

Finalmente, en el último capítulo se presentan las conclusiones principales que pueden ser extraídas de est tesis. Asimismo, se discuten algunas de las extensiones posibles a las que este trabajo puede dar lugar. Los resultados presentados aquí tratan con temas de un amplio interés, y se espera que inicien nuevas investigaciones en las líneas que se desprenden de ellos.

Prefaci

En el darrer segle, degut inicialment al descobriment de l'origen del *moviment Brownià*, i després amb la proliferació dels aparells electrònics, l'estudi dels efectes del soroll en sistemes dinàmics va atreure molt interès. El soroll simbolitza la reducció d'aquells graus de llibertat d'un sistema dinàmic que no poden ser modelats d'una manera senzilla. La imatge típica del seu efecte, és el d'una pertorbació en l'evolució del sistema d'una forma erràtica i de caràcter impredictible. Degut a això, la recerca es va centrar inicialment en trobar formes de reduir els seus efectes, tot i que es consideraven una molèstia que calia ser evitada.

Durant les dues darreres dècades, no obstant, es va descobrir que el soroll pot tenir un rol constructiu en sistemes dinàmics no lineals. Entre els exemples més significatius, cal mencionar la *ressonància estocàstica* i les *transicions de fase induïdes per soroll*. En la primera, una intensitat de soroll òptima produeix una gran amplificació d'un senyal feble que actua sobre el sistema considerat. En el segon fenomen, s'observa un dràstic canvi de les propietats macroscòpiques del sistema.

D'entre els sistemes dinàmics, uns que han despertat molt interès han estat els *sistemes excitables*. Aquests sistemes romanen en un estat d'equilibri fins que una pertorbació externa prou fort els duu fora d'aquell. Després d'un canvi temporal en la seva configuració, el sistema torna al seu estat d'equilibri original. Aquesta excursió s'anomena *pols* o *tret*. Tal vegada, l'exemple més esmentat d'aquest tipus de sistema son els models matemàtics per descriure l'evolució temporal dels potencials d'acció en neurones i altres cèl·lules. Els primers models daten de la dècada del 1940. Els sistemes excitables són, així i tot, molt generals i es poden trobar en sistemes físics, òptics, en models de propagació de malalties, incendis de boscos, etc.

Un tipus de pertorbació pels sistemes excitables que es troba molt sovint és, precisament, el soroll. Un fenomen que posa de manifest un efecte contraintuïtiu del soroll actuant en sistemes dinàmics va ser trobat en l'última dècada: l'augment en la regularitat dels polsos quan la intensitat del soroll té una determinada intensitat (intermèdia). Aquest fenomen rep el nom de *ressonància de coherència* o *coherència estocàstica*.

Una extensió natural per analitzar els esmentats resultats, és l'estudi de sistemes dinàmics acoblats en presència de soroll. Com interaccionen aquests

sistemes i quins efectes emergeixen d'aquesta interacció han obert línies d'investigació molt interessants, trobant entre els exemples més notables el de la *sincronització* i és un molt bon exemple de l'enfocament minimalista, típic de la física a l'hora de modelitzar. Un fenomen sorprenent, que no va ser comprès fins la segona meitat del segle vint, és el del pampalluguejar de les cuques de llum al sud-est asiàtic. S'havia observat que al capvespre grans quantitats de aquests coleòpters pampalluguegen a l'unís on després d'un període transitori inicial. El mecanisme biològic no és completament entès encara avui, però models molt simplificats van demostrar que la feble interacció donada pels senyals visuals originen aquest fenomen col·lectiu. Aquest exemple mostra clarament que les unitats interactuants no han de ser necessariament idèntiques, però poden ser, tanmateix, *diverses*. L'efecte de la diversitat s'assembla en aquest context al que habitualment es concebeix com el típic efecte del soroll: si les unitats interactuen però són molt diferents entre sí, evolucionaran de manera molt distinta. Aquest problema és molt important, tot i que la diversitat és un ingredient habitual en molts sistemes naturals.

El propòsit d'aquesta tesi es aprofundir en el rol constructiu que els elements que *produeixen desordre* poden tenir en sistemes dinàmics. Quan es parla d'*elements que produeixen desordre*, es fa referència a elements que provoquin que cada unitat evolucioni d'una manera distinta. Per exemple, es poden citar fonts de soroll sense correlació actuant sobre els components del sistema. A més, es pot considerar la *diversitat*: en molts casos les unitats que constitueixen els sistemes no són idèntiques. Sorprenentment, es troba que és precisament la pèrdua d'ordre la que causa que els sistemes exhibeixin un comportament més coherent. També es consideren l'efecte de diferents tipus d'interacció, i es mostra que a través de les mateixes es pot generar una àmplia varietat de fenòmens: des de dur a un comportament més coherent a tot el sistema, a causar fenòmens dinàmics molt interessants en cadenes d'elements diversos.

Descriurem a continuació totes les parts d'aquesta tesi en més detall, juntament amb els principals resultats.

Part I: Introducció

La primera part d'aquesta tesi està dedicada a introduir els conceptes més importants utilitzats durant els capítols següents, ja que es pretèn que aquesta tesi sigui tant auto-continguda com sigui possible.

El primer capítol d'aquesta part, es concentra en les definicions generals que pertoquen als sistemes dinàmics. Després es realitza una breu introducció a la teoria de bifurcacions, definint aquelles que apareixen en els capítols posteriors. Finalment, es defineix un cas particular de sistemes dinàmics: aquells que estan definits en un cercle.

En el segon capítol, es descriu l'efecte que el soroll té sobre els sis-

temes dinàmics. Després d'una secció d'introducció (tant conceptual com històrica), es defineixen les eines matemàtiques que s'utilitzen a l'estudiar aquest tipus de sistemes. Després es descriu l'efecte constructiu que el soroll pot tenir sobre sistemes dinàmics, esmentant el fenomen de *ressonància estocástica*: després d'explicar qualitativament el fenomen, es detalla el marc teòric que facilita en la seva comprensió.

Existeix una àmplia varietat d'exemples de *sistemes excitables* a la natura. Al llarg del tercer capítol, aquests sistemes són definits i es presenta una classificació d'acord amb les seves propietats dinàmiques. Dos exemples prototípics d'excitabilidad són els models de *FitzHugh–Nagumo* i els *rotors actius*. Es comenten breument algunes de les seves propietats en ambdós seccions. El soroll actuant sobre sistemes excitables produeix el fenomen de *ressonància de coherència*, que és breument descrit en la secció final d'aquest capítol.

L'últim capítol d'aquesta part de la tesi està dedicat a ressenyar el fenomen de *sincronització*. En particular, es detalla un exemple paradigmàtic d'aquest fenomen: *el model de Kuramoto*, i s'enfatitza el paper similar que soroll i diversitat generen sobre aquest sistema.

Part II: Resultats

La diversitat, que ha estat típicament considerada com un factor de degradació en les característiques globals de sistemes acoblats, pot tenir un paper constructiu en molts sistemes dinàmics. En particular, en aquesta part de la tesi es mostra que la diversitat pot ser, de forma contra-intuïtiva, font d'un comportament més regular. Es troba que aquests resultats són molt generals, i s'espera que els mateixos siguin aplicables a una àmplia varietat de fenòmens, ja que es poden preveure moltes extensions possibles.

Al capítol 5 d'aquesta tesi, s'estudia un conjunt de sistemes excitables acoblats de rotors actius. La principal descoberta de aquest capítol és una teoria senzilla, però que permet una comprensió completa del mecanisme que provoca l'aparició de polsos col·lectius per part de les unitats que composen el sistema. Es troba que aquest comportament ocorre quan les posicions de les unitats estan prou desordenades. Aquest mecanisme és molt general i és independent de la font exacta de desordre. Això és estudiat en detall, al capítol 6, on es considera un conjunt d'unitats de FitzHugh–Nagumo acoblades. El mateix fenomen apareix en aquest tipus de sistema.

D'aquests resultats es conclou que aquest fenomen és independent del tipus d'excitabilitat que el sistema exhibeixi. Així mateix es comparen els resultats que s'obtenen amb soroll i diversitat, trobant qualitativament el mateix comportament.

El següent capítol 7, es focalitza en una altra font de desordre: l'efecte d'enllaços repulsius actuant en un conjunt d'unitats de rotors actius idèntics. El resultat que es troba és que, sota determinades condicions, la presència

d'alguns enllaços repulsius pot provocar també un estat en el què totes les unitats polsen al unís on. S'analitzen, també, les propietats que ha de tenir la xarxa subjacent de connexions repulsives perquè aquest fenomen global ocorri. Es troba que cert grau d'*heterogeneïtat* en la xarxa d'enllaços repulsius és necessària perquè s'observi aquest comportament coherent: la intensitat de repulsió ha de ser més important en unes unitats que en altres perquè això sigui possible.

Al següent capítol, el 8, es presenta un fenomen anàleg al de ressonància estocàstica, però induït per diversitat en lloc de soroll: la *ressonància induïda per diversitat*. En particular, es mostra que un sistema compost per molts unitats interactuants *diverses*, pot respondre millor a un senyal extern *feble* si les unitats no són totes idèntiques, però hi ha un grau intermedi de diversitat. La qualitat de la resposta global es degrada si la diversitat és massa gran o massa petita. Així mateix, es desenvolupa una teoria de camp mitjà que explica de forma convincent l'orígen del fenomen i ajusta quantitativament amb els resultats de les simulacions numèriques. Es mostra que, a més, el fenomen apareix en sistemes excitables. Aquests resultats obren un nou escenari per a l'aparició d'una resposta gran a senyals externs en sistemes composts per moltes unitats diverses, tal i com succeeix en conjunts de neurones.

Al capítol 9, s'estudia un model de formació d'opinió que incorpora tres ingredients bàsics per a l'evolució de l'opinió mantinguda per un individu: imitació, influència de la moda i aleatorietat. Es mostra que, en absència de moda, el model es comporta com un sistema biestable, amb salts aleatoris entre els dos estats estables, que segueixen una distribució de temps d'acord a la llei de Kramers. També es demostra l'existència de ressonància estocàstica dependent de la grandària, per la qual existeix un número òptim d'individus tal que el valor mitjà de l'opinió segueix millor els canvis de la moda. Per altra banda, es proposa una extensió del model que permet estudiar l'efecte de diversitat, trobant que pot tenir el mateix paper constructiu que la aleatorietat.

Els resultats següents s'endinsen en l'estudi de cadenes d'elements excitables. Al capítol 10, es mostra l'efecte que l'acoblament mitjançant la variable inhibitòria té en petites cadenes d'elements diversos excitables o oscil·latoris. L'acoblament inhibitori està present en molts sistemes neuronals. En aquest capítol es dona particular atenció als seus efectes en sistemes subjectes a soroll i a un forçament periòdic que actua sobre un dels fins de la cadena. Es mostra que hi ha un règim dinàmic en el qual les unitats situades a ambdós extrems de la cadena poden respondre a l'estímol extern, mentre que les interiors romanen realitzant oscil·lacions sub-llindars. Això ocorre també si les unitats intermèdies, en absència d'acoblament, són oscil·latòries. El mecanisme d'aquest fenomen és una interrelació entre soroll i la transmissió del senyal, per a certs valors de l'acoblament inhibitori.

L'últim capítol de la part de resultats, mostra un estudi del fenomen

de ressonància estocàstica en sistemes espacialment extesos. En particular, s'estudia una versió simplificada del model de FitzHugh–Nagumo, on la difusió en la variable activadora depèn del valor del camp mateix. Els camps es troben acoblats a través de totes dues variables: la inhibidora i l'activadora. Es mostra que la resposta col·lectiva del sistema millora deguda a aquesta forma particular de la difusió.

A l'últim capítol es presenten les conclusions principals obtingudes en aquesta tesi. Així mateix, es discuteixen algunes extensions possibles a les que aquest treball pot donar lloc. Els resultats presentats aquí tracten temes d'un ampli interès, y s'espera que siguin el punt de partida per noves línies que el prenguin com a punt de partida.

Part I

Introduction

Chapter 1

Dynamical systems

Along this chapter we will enumerate the most relevant features of the dynamical systems considered in the next chapters. It is not our intention in this brief introductory chapter to go into a detailed review of all the knowledge about these systems. But we hope that the bibliography mentioned in the text will be a good starting point for the interested reader to deepen into these topics.

In the following section 1.1, we will briefly define some basic concepts and definitions on dynamical systems that will be used all along this presentation.

To gain more insight on the terminology used in this chapter and subsequent ones, in section 1.2 we will present the kinds of bifurcations that can be observed in one-dimensional systems. We will continue with those bifurcations in two dimensions that are relevant to our results.

Later, in the last section of this chapter, 1.3, we introduce the concept of dynamical systems in a circle. These are a particularly interesting reduction of dynamical systems that appear when the relevant dynamics can be reduced to a limit cycle. Among them, we will introduce the *active-rotator model*, a system that we will encounter often along this thesis.

1.1 Definitions

A *dynamical system* is one that evolves in time. The time variable can change either continuously or in a discrete way. Dynamical systems have been studied in Physics since four centuries ago. Thus, it is of no surprise that most of the vocabulary employed is rooted in these original mechanical applications, although since the last part of the XIXth century, the study of dynamical systems has become relevant for other different scientific disciplines, ranging from Biology (where the field of applicability is by itself very broad) and Climatology to Economics, the relevance of these systems is widespread in science.

1.1.1 Continuous dynamic systems

From a mathematical point of view [1], a *continuous dynamical system* is defined by a set of ordinary differential equations

$$\begin{aligned} \dot{x_1}(t) &= F_1\left[x_1(t), x_2(t), \ldots, x_n(t)\right] \\ \dot{x_2}(t) &= F_2\left[x_1(t), x_2(t), \ldots, x_n(t)\right] \\ &\ldots \\ \dot{x_n}(t) &= F_n\left[x_1(t), x_2(t), \ldots, x_n(t)\right]. \end{aligned} \tag{1.1}$$

The state is determined by the vector $\mathbf{x}(t) = (x_1(t), x_2(t), \ldots, x_n(t))$. The dot denotes the time derivative: $\dot{x_i}(t) \equiv dx_i(t)/dt$. The solution of this set of equations allows to determine the time-evolution of the variable $\mathbf{x}(t)$, given any initial state $\mathbf{x}(0)$.

The $n-$dimensional space in which the system evolves is known as *phase space*. The trajectory the system performs in the phase space is known as *orbit*.

This definition is more general than the Hamiltonian or Newtonian dynamics in Physics [2], including them as particular cases. This broader definition also includes as dynamical systems those from other disciplines [3]. A function $V(x_1, x_2, \ldots, x_n)$, such that

$$\begin{aligned} -\partial V(x_1, x_2, \ldots, x_n)/\partial x_1 &= F_1\left[x_1(t), x_2(t), \ldots, x_n(t)\right] \\ -\partial V(x_1, x_2, \ldots, x_n)/\partial x_2 &= F_2\left[x_1(t), x_2(t), \ldots, x_n(t)\right] \\ &\ldots \\ -\partial V(x_1, x_2, \ldots, x_n)/\partial x_n &= F_n\left[x_1(t), x_2(t), \ldots, x_n(t)\right], \end{aligned}$$

is called *potential* of the dynamics. This is an extension of a well-known physical concept.

1.1.2 Fixed points

A *fixed point* is a state $\mathbf{x}^*$ such that $F_i(\mathbf{x}^*) = 0$ for $i = 1, \ldots, n$. These equilibria points can be either stable, unstable or saddle-points [4].

An asymptotically stable fixed point is one such that the system will tend towards it, whenever the system evolves starting from an initial condition sufficiently close to it. From a mathematical point of view, this can be formalised by *linearising* the system around the fixed point. This corresponds to making a Taylor expansion around the fixed point, and keeping only the first order terms. Let $\mathbf{x} = \mathbf{x}^* + \delta\mathbf{x}$. This procedure leads to the expression

$$\delta\dot{\mathbf{x}} = \mathbb{J}_{\mathbf{x}^*} \times \delta\mathbf{x}, \tag{1.2}$$

with $\mathbb{J}_{\mathbf{x}^*}$ is the Jacobian matrix evaluated at the fixed point. For an stable fixed point, the Jacobian matrix has only eigenvalues whose real part is non-positive.

On the other hand, an *unstable* fixed point is one that independently on how close an initial condition is to it, the system will depart from it. Linearising the system around such a fixed point, it is found that the Jacobian matrix has at least one eigenvalue whose real part is positive.

A particulat kind of unstable states are the saddle points. Their stability depends on the initial condition from which the system is left evolve: For some of them, the saddle-point will behave as a stable one, while for some others, will behave like an unstable. In one dimension, this nomenclature is a little bit abusive, and these points can be named as *half-stable*. The Jacobian matrix, in this case, has some eigenvalues with positive real part and some negative.

For systems defined in spaces with dimension greater than one, the eigenvalues can be complex. If this happens, the behaviour around the fixed point can be oscillatory.

1.1.3 Discrete dynamic systems

The *discrete dynamical systems* are those in which time changes discretely. In general the time evolution is given by the set of maps

$$\begin{aligned} x_1(t+1) &= F_1\left[x_1(t), x_2(t), \ldots, x_n(t)\right] \\ x_2(t+1) &= F_2\left[x_1(t), x_2(t), \ldots, x_n(t)\right] \\ &\ldots \\ x_n(t+1) &= F_n\left[x_1(t), x_2(t), \ldots, x_n(t)\right]. \end{aligned} \tag{1.3}$$

They are important as many properties of dynamical systems can be more easily understood in this simplified formulation, and easily extended to continuous processes.

1.2 Bifurcations

The bifurcation theory delves on abrupt changes in the dynamical properties of a system when a parameter changes. Although being more descriptive than predictive, it is important when trying to understand general mechanisms that can arise in particular circumstances.

In the following section we will introduce some common vocabulary on this field. Next we will enumerate the types of bifurcations in one dimension, and later on, two special cases of bifurcations in two dimensions: the Hopf bifurcation and the Saddle-node in an Invariant Circle.

A dynamical system exhibits a *bifurcation* when the properties qualitatively change when a control parameter is varied. The parameter value at which this change takes place is called *bifurcation point* [5].

A common convention when depicting dynamical systems in its phase space, is to plot the stable fixed points as black circles, the unstable ones

as white circles; and the saddle points as an circle half-white, half black, we will stick to this convention from now on.

In order to exemplify simple dynamical systems that show the different kinds of bifurcations, it is useful to consider the *normal forms* (as we will do below): on them, the functions F_i are polynomials such that their degree is the lowest one allowing the given bifurcation. Their interest lies on the fact that around the bifurcation point, *any* set of functions $\{F_1, \cdots F_N\}$ will expand into the normal form of the bifurcation.

1.2.1 One dimensional bifurcations

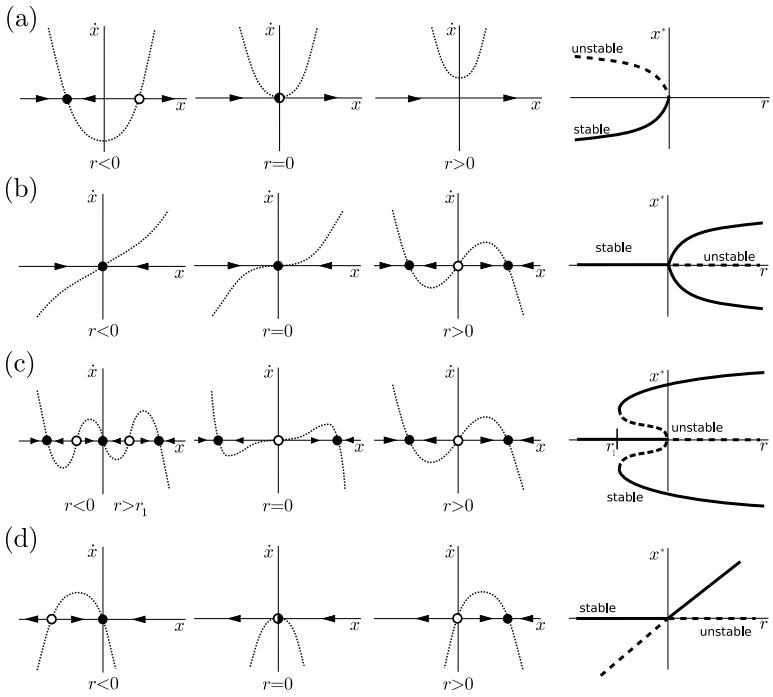

Figure 1.1: In this figure we plot four bifurcation types: (a) Saddle-node bifurcation, (b) and (c) supercritical and subcritical Pitch-fork bifurcations, respectively, and (d) Transcritical. The first three columns show the phase portrait at both sides of the bifurcation and at the bifurcation point itself. The relative stability of the fixed points is depicted using the standard convention: black circles represent the stable ones, white circles the unstable ones, and two semicircles black and white represent a saddle point. The last column represents the bifurcation diagram of the system as the control parameter is varied.

Saddle-node bifurcation

This type of bifurcation (see figure 1.1(a)) is one by which a fixed point is created or destroyed when the control parameter is varied. The normal form associated to it is

$$\dot{x} = x^2 + r, \tag{1.4}$$

being r the control parameter. For positive values of r, there are no fixed points in the system. The bifurcation point is found for $r = 0$: at that value, there is one unstable fixed point found at $x = 0$. Finally, for $r < 0$, there are two fixed points: a stable and an unstable one located respectively, at $x_s^* = -\sqrt{|r|}$ and $x_u^* = \sqrt{|r|}$. These changes can be seen in the first three columns of figure 1.1(a). Finally, the stability of the fixed point and its variation with the control parameter is depicted in the bifurcation diagram shown in the last column of the same figure.

It is important to mention that after the fixed points dissappear, the resulting dynamics near its location, remains very slow. This phenomenon is known as *ghost* fixed point, and constitutes a bottleneck of the dynamics.

We just briefly mention this bifurcation in this section, and there will be a throughout discussion when we present the *active rotator* systems, in section 1.3.

Supercritical pitchfork bifurcation

There are two types of pitchfork bifurcations, that we will detail in separated subsections, as they have interest in different kinds of physical systems. In both of them, we will assume that the systems have an invariance according to the transformation $x \to -x$.

The supercritical pitchfork bifurcation has an associated normal form

$$\dot{x} = r\,x - x^3. \tag{1.5}$$

The effect of the cubic term is *stabilising*: it is a restoring force that pulls the system to the origin. When $r < 0$ the point $x^* = 0$, is the only fixed point, which is a stable one. For $r > 0$, this point is unstable, while there are two stable ones, located at $x^* = \pm\sqrt{r}$. At the bifurcation point, $x^* = 0$ is the only (stable) fixed point. These different regimes are depicted in the three first columns of figure 1.1(b).

At the bifurcation point: $r = 0$, the system is $\dot{x} = -x^3$, whose solution for a system located at x_0 for $t = 0$, reads

$$x(t) = \frac{x_0}{\sqrt{2}\sqrt{2x_0^2\,t + 1}}, \tag{1.6}$$

which is an algebraic function of time. Then, there is a *critical slowing down* of the dynamics near this point.

This bifurcation is of special relevance in Physics: several models, even the prototypical *A-model*, present a *second order phase transition* which is signalled by this bifurcation. The critical slowing down mentioned above, is a typical consequence of these phase transitions.

Subcritical pitchfork bifurcation

For this bifurcation, the associated normal form is

$$\dot{x} = r\,x + x^3 - x^5. \tag{1.7}$$

Note that the cubic term is now *positive* at difference with the supercritical pitchfork bifurcation. Then, its effect is *destabilising*: The system is pulled to the stable branches of the 5th-order term (see figure 1.1)(c). The fact that the prefactors of the 3rd- and 5th-order terms is 1, implies no loss of generality.

As can be seen in the first and last columns of figure 1.1(c), there is a region for the parameter r, $r \in [r_1, 0]$ such that there are *three* stable fixed points, and *two* unstable ones. If $r < r_1$, the system exhibits only one stable fixed point at the origin. For positive values of r, there are two stable fixed points and an unstable one at $x_u^* = 0$. The non-zero branches of stable solutions, are often referred to as *large amplitude* branches.

Of particular interest is the region $[r_1, 0]$. Here, the point $x^* = 0$ is *locally* stable, as large enough perturbations drive the system away to the large amplitude solutions. This also implies that the system would evolve in a *hysteretic* fashion if the parameter r is varied: let us suppose the system starts at the stable fixed point $x^* = 0$ for a negative value of r. If the control parameter is increased up to $r > 0$, any infinitesimal perturbation will drive it to the large amplitude branches, the only stable positions the system has for those values of r. If now the control parameter is decreased, the system will stay near the large amplitude solutions; but whenever $r < r_1$, these solutions disappear, and the system will go back to the $x^* = 0$ stable point.

It is interesting to note that the bifurcation at $r = 0$ is a saddle-node bifurcation, as for increasing r, two fixed points are born, one stable and the other one, unstable.

Transcritical bifurcation

The associated normal form is

$$\dot{x} = r\,x - x^2. \tag{1.8}$$

In this bifurcation there are two fixed points, one located at $x = 0$ and the other at $x = r$, that exchange their stability at the bifurcation point $r = 0$. A representation of this bifurcation can be seen in the last column of figure 1.1(d).

For $r < 0$, the stable fixed point is $x^* = 0$, whilst $x_u^* = r$ is an unstable one (see figure 1.1(d), first column). On the other hand, if $r > 0$, the stable fixed point becomes $x_s^* = r$, being unstable $x_u^* = 0$ (as depicted in the third column of figure 1.1(d)). The two fixed points, collide at $r = 0$, and at that point the fixed point is a saddle (second column, figure 1.1(d)).

1.2.2 Two dimensional bifurcations

The generalisation of the one-dimensional bifurcations

Many bifurcations appear in two-dimensional dynamical systems. However, we will focus on the Hopf and Saddle-Node in an Invariant Circle bifurcations, the two that will be considered in the forthcoming chapters. Also, and in order to complete the previous discussion, we will briefly comment on the two-dimensional generalisations of the already mentioned bifurcations.

Let us consider a generic two-dimensional dynamical system

$$\begin{aligned} \dot{x} &= f(x, y) \\ \dot{y} &= g(x, y), \end{aligned}$$

where the functions (f, g) depend on a bifurcation parameter r. The system has a fixed point at (x_0, y_0), i.e. $f(x_0, y_0) = g(x_0, y_0) = 0$. At first approximation, and near the fixed point, it is possible to obtain a reduced description of it. Effectively, by writing $\delta x = x - x_0$, $\delta y = y - y_0$, the time evolution can be written in a linearised form as

$$\begin{pmatrix} \dot{\delta x} \\ \dot{\delta y} \end{pmatrix} = \mathbb{J}_{x_0,y_0} \times \begin{pmatrix} \delta x \\ \delta y \end{pmatrix}.$$

Once again, $\mathbb{J}_{x_0,y_0}$ is the Jacobian matrix of the functions (f, g) evaluated at the fixed point. The stability of that point, is given by the value of the eigenvalues λ_1, λ_2 of the Jacobian matrix. If $\mathcal{R}(\lambda_1) < 0$, $\mathcal{R}(\lambda_2) < 0$, the fixed point will be stable.

As $\mathbb{J}_{x_0,y_0}$ is a 2×2 real-valued matrix, its eigenvalues come from a quadratic equation, so there are only two possible scenarios for λ_1, λ_2: either they are both real, or complex conjugate.

The bifurcations described in the previous subsections for one-dimensional systems are also present in two-dimensional ones. Their generalisation in two dimensions are straightforwardly derived, and the corresponding dynamics are given by the set of equations

$$\begin{aligned} \dot{x} &= F(x) \\ \dot{y} &= -y. \end{aligned}$$

Where $F(x)$ is the normal form of the corresponding one-dimensional bifurcation. If the one-dimensional system undergoes a given one-dimensional

bifurcation, the complete system will undergo the same bifurcation, as the time evolution for the y variable, simply is a restoring term, that causes the system to drift towards the *locus* $y = 0$. In this case, the eigenvalues of the Jacobian are real, and the same stability analysis is valid in this case.

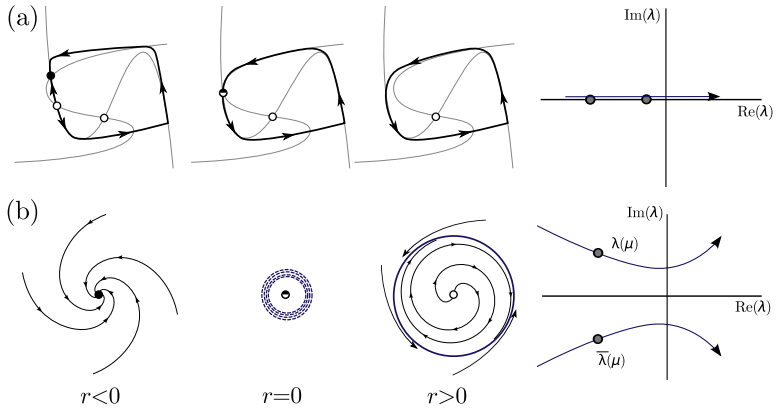

Figure 1.2: Schematic representation of two-dimensional bifurcations. In the (a) panel we show the two-dimensional Saddle-node on Invariant Circle (SNIC) bifurcation: as the bifurcation parameter is varied, a pair of stable-unstable nodes collide and dissappear, leaving a stable limit cycle. In (b), it is shown a schematic representation of the a supercritical Hopf bifurcation: When the control parameter is varied, a stable fixed point, loses its stability and a stable limit cycle appears. In the last column of both panels, we plot the change in the eigenvalues of the Jacobian matrix for the linearised version of a two-dimensional system, near a fixed point as the bifurcation parameter varies: in (a) the eigenvalues vary through real values; while in (b), the eigenvalues are a pair of complex conjugate values.

Saddle-node on Invariant Circle bifurcation

The *Saddle-node on Invariant Circle* (SNIC) bifurcation is a particular case of the two-dimensional Saddle-node one: It appears when the stable and unstable fixed points that collide at the bifurcation point are located *on* a limit cycle (see panel (a) in figure 1.2). After the bifurcation, it is this limit cycle the one that is converted in the only attractor of the dynamics.

Topological arguments [6], show that there is a slowing in the dynamics between the unstable and stable points, when the bifurcation parameter approaches to the bifurcation point. Due to this fact, the frequency of the oscillations vanishes at the bifurcation. In fact close to the bifurcation, the frequency of oscillations is proportional to $\mathcal{O}(\sqrt{r})$, being r the distance to the bifurcation point. The amplitude of the oscillations, however, start from a

non-zero value as the limit cycle is already present in the phase space before the oscillatory regime emerge.

For the particular case of the active-rotator system, we will compute these quantities in section 3.2.

Hopf bifurcation

Also, of particular interest for the results that will be shown in the upcoming chapters is the *Hopf bifurcation*. The last column of figure 1.2(b), shows a simplified picture of what happens. The eigenvalues of the Jacobian matrix remain complex while varying the bifurcation parameter. So, an oscillatory behaviour is found when the system is perturbed around the fixed point.

There are two possible routes to bifurcation in this scenario: In the particular case we will be more interested in, a stable fixed point changes stability at the bifurcation point, becoming unstable whilst a stable limit cycle appears (see figure 1.2(b)). This bifurcation is known as *supercritical Hopf bifurcation*. Interestingly enough, due to the vanishing of the real part of the eigenvalues of the Jacobian matrix, at the bifurcation point, a degenerate state with limit cycles of different radius appears.

Considering that the bifurcation occurs at $r = 0$, it is worthwhile noting that the characteristic size of the limit cycle grows proportional to $\mathcal{O}(\sqrt{r})$ near the bifurcation. Also, the period of the oscillations near the bifurcation point is given by $T = 2\pi/\mathrm{Im}(\lambda) + \mathcal{O}(r)$.

Other possibility for this kind of bifurcation, is that the fixed point changes its stability, whilst a limit cycle remains stable. In this case, the bifurcation is called *subcritical Hopf bifurcation*.

1.3 Dynamical systems in a circle

So far, we have explained some properties of dynamical systems in one- and two-dimensional systems. Under some circumstances, however, a cyclic motion in two dimensions can be approximated by considering that the system is constrained to move in the limit cycle. These simplified models, then, usually allow for a better understanding on the underlying dynamical properties of the system. Further, in many cases analytical calculations can be done in these models, allowing the understanding of mechanisms present in more complex ones. A typical example is the Kuramoto model [7], which became a paradigm in synchronisation phenomena, and to which chapter 3 is devoted to.

In the next subsection, we will introduce in general the dynamical systems defined in a circle, and in the next one, we will extensively describe the active-rotator system.

1.3.1 Definition

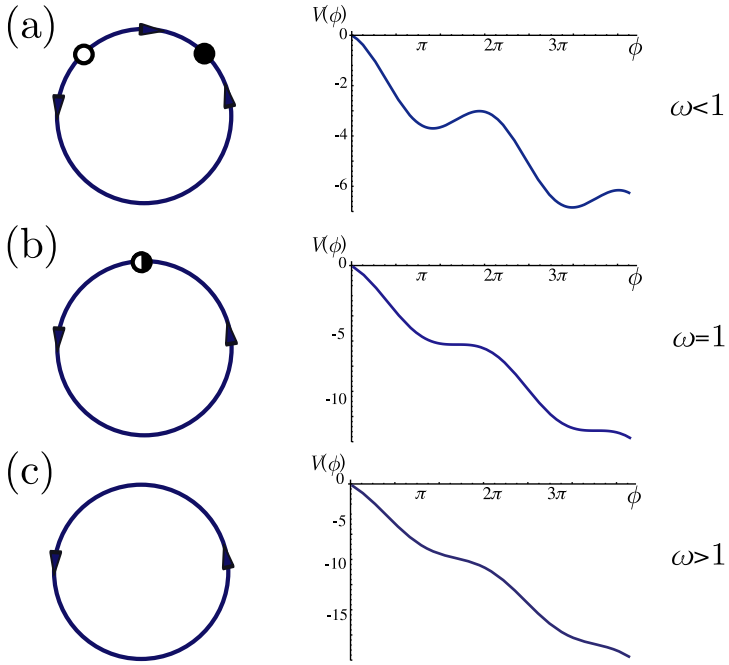

Figure 1.3: The stable and unstable points of the active-rotator model is shown for various values of the natural frequency ω in the left column. The right column depicts the different associated potentials for the corresponding parameters. It is observed that the fixed points disappear for $\omega = 1$ (signalled also the fact that there are no equilibrium points in the potential for $\omega > 1$). The bifurcation in this case is a SNIC one.

Let $\phi(t)$ be a dynamical variable describing a motion of a particle on a circle. Let us assume that the variable $\phi(t)$ obeys the differential equation

$$\dot{\phi}(t) = f(\phi, t). \tag{1.9}$$

Although being one-dimensional, and subjected to an over-damped dynamics, these systems exhibit the interesting behaviour that, although flowing in one direction, the particle eventually returns back to the initial point. Due to this fact, flows in a circle have been used to model simple oscillatory systems. The dynamic variable $\phi(t)$ is referred to as *phase* or *angle*. For these motions, it is of no relevance the amplitude of the oscillations.

It is important to remark that the function $f(\phi, t)$ must be a $2\pi-$periodic function, such that each time the system reaches the same point in the circle, the dynamics is univocally determined.

The simplest example of these systems is the *rotator* model. It represents a motion on a circle with fixed velocity. Its dynamics is given by the

expression

$$\dot{\phi}(t) = \omega. \tag{1.10}$$

The constant parameter ω is the angular velocity (also named as "frequency") of the oscillations. The time it takes to the system to complete a turn is $T = 2\pi/\omega$ (*period* of the oscillations). The position of the unit at time t is simply given by $\phi(t) = \phi_0 + \omega\, t$, with ϕ_0 the position at $t = 0$.

In chapter 4, this system will be studied in more detail, when we present the synchronisation phenomenon in the Kuramoto model.

1.3.2 Active rotator model

A very simple modification of the previous model leads to a very interesting behaviour. Let us consider a system whose dynamics is given by the first order differential equation

$$\dot{\phi}(t) = \omega + b\, \sin(\phi)\,. \tag{1.11}$$

This model was first introduced in other contexts by R. Adler [8], and then is usually named after him. The parameter ω is also called *natural frequency* of the active-rotator, although the relationship with the effective frequency is not trivial, as we will show below. The value of b determines the strength of the force that depends on the position of the particle. For $b > 0$, it is useful to consider the rescaling: $b \to 1$, $\omega/b \to \omega$, $b\,t \to t$. Then, the resulting system is independent of the parameter b. With this in mind, we will fix $b = 1$ from now on.

For this system, it is possible to write an associated potential of the form

$$V(\phi) = -\omega\phi + \cos(\phi)\,. \tag{1.12}$$

It is worth remarking that in this prescription, the system (after completing a cycle) does not return to the original point, but to one with a different potential, $V(\phi) \neq V(\phi + 2\pi)$. Let us remark that in section 1.3 it was said that *from a dynamical point of view* the points ϕ and $\phi + 2\pi$ are equivalent. Thus, keeping in mind this, we will talk about the potential function of this system in order to clarify some of its properties and later for performing computations on it.

This dynamical system displays a Saddle-nod in a Invariant Circle bifurcation as a function of the natural frequency ω. First, for $\omega < 1$, there are two fixed points for the system: a stable one located at $\phi^* = \arcsin(\omega)$ and another unstable situated at $\phi_u^* = -\arcsin(\omega)$. It can be seen in figure 1.3(a), second column, the associated potential has a local minimum and a local maximum at those points.

Both fixed points collide at $\omega = 0$, and a saddle-point appears at $\phi^* = \pi/2$ (see figure 1.3(b)). As the second column of this figure shows, the

$-dV(\phi)/d\phi$ (which is the force the particle is experimenting) near the fixed point is much lower than in the rest of the interval.

For values $\omega > 1$, there are no stable points in the dynamics, and the system completes cycles with a well-defined frequency around the circle: The velocity has the same sign for all the circle. The period of oscillations T can be determined, by means of

$$T = \int_0^{2\pi} \frac{d\phi}{\dot{\phi}} = \int_0^{2\pi} \frac{1}{\omega + \sin(\phi)} d\phi. \tag{1.13}$$

this leads to the result

$$T = \frac{2\pi}{\sqrt{\omega^2 - 1}}. \tag{1.14}$$

Conversely, the frequency of the oscillations is $f = \sqrt{\omega^2 - 1}$. Near the bifurcation point, $\omega \gtrsim 1$, the frequency of oscillations can be approximated by

$$f = \sqrt{\omega^2 - 1} = \sqrt{(\omega - 1)(\omega + 1)} \approx \sqrt{2}\sqrt{\omega - 1}. \tag{1.15}$$

The frequency grows as the square root of the distance to the bifurcation point. This is also in accordance to what was said in section 1.2.2 about the slowing down of the dynamics near the bifurcation point.

Chapter 2

Noise in dynamical systems

The effect of stochastic terms acting on dynamical systems gives raise to very interesting phenomena. Before going into the description of those, it will be useful to very briefly introduce some concepts that are common to this kind of systems.

This chapter is divided in two sections. First, in the next section, we will briefly review some concepts involved in stochastic dynamical systems. There are many text books dedicated to this very broad research field [9, 10, 11] and also very interesting reviews [12]. So our intention here, is not to give a thorough introduction of the subject, but rather mention some basic vocabulary that will be used along this Thesis.

As it has been said before, of particular interest is the constructive role that noise may play on non-linear systems. The last section of this chapter, is devoted to a particularly interesting phenomenon present in noisy non-linear systems, which is called *stochastic resonance*. This phenomenon has attracted a lot of interest after being discovered, at the beginning of the 1980 decade. It appears in systems subject to both: a *weak* forcing signal, and some random term. Its basic footprint, is the (at first glance) counter-intuitive effect that noise *enhances* the power of the weak signal. But this only happens for an intermediate range of noise intensities: either when the noise is too large (then governing the dynamics) or too weak (making its effects negligible), the phenomenon disappears.

A related phenomenon to that of stochastic resonance arises in *excitable systems* (see chapter 3) subjected to the effect of noise and its is called *coherence resonance* or *stochastic coherence*. In this phenomenon, and also for intermediate noise intensities, it is found a mode regular behaviour of system's dynamics. We will briefly review it in section 3.3.4.

2.1 Dynamical systems affected by noise

2.1.1 Historical notes

The study of stochastic terms on dynamical systems, started in the beginning of the XXth century. Although the first comprehensive study of an unpredictable, fluctuating, behaviour was performed in 1827 by the Scotish botanist Robert Brown [10]: he observed the irregular motion of small particles when looking through the microscope at small pollen grains suspended in water. He went on showing that the same phenomenon occurs independently of the suspended substance –even also glass, minerals–, discarding, then, an organic explanation for the observations.

An explanation of the origin of the *Brownian motion*, as it is known nowadays this phenomenon, was not found until 1905, by Albert Einstein [13] and independently by Marian Smoluchowskii [14]. The two main points raised in Einstein's work are the following: (i) The motion of the pollen grains is caused by the impact of incessantly moving molecules of liquid in which they are suspended. (ii) The motion of water molecules is so complicated, that its effect on pollen particles can be only described probabilistically.

Langevin, gave in 1908 an alternative explanation of the phenomenon [15]. He introduced by the first time a *stochastic differential equation*, i.e. an ordinary differential equation with stochastic terms. Although coincident with previous formulations, his method was more direct and allowed for generalisation to other scenarios. He basically considered that there are *two* forces acting on the particle: (i) *a viscous dragging force*, as in any macroscopic object moving in a fluid; (ii) *a fluctuating force*, of random nature, that models the incessant impacts of the liquid molecules on the Brownian particle. All that is known about this last term is that it should be equal to zero on average.

During the first two decades of the last century, there was a broad interest (both, theoretical and experimental) on the Brownian motion problem. With the advent of electronic circuits and radio transmission, it was evident that there are sources of irregular electrical signals in the atmosphere, the receiver and even the transmitter itself. These fluctuating signals, received the collective name of *noise*. It was usual to find what is called *shot noise* [16]. This discrete process was found in vacuum tubes, used as amplifier and rectifier devices, where it is generated by the individual electrons arriving to the catode.

Other type of noise, which will concern us during this thesis, is a continuous one: the *thermal noise*. It is present in systems in thermal equilibrium. A good example is that of a resistor at temperature T. It can be shown that if one measures the output power with frequency f, $S(f)$, it is *flat*, i.e. it is independent of the frequency, up to very large frequencies ($f \sim 10^{13}$Hz).

Due to this fact, this noise is usually called *white noise*, all the frequencies are present, like in white light.

The white noise has a zero correlation time. This is the assumption made by Langevin about the stochastic force acting on the Brownian particle. It is worthwhile remarking that the white noise as such is not feasible experimentally, but it is a good approximation in those stochastic processes whose temporal autocorrelation decreases much faster than the time between measures of the state of the system.

As the effect of noise was first studied when acting on top of a signal, it has always seen as a empovering factor on the dynamics of a system. The fact that stochastic terms can have a constructive role on non-linear dynamic systems has attracted much attention in the last two decades. In particular, it was found that noise can drive systems into a more *ordered* behaviour, as we explain in a forthcoming section. In particular we will focus on a phenomenon called *stochastic resonance* [17], which appears on systems driven by a weak external signal and subject to noise: when the right amount of noise is applied to the system, it responds more coherently with the external forcing. However, such coherence is lost whenever the noise is too large, or too weak.

2.1.2 Random Walk

This is a classical problem in Statistical Physics. It can be stated as follows: A particle moves along a line and time increases discretely by an amount Δ. At each time step, the particle, moves a distance l either to the left or right at random. Given this discretisation in space, the only allowed positions are $x = i\,l$, where $i \in \mathbb{Z}$. It is easy to show that the probability of finding the particle at position i after τ steps, follows the binomial distribution

$$P(x(\tau\Delta) = i\,l) = \left(\begin{array}{c} \tau \\ \frac{\tau+i}{2} \end{array} \right) 2^{-\tau}.$$

From this expression, it follows that $\langle x(\tau\Delta)\rangle = 0$ and $\langle x(\tau\Delta)^2\rangle = n\,l^2$. For large times, the discrete distribution can be approximated by a Gaussian one [12], yielding

$$P(x(\tau) \leq i\,l) = \frac{1}{2} + \mathrm{erf}\left(\frac{i}{\sqrt{\tau}}\right). \tag{2.1}$$

This problem, constitutes an example of a *Markovian process*: the state of the system on the next time step only depends on the actual position, and not of its previous history.

2.1.3 White noise

Noise, being a fast varying, irregular function, is not trivial to define. In order to do so, we will first introduce the concept of a *Wiener process*. Let us

consider a random walk process, such that the space and time discretisations (Δ and l, respectively), tend to zero whilst $l^2/\Delta = 1$. Also, let us write $x = i\,l$, $t = \Delta\,\tau$. In the limit of large τ, when the continuous limit of equation (2.1) can be taken, the cumulative probability distribution reads

$$P(W \leq x; t) = \frac{1}{2} + \mathrm{erf}\left(\frac{x}{\sqrt{t}}\right). \tag{2.2}$$

In this limit, the process $W(t)$ is called a *Wiener process*. It has a Gaussian distribution with zero mean and variance t. The process generated in this way is continuous; it also has a Haussdorf dimension equal to 2 [18]. The associated probability distribution function to it, is given by,

$$f(W; t) = \frac{1}{\sqrt{2\pi t}} \mathrm{e}^{-\frac{W^2}{2t}}. \tag{2.3}$$

Since this is a Gaussian distributed process, it is fully determined by its mean and two-time correlation functions

$$\langle W(t) \rangle = 0 \qquad \langle W(t)\, W(t') \rangle = \min(t, t'). \tag{2.4}$$

A *white noise* is defined as the derivative of the Wiener process defined previously. It has been said that the Haussdorf dimension in greater than the space in which the process is defined, so the process is infinitely *rough* and the derivative must be defined in a special way. To proceed, the derivative must be taken before the continuous limit is performed. If $x(t)$ is the random walk process, let $\xi_\epsilon(t)$ be the process defined as

$$\xi_\epsilon(t) = \frac{x(t+\epsilon) - x(t)}{\epsilon}; \tag{2.5}$$

which is a discretised version of the time derivative. ξ_ϵ is a Gaussian process (because it is a linear combination of Gaussian processes), and then it is completely defined by

$$\begin{aligned} \langle \xi_\epsilon(t) \rangle &= 0 \\ \langle \xi_\epsilon(t)\, \xi_\epsilon(t') \rangle &= \begin{cases} 0 & \text{if} \quad |t_1 - t_2| \geq \epsilon \\ l^2(1 - |t_1 - t_2|/\epsilon)/(\Delta\,\epsilon) & \text{if} \quad |t_1 - t_2| < \epsilon \end{cases} \end{aligned}$$

The *white noise* is the process obtained in the limit $\xi(t) \equiv \lim_{\epsilon \to 0} \xi_\epsilon(t)$. Physically, this limit corresponds to the vanishing of the correlation time. It is Gaussian distributed with

$$\begin{aligned} \langle \xi(t) \rangle &= 0 \\ \langle \xi(t)\, \xi(t') \rangle &= \delta(t - t'), \end{aligned}$$

with $\delta(x)$ is the Dirac's delta function.

All the experimentally generated (or found) noise sources, however, are not delta-correlated in time. These noises are called *coloured* in oposition to the white ones. Those sources are not studied in this thesis, and the interested reader can consult the comprehensive review [19].

2.1.4 Langevin formulation

In the example in the dynamics of a Brownian particle, its rapidly changing trajectory appears due to the incessant kicks of water molecules. Thus, to understand the complete dynamics of the particle in a microscopic prescription one should solve a *very large* system that involves the dynamics of all the water molecules that compose also the system (the order of magnitude being $\sim 10^{23}$). In a similar way, for radio signals, also one should know all the electromagnetic sources that are being detected in addition to the main signals. These ingredients would make it infeasible the solution of such systems. Langevin proposed a simplified formulation of these dynamical systems: in it, all variables whose dynamics are not the *relevant* ones, are neglected; and its influence is put into a *stochastic term*.

The Langevin representation of dynamical systems evolving under the effect of the random forcing is based on writing a stochastic differential equation. In this formulation, the stochastic term enters linearly. For a one-dimensional system, the equation reads

$$\dot{x}(t) = F\left[x(t)\right] + G\left[x(t)\right]\xi(t). \tag{2.6}$$

Here, $\xi(t)$ is the noise term. The exact time-evolution of the dynamical variable depends not only on the initial condition, but also on the particular realization of the stochastic process. To solve this equation means to find at least the probability distribution function $p(x,t)$ of finding the particle at the position x for every time t in the evolution of the system.

In the particular case of $G \equiv \sqrt{D}$, with D a positive constant (i.e. $D \in \mathbb{R}^+$), the noise is called *additive*

$$\dot{x}(t) = F\left[x(t)\right] + \sqrt{D}\xi(t). \tag{2.7}$$

This will be the only case considered along this thesis. If $G\left[x(t)\right]$ is any non-constant function, the noise is called *multiplicative*.

From a numerical perspective, it is often prohibitive to solve a stochastic differential equation in its formal sense. Instead, one usually implements methods such as Heun's [20] that allow to obtain a trajectory for a given realization of the stochastic process $\xi(t)$. Averaging over different trajectories constructed in this way, one obtains the aforementioned $p(x,t)$.

2.1.5 Fokker–Planck equation

The Fokker–Planck equation [21, 22] describes the evolution of an ensemble of stochastic dynamical systems. It is a differential equation for the probability $p(x,t)$ of finding the particle at a position x at time t. Then, any average of macroscopic variables is done by direct integration of this distribution.

Deriving the Fokker–Planck equation from the Langevin prescription is not univocally determined in the case of multiplicative noise [11]. The problem arises, basically, depending on how the integral (that appears in the derivation)

$$\int_t^{t+h} dt'\, G\left[x(t')\right] \xi(t'),$$

is defined. This gives raise to different Fokker–Planck equations for a given Langevin one. The two most prominent formulations were developed by Stratonovič and Itô [10, 11, 12]). Thus, a problem involving multiplicative noise is not fully determined if it is not said in which prescription it is defined. In the case of additive noise, both formulations coincide.

To derive the Fokker–Planck equation in the simple case of additive noise, we can proceed as follows: given an ensemble over systems, let $\rho(x, t = 0)$ be the initial density distribution of particles located at position x. Then, $\rho(x, t)$ describes the time evolution of such density.

Let us consider a noise realization ξ_w of the white noise term. The density ρ obeys the Liouville's continuity equation

$$\frac{\partial \rho}{\partial t} + \frac{\partial}{\partial x}\left(\dot{x}\,\rho\right) = 0.$$

By inserting equation (2.7) in it, we get

$$\begin{aligned} \frac{\partial \rho}{\partial t} &= -\frac{\partial}{\partial x}\left(F\left[x(t)\right]\,\rho\right) - \sqrt{D}\frac{\partial}{\partial x}\left(\xi_w(t)\rho\right) \\ &\quad -\frac{\partial}{\partial x}\left(F\left[x(t)\right]\,\rho\right) - \sqrt{D}\xi_w(t)\frac{\partial \rho}{\partial x}. \end{aligned} \tag{2.8}$$

The one-time distribution function $p(x, t)$ is an ensemble average over different noise realizations. In this average, we get

$$p(x, t) = \langle \rho(x, t)\rangle_{\xi_w},$$

And then, applying this average to equation (2.8), we get

$$\frac{\partial p}{\partial t} = -\frac{\partial}{\partial x}\left(F\left[x(t)\right]\,p\right) - \frac{\partial}{\partial x}\langle \xi(t)\,\rho(x, \xi(t))\rangle.$$

Where $\rho(x, \xi(t))$ is a functional of the particular realization of the noise. By means of differential functional calculus, it can be shown that

$$\langle \xi(t)\,\rho(x, \xi(t))\rangle = -\frac{1}{2}\frac{\partial}{\partial x}p(x, t).$$

Finally, the Fokker–Planck equation for the probability distribution function, reads

$$\frac{\partial p(x, t)}{\partial t} = -\frac{\partial}{\partial x}\left(F\left[x(t)\right]\,p(x, t)\right) + \frac{\sqrt{D}}{2}\frac{\partial^2 p(x, t)}{\partial x^2} \tag{2.9}$$

For problems related with transport phenomena, it is very useful to write down the Fokker–Planck as a continuity equation,

$$\frac{\partial p(x,t)}{\partial t} = -\frac{\partial J(x,t)}{\partial x}, \tag{2.10}$$

where the probability current $J(x,t)$ is defined as

$$J(x,t) = F\left[x(t)\right]\, p(x,t) - \frac{\sqrt{D}}{2}\frac{\partial p(x,t)}{\partial x}. \tag{2.11}$$

For stationary solutions, the current is a constant,

$$\partial p(x,t)/\partial t = -\partial J(x,t)/\partial x = 0. \tag{2.12}$$

But there are two qualitatively very different solutions: $J = 0$ (where no transport is present in the system), and $J \neq 0$ (there is a uniform motion of particles in the system).

2.2 Stochastic Resonance

2.2.1 Historical background

The origin of the periodicity between ages where the global Earth climate was warm and glacial is a withstanding question. It is interesting that such periodicity (about $\sim 10^5$ years) coincides with the ratio of variation of eccentricity of the Earth's orbit. Nevertheless, the changes in the Earth's orbit do not suffice to explain such large variations in the global temperature (the variation in the solar influx onto Earth surface is of the order of 10^{-1}). In 1980, Benzi *et al.* [23, 24], and independently, Nicolis [25, 26] developed a very simple model that is able to explain such a phenomenon, although there is not general consensus on whether the explanations developed in those works are valid or not.

The simple model proposed by these authors is as follows: they first consider that the problem can be recasted into a time-evolution of the *global* temperature, $T(t)$ (i.e. the *mean* temperature on the planet). Further, it is considered that the evolution of $T(t)$ follows, mainly, a bistable potential. Each minima corresponds to a stable climate situation (i.e. the warm and glacial states). Over this potential a small (periodic) perturbation that corresponds to the changes in eccentricity of Earth's orbit, periodically drives one or other minima to being more stable. Nevertheless, it is important to remark that this forcing *is not enough* to cause jumps between the minima. Finally, the fast fluctuations due to internal dynamics of the weather and variations of solar radiation, are considered to be a noise source that also drives the system. The counterintuitive result is that exists an intermediate range of noise intensities such that $T(t)$ jumps between minima following

(statistically) the same periodicity than the signal. This phenomenon, however, disappears for noise intensities too large or too weak.

Two years later, there was an experimental [27] verification of the phenomenon on the Schmitt trigger electronic circuit. This circuit is an histeretical binary switch whose output is constant $V_0(-V_0)$ until its input crosses the threshold value V_t ($-V_t$, respectively). Then, any periodic signal whose amplitude is $|V_a| < V_t$, will produce no change in the output of the circuit. However, if such a subthreshold signal is injected in conjunction with noise, the stochastic resonance phenomenon is observed. Later on, in 1988 [28] there was also an experimental finding of the phenomenon in non-linear optical devices as the *laser ring*.

However, it was not until 1989, that the phenomenon was quantitatively analysed from a theoretical point of view. In reference [29], the authors performed a two-state approximation for the dynamics (due to the fact that most of the time the system is near one or other minima). They proved that the resonance is due to the matching between the Kramers' time (i.e. the mean time for a randomly driven particle to hop over a potential barrier due to the fluctuations), and the time-periodicity of the external signal.

In reference [30], it was proven that stochastic resonance also exists in neural (*excitable*) systems. As it was found experimentally in mecanoreceptor neuron in the tail of a crayfish. The experiment consisted in measuring the firing activity of the receptor when put in saline water stirred with a combination of a subthreshold signal and noise. In that work, it was stressed the existence of an internal noise within the neuron, that could not be avoided. Later, it was found that stochastic resonance is present in a wide range on neural activities. For example, in reference [31], a combination of a periodic electric signal and noise was directly injected in the brain of a mammalian, and it was observed a neural activity with the periodicity of the signal. Also it was found that vision near penumbra [32] is enhanced by noise causing dark images to be detected, nevertheless. Finally, it is worth mentioning here the very interesting result that if a signal is injected through an eye and a noisy image on the other, there is a response to the signal at brain level [33].

In all the examples given so far, the dynamical variables are continuous. However, the stochastic resonance phenomenon was also found for time-discrete models such that the Ising model in a two-dimensional lattice [34].

2.2.2 Description of the phenomenon

The most typical example of a system displaying stochastic resonance is that of a Browian particle moving in a one-dimensional, double-well potential. Further, it is assumed that the particle moves in the over-damped limit. Let us denote its position by $x(t)$. The particle is also subject to a periodic signal with amplitude A and frequency $\Omega = 2\pi/T_s$. Finally, there is a noise

source $\xi(t)$ that enters additively into the equation. With this ingredients, the Langevin equation for this system is

$$\frac{d}{dt}x(t) = -x(t)^3 + b\,x(t) + A\,\sin\left(\frac{2\pi}{T_s}t\right) + \xi(t) = -\frac{\partial V}{\partial x} + \sqrt{D}\xi(t) \quad (2.13)$$

The deterministic potential reads

$$V(x) = \frac{x^4}{4} - b\,\frac{x^2}{2} - A\,x\,\sin\left(\frac{2\pi}{T_s}t\right).$$

In absence of signal ($A = 0$), the potential has two stable minima, located at $x^* = \pm\sqrt{b}$, and an unstable one (at $x_u^* = 0$). The height of the potential barrier is $\Delta V = \frac{b^2}{4}$.

It will be considered that any motion of the particle within one of the well produces no detectable output. In this sense, any signal such that fulfils $A < b/\sqrt{3}$ will be subthreshold, due to the fact that for all t no minima will disappear. Nevertheless, in general the signal amplitude can be set much lower than this limit ($A \sim 10^{-2}\,b$), and the phenomenon will remain.

Regarding the noise source, most of the work done on stochastic resonance considers it to be a Gaussian distributed, zero mean noise. It is defined by its two first moments $\langle\xi(t)\rangle = 0$, $\langle\xi(t)\xi(t')\rangle = \delta(t-t')$, where $\delta(t)$ represents the Dirac delta function, and D is the noise intensity. Further, it is a common assumption that the noise enters in an additive way. Although in this introductory section we will stick with this basic setup, there are works where the authors study the influence of time-correlation in noise, as well as multiplicative noise in conjunction with an additive one. In the case of coloured (time-correlated) noise, it was found [35, 36] that such correlation *degrades* the phenomenon, getting a lower response and a shifting in the value of optimal D to higher values than in the case of white noise. In the case of multiplicative noise (uncorrelated with the additive one) [37] the phenomenon exists as a function of multiplicative noise strength. Although the results that arise in other cases are interesting, from now on, we will consider in this introduction the noise to be additive, Gaussian and white.

The main effect of noise is to cause random jumps between both minima. Between consecutive jumps, the particle fluctuates near the potential minima. The mean first passage time (τ_K) for a stochastic system to overcome the potential barrier was first computed by Kramers [38]

$$\tau_K = \frac{2\pi}{\sqrt{V''(x_u^*)\,|V''(x^*)|}}\mathrm{e}^{2\Delta V/D} = W_K^{-1}, \quad (2.14)$$

i.e. the second derivative of the potential has to be computed in the potential minimum (in the symmetric case, it is indistinctly, $x^* = \pm\sqrt{b}$), and in the local maximum (in the case considered here, $x_u^* = 0$). In the considered case,

$V''(x_u^*) = -b, V''(x^*) = 2b$. The transition rate W_k, is simply the inverse of τ_K. For the double well potential, it reads

$$\tau_K = \frac{\sqrt{2}\pi}{b} \mathrm{e}^{2b^2/D}, \tag{2.15}$$

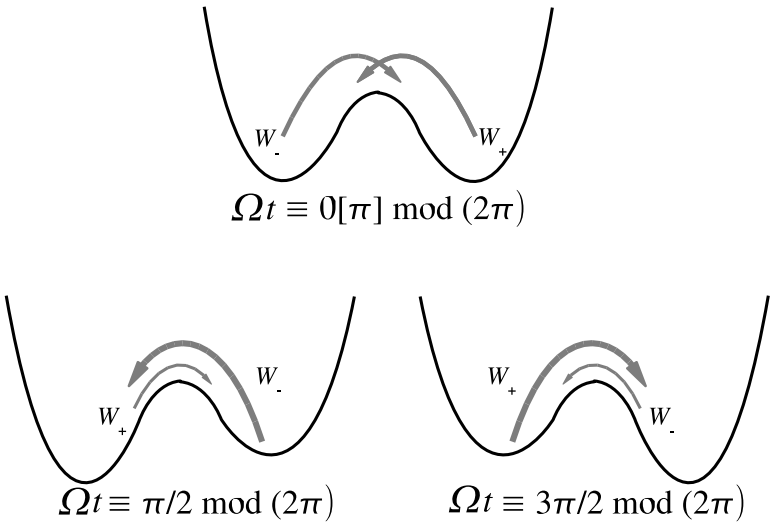

Figure 2.1: It is schematically depicted a bistable potential modulated by a periodic forcing of the form $A\sin(2\pi t/T_s)$. Successively, representations of the potential at times $\Omega t \equiv 0 \mod(2\pi)$ and $\Omega t \equiv \pi \mod(2\pi)$ in the first plot, $\Omega t \equiv \pi/2 \mod(2\pi)$ in the second, and $\Omega t \equiv 3\pi/2 \mod(2\pi)$ in the third, are shown. The arrows within the plots display the probability of hopping between the minima (see text for details). When a well in deeper than the other, the probability of transition to that is greater that the other represented by thicker lines. There is a characteristic time $\tau_K \propto \exp(\Delta V/D)$ associated with these jumps (ΔV, the height of the potential barrier, D the noise intensity). The optimal value of D is found for the condition $2\tau_K = T_s$, i.e. the time periodicity of the signal.

When a modulation is applied, as pictured in figure 2.1, the transition rate from one minimum to another will differ from the reverse. Due to the exponential dependence of the transition rate on the potential barrier height, even the small amplitude of the signal causes large changes in the transition probabilities.

In order to characterise the phenomenon of stochastic resonance, several kinds of measures have been proposed [17]. In this section we will briefly introduce two of them, the *signal to noise ratio* (at the signal frequency), and the *spectral amplification factor*. In the early stages of research, the measure used to characterise stochastic resonance was *interspike time interval*,

although we will not concentrate on it.

2.2.3 Power spectrum density and signal to noise ratio

The *power spectrum density* $S(\omega)$, is computed as the Fourier transform of the self-correlation function

$$K(\tau) \equiv \langle x(t)x(t+\tau)\rangle \,. \tag{2.16}$$

Here, $\langle\cdot\rangle$ represents time average. $S(\omega)$ gives the spectral decomposition of the evolution in time of a given quantity. Given a time-evolving variable $x(t)$, its power spectrum density is, then

$$S(\omega) = \langle \mathcal{F}\left[x(t)x(t+\tau)\right]\rangle \,. \tag{2.17}$$

Regarding the phenomenon of stochastic resonance, in a system like the one described by equation (2.13), what is observed is the following: for the optimal noise intensity a main peak in $S(\omega)$ will appear at the driving frequency over a noisy background (see the third panel of figure 2.2). For higher noise intensities than the optimal, the height of such peak will decrease (last panel in figure 2.2). Concerning lower noises than the optimal one, there are two regimes: in an intermediate region such peak decreases once again (i.e. the synchronisation with the modulation worsens, second panel in figure 2.2), but in the limit $D \to 0$ both, the height of the peak and the noisy background tend to zero. It is important to remark that in this limit such a peak is only due to the *intrawell* motion of the particle, as seen in the first panel of figure 2.2. Finally, it is worth to mention that also higher odd harmonics of the driving frequency may be seen in the power spectrum.

The computation of the *signal to noise ratio* (SNR), at the driving frequency is

$$SNR = 10\log_{10}\left(\frac{S_s}{S_n}\right), \tag{2.18}$$

where S_s represents the power spectrum evaluated at Ω (i.e. the power of this component). While S_n, is the power of the noisy background also evaluated at the same frequency. The result is given in dB (decibels).

In figure 2.3, it is shown a typical result of the SNR versus noise intensity for the double well system. With the full line, the results for the whole dynamics of the system are shown. What is observed is that for a value of $D \cong 14$ a local maximum is obtained for the SNR. However, in the limit $D \to 0$, SNR diverges. The reason for this can be easily understood looking at the first plot in figure 2.2: for vanishing noise intensities, the value of S_n (the background), vanishes, while S_s remains finite, thus causing the divergence in the SNR.

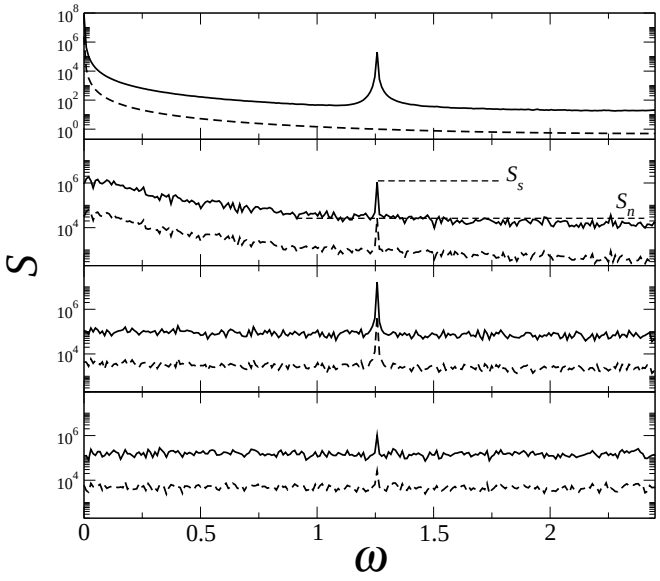

Figure 2.2: The power spectrum density of the double well system defined in equation (2.13). Here, $b = 4\sqrt{2}$, $A = 3\sqrt{2}$, $T_s = 5$ ($\Omega = 2\pi/T_s = 1.256\ldots$). From top to bottom the noise intensities are, respectively, $D = 0.1, 8, 14, 40$ (please, note the different vertical scales in the first plot with respect to the others). The full lines show the PSD for the dynamics of the system, while the dashed ones, correspond to *digitised* time-series (see text for details). It is apparent that there is an intermediate value of D such that the height of the peak with respect to the background is maximum. In the second plot, also a schematic view of S_s (signal power) and S_n (power of the noisy background) is shown.

As has been said previously, the contribution in S_s is only due to intrawell motion. For some applications, this motion is not relevant. A way to extract it, is to perform a *digitalisation* of $x(t)$; the simplest way to do so it to construct a binary signal $s(t)$

$$s(t) = \begin{cases} 1 & \text{if } x(t) < x_u^* \\ -1 & \text{if } x(t) \geq x_u^* \end{cases} ,$$

where x_u^* is the position of the unstable minimum, separating both wells. When processing this signal, the divergence at $D = 0$ disappears, as seen in the dashed line of figure 2.3.

2.2.4 Linear response and spectral amplification factor

Another useful measure for the stochastic resonance phenomenon is the spectral amplification factor [39]. As will be seen, this measure is related with the

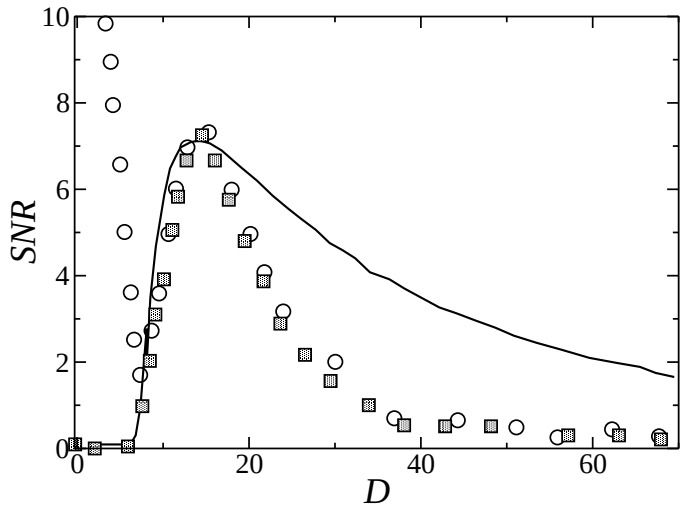

Figure 2.3: The signal to noise ratio, *SNR*, versus noise intensity for the bistabel system. The results, show a noise intensity such that the signal is better transmitted. The white circlesrepresent the numerical results for $x(t)$, while the gray circles show the *SNR* for the digitised output. The line represents the theoretical prediction of the two-state model (see section 2.2.5 for details). Same parameters as in figure 2.2.

statistical synchronisation of the system dynamics with the external signal.

Averaging over different realizations of noise, the system defined by equation (2.13) (and a broad variety of dynamic systems), asymptotically (and independently of the distribution of initial conditions) tends to an asymptotic value which happens to be time-periodic $x_{as}(t)$, with the time-periodicity of the signal, and its higher order harmonics. So, this asymptotic function can be decomposed in a Fourier expansion

$$x_{as}(t) = \lim_{t_0 \to -\infty} \langle x(t)|x_0, t_0\rangle = \sum_{n=-\infty}^{\infty} M_n \, \sin(n\,\Omega\, t), \tag{2.19}$$

where the average runs over different initial conditions.

For the self-correlation function, alternatively, the same result holds

$$\begin{aligned} \hat{K}_{as}(\tau) &= \lim_{t_0 \to -\infty} \langle x(t)x(t+\tau)|x_0, t_0\rangle \\ &= \sum_{n=-\infty}^{\infty} M_n^2 \mathrm{e}^{\imath\, n\Omega\, \tau}. \end{aligned} \tag{2.20}$$

A result following from the orthogonality of the base functions.

It is important to remark that M_1 is exactly the same as the PSD evaluated at the driving frequency. The power of the $n-$th harmonic of the frequency Ω is given by $P_n = 4\pi|M_n|^2$. While integrating the input power over a period, one gets that the total power of the signal contained in the input is $P_i = \pi A^2$, being A the signal intensity.

The spectral amplification factor, η, is then

$$\eta = \frac{P_1}{P_i} = 4\left(\frac{|M_1|}{A}\right)^2 \tag{2.21}$$

This method has two interesting properties, first, it does not have the problem of divergence in the limit $D \to 0$, it only decreases monotonically with vanishing noise. When not digitised, reaches a small non-zero value (once again, due to the intrawell motion). When the output is digitised, η does goes to zero when no extra-well motion exists. The second property, is that it can be computed more accurately than the SNR because there is only one magnitude to be calculated. At difference, for the signal to noise ratio, all the power spectrum density must be computed. In figure 2.4 the results for the archetypical double-well system are shown.

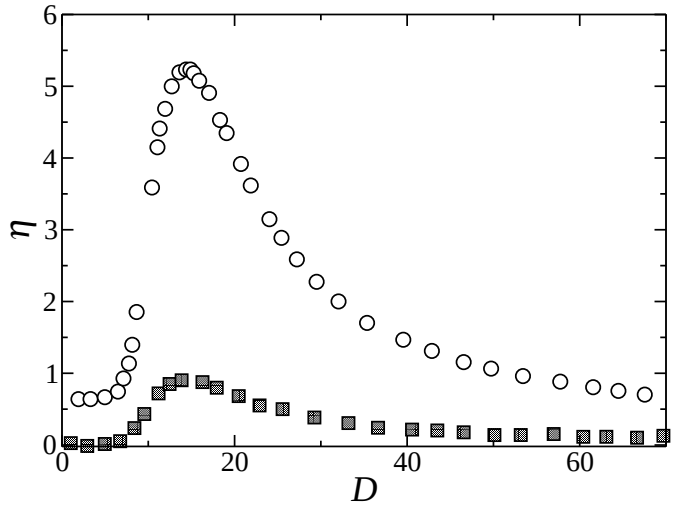

Figure 2.4: The numerical results for the spectral amplification factor, η, are plotted as a function of noise intensity, showing a maximum for an intermediate amount of noise. The white circles represent the results for $x(t)$, while the gray circles show the resulting η for the digitised output. Same parameters as in figure 2.2.

2.2.5 Two-state model

In this subsection we will introduce the two-state model [29], which is the simplest approach that successfully explains (with qualitative and quantitative agreement) the phenomenon of stochastic resonance for a bistable system, whose transition rate as a function of noise and system parameters is known.

It is based on the fact that for signals with large time-periodicity the system reaches stationary behaviour in each well (i.e. an *adiabatic approximation*), before hopping back. Further, it is assumed that, at time t, the particle coordinate can have one of two different values: $x^*_\pm$ (corresponding to the potential minima), with a probability $n_\pm(t) = \mathrm{Prob}(x = x^*_\pm|t)$. If in the original bistable system the coordinate $x \in \mathbb{R}$, these quantities are given by

$$n_-(t) = 1 - n_+(t) = \int_{-\infty}^{x^*_u} P(x,t)\, dx.$$

where x^*_u is the position of the local maximum in the potential. Let $W_\pm(t)$ be the *transition rate* from the state $x^*_\pm$. This is a periodic function of time, due to the periodicity of the signal and the adiabatic approximation. Thus, the master equation for the populations $n_\pm$ yields

$$\frac{d}{dt}n_-(t) = -\frac{d}{dt}n_+(t) = W_+(t)\, n_+(t) - W_-(t)\, n_-(t) \tag{2.22}$$

The functions $W_\pm(t)$, in general, can not be found exactly. However, for small modulation amplitudes, it is possible to expand them into a Taylor series

$$W_\pm(t) = W_0 \mp a_0 \sin(\Omega t) + \mathcal{O}(A^2)\cdots, \tag{2.23}$$

where W_0 is the transition frequency evaluated in absence of signal and

$$a_0 \;=\; -\frac{d}{dA}W_k\bigg|_{A=0} A \tag{2.24}$$

The reduction from a continuous bistable system (whose probability evolves according a Fokker–Planck equation) to a discrete two-state system (governed by a master equation) has been solved formally [10, 40]. Given initial conditions (x_0, t_0), the solution for $n_+(t)$ at first order in the modulation

$$n_+(t|x_0,t_0) \;=\; \mathrm{e}^{-W_k|t-t_0|}\left(\frac{a_0\, A\cos(\Omega\, t_0 - \phi)}{\sqrt{W_k^2+\Omega^2}} + 2\delta_+ - 1\right). \tag{2.25}$$

Where $\phi = \tan^{-1}(\Omega/W_k)$. The function δ_+ is equal to 1 if $x(t_0) = x_+$ and 0 otherwise. From the former equation the self-correlation function can be

computed and then the power spectrum, which gives

$$S(\omega) = \left(\frac{2W_k}{W_k^2+\omega^2}\right)\left(1-\frac{(a_0\,A)^2}{2(W_k^2+\Omega^2)}\right)+ \frac{\pi\,(a_0\,A)^2}{2(W_k^2+\Omega^2)}[\delta(\omega-\Omega)+\delta(\omega+\Omega)]. \quad (2.26)$$

Equation (2.26) gives a very interesting result: the power spectrum of a bistable system will be composed of a part term with Lorentzian shape and two peaks at (plus/minus) the driving frequency. The first term corresponds mainly to the noisy dynamics, i.e. the random hoppings. Further this expression allows us to determine the *SNR* in this approximation. The result obtained, is

$$SNR = 10\log_{10}\left(\frac{(\pi a_0\,A)^2}{W_k}\left(1-\frac{(a_0\,A)^2}{2(W_k^2+\Omega^2)}\right)^{-1}\right), \quad (2.27)$$

being A the intensity of the small modulation, the leading term to the computation of the SNR is, for the double-well potential (by replacing in equation (2.15)),

$$SNR = 10\log_{10}\left(1+\frac{\sqrt{2}b^2\,A^2}{D^2}\exp\left(\frac{-2b^2}{D}\right)+\mathcal{O}(A^4)\right).$$

In figure 2.3 the theoretical line shows the good agreement of this simple formalism with the numeric results. The intrawell motion is neglected (due to the two-state approximation), thus the predicted value goes to zero for vanishing noise.

Chapter 3

Excitable Systems

Excitable behaviour appears in a large variety of physical, chemical and biological systems [3, 41]. Typically this behaviour occurs for parameter values close to an oscillation bifurcation, and is characterised by a nonlinear response to perturbations of a stationary state: while small perturbations induce a smooth return to the fixed point, perturbations exceeding a given threshold induce a return through a large phase space excursion (firing), largely independent of the magnitude of the perturbation. Furthermore, after one firing the system cannot be excited again within a refractory period of time. In many situations of interest, the firings are induced by random perturbations or noise [42].

Excitable systems are widespread in nature, the most paradigmatic being those coming from Biology: The most typical example is that of neurons [43, 44], but also in cardiac tissues, pancreatic $\beta-$cells. The Hodgkin–Huxley model, the first mathematical model for excitable dynamics, was proposed in 1952 [43]. This four-dimensional dynamical system was introduced to explain the voltage dynamics of the giant axon of a squid.

These systems also are present in multi-species chemical reactions, such as the Belousov–Zhabotinskii [45], in what constitutes an extended medium. Also, it was found that the cycle of some contagious diseases also follows this kind of dynamics, as shown by the SIRS (standing for susceptible-infected-recovered-susceptible) model [46]. Interestingly enough, this model is also excitable in its discrete three-state version.

A typical ingredient in these systems is the existence of a *refractory time*: a minimum time interval such that the system can not spike more than once during it. This is related to the fact that, during the excursion, the trajectory in the phase space of the system is basically deterministic. Then, the refractory time is approximately equal to the time it takes to the system to move through this excursion.

As has been said, the excitable systems must be *perturbed* by some means in order to spike. Typical *stimuli* are external (periodic or aperiodic) sig-

nals. These deterministic perturbations are rather well understood [47, 3]. In the last two decades, however, the *ordering effect* that noise has on different systems [23, 26], was unveiled, and then, many works were related to establish the constructive effect of noise in this kind of systems (for a recent and comprehensive review, see [42]).

This chapter is organised as follows. In the next section we introduce a classification of excitable systems according to the bifurcation they undergo. Later, we introduce the active-rotator system as a paradigm of *type I* excitability and the FitzHugh–Nagumo model, prototypical example of *type II* excitability. In the final section, we review the *coherence resonance* phenomenon, by which an excitable system exhibits a more coherent behaviour under the proper value of the noise.

3.1 Classification

In general, an excitable behaviour appears when the systems considered are close to a bifurcation point: the stable configuration being signalled by a fixed point, while the other regime might be, for example, an oscillatory one. The perturbations aforementioned, drive the system from one behaviour to the other.

In general, this bifurcation can be of different kinds, and this fact allows for a simple classification of the excitability of the systems according to this transition [48, 6]. It was first proposed by Hodgkin [49], when studying the response of neuron cells to an external stimulus. He noticed that the change from a resting state to oscillations, could occur in two different ways: (i) through oscillations of arbitrarily low frequencies, that would grow if the perturbation strength would we increased; (ii) The oscillations are generated in a given interval of frequencies. This classification was later formalised by Rinzel and Ermentrout [50], by using bifurcation theory.

Type I

Excitable systems of type I are characterised by the fact that the oscillatory regime just above the bifurcation exhibits frequencies with arbitrarily low values. Figure 3.1(a) depicts a representation of the typical situation.

It is important to stress that, altough in much of the bibliography on excitable systems it is common to find that class I excitability appears near a Saddle-node bifurcation, this is not the case [6]. For this excitability to exist, the kind of bifurcation must be a saddle-node on an invariant circle one. The reason for this is that the fixed points must be *in* the limit cycle. Otherwise, even in the excitable regime, a well-defined frequency would exist: that of the limit cycle. the saddle node on an invariant circle bifurcation ensures a slowing-down of the frequency near the bifurcation point (see section 1.2.2 for full details).

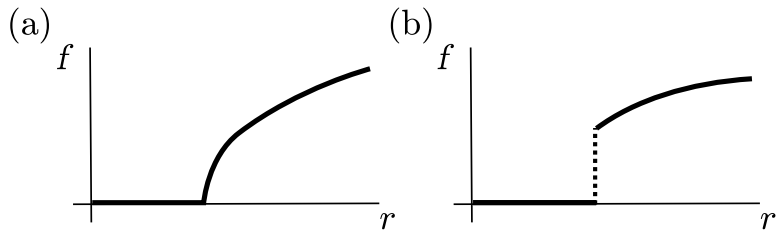

Figure 3.1: It is shown a schematic representation the frequency of oscillations for the bifurcation of different excitable systems. Panel (a) depicts the transition for an excitable system of *type I*. For these systems, near the bifurcation point, oscillations of frequencies arbitrarily slows can be found. Panel (b) represents such transition for a *type II* excitable system. At the bifurcation point, oscillations with non-zero frequency are born.

Among the dynamical systems displaying this kind of excitability we highlight: (i) active-rotator (or Adler) model, used to study Josephson junctions, neuron dynamics, surface growth. (ii) the Hodgkin–Huxley neuronal model [49, 43], for some parameter values.

An interesting example exhibiting this kind of excitability, is the cortical excitatory pyramidal neurons. Interestingly enough, the strength of the input stimulus is encoded in the firing frequency of these neurons, as the frequency range these neurons can fire is broad [6].

Type II

This type of excitability arises in systems showing Hopf (either subcritical or supercritical), or Saddle-node bifurcations. It is characterised by the fact that at the bifurcation point the system shows oscillations of a non-zero frequency. In fact, the interval of frequencies at which these systems oscillate is in general narrow. A representation of the dependence of oscillation frequency on the bifurcation parameter, can be seen in figure 3.1(b).

Among the mathematical models that show this excitability, we may mention (i) FitzHugh–Nagumo model [51, 44]; this is a paradigmatic example of excitable dynamics, and is used to model from chemical reactions to neuron dynamics. A section will be devoted to this system in this Chapter. (ii) The Hodgkin–Huxley neuronal model in some parameter range. In fact, the FitzHugh–Nagumo model was first introduced as a simplification –for some parameter region– of this model. (iii) the Morris–Lecar model, for nervous cells [52].

There are also neurons that exhibit this kind of excitability: for example the cortical inhibitory interneuron. These neurons are fast-spiking, and fire in a relatively narrow frequency. In another field of sciences, the Belousov–Zhabotinskii chemical reaction is an example of this excitability [53, 54].

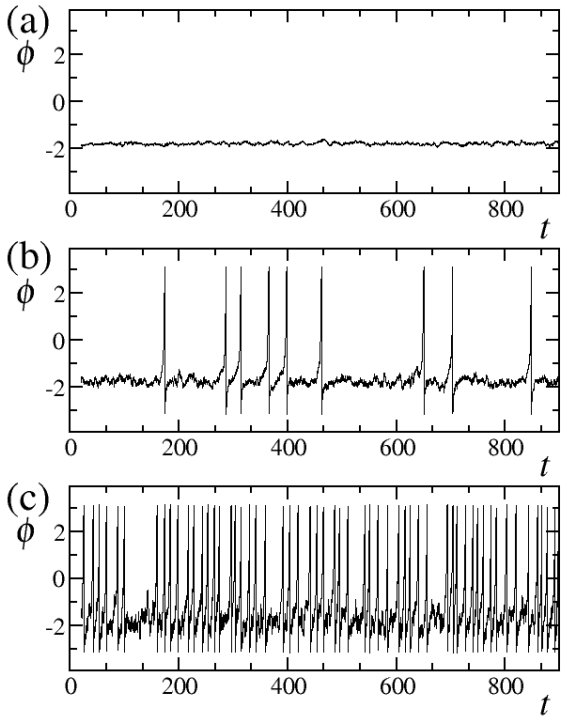

Figure 3.2: We plot trajectories obtained numerically of the active-rotator model for different noise intensities and a fixed value of $\omega = 0.98$, in the excitable regime and close to the bifurcation point. The value of noise intensity is $D = 5 \times 10^{-3}, 10^{-2}, 0.1$, in panels (a), (b) and (c), respectively.

3.2 Active-rotator as an excitable system

In section 1.3 we introduced the active-rotator model. However, we restricted ourselves to briefly discuss the properties of this system when the dynamics are purely deterministic. We also shown that the oscillation time diverges near the saddle-node in and invariant circle bifurcation this model undergoes.

The active rotator model, under the effect of noise, was first studied by Kuramoto and Shinomoto in the context of coupled oscillators [55, 56]. Since then, a lot of work has been devoted to the study of this generic model. For example, this model has been employed when modelling neurons [57, 58], flashing fireflies [59, 60], human circadian pacemaker cells [61], Josephson junctions and charge-density waves [62], etc.. Thus, the active-rotator model is used as a paradigm of class I excitable systems.

The dynamics is simply given by

$$\dot{\phi} = \omega + \sin(\phi) + \sqrt{D}\xi(t). \tag{3.1}$$

Although we only consider the white noise one, it is worth mentioning that coloured noise can give raise to interesting phenomena, such as *ratchet* behaviour [63].

Some typical dynamic trajectories of this system are shown in figure 3.2. It is seen the large variation in the time-scale between pulses due to changes in the noise intensity. This is related to the slowing down of the systems undergoing a saddle-node bifurcation close to the bifurcation point. Then, there is not a "typical" time-scale for this system. It only depends on the distance to the bifurcation point.

The time it takes the system to escape from the basin of attraction near the fixed point has been computed in [64]:

$$T = \frac{\int_0^{2\pi} d\phi\, I(\phi)}{1 - \mathrm{e}^{-2\pi\omega/D}}, \tag{3.2}$$

where the function $I(\phi)$ is defined as

$$I(\phi) = \frac{1}{D}\mathrm{e}^{-V(\phi)/D} \int_{\phi-2\pi}^{\phi} d\varphi\, \mathrm{e}^{-V(\varphi)/D}. \tag{3.3}$$

3.3 FitzHugh–Nagumo model

3.3.1 The Bonhoeffer–van der Pol model

In [65], B. van der Pol, introduced a model to qualitatively describe the relaxation oscillators. It was later used by Bonhoeffer [66] to study the behaviour of passivated iron wires. It was later used –for analogy– as a model for nerve excitation [67]. The model considered is as follows

$$\ddot{x} + \epsilon^{-1}(x^2 - 1)\dot{x} + x = 0. \tag{3.4}$$

It is interesting that this model, under the variable change

$$y = \frac{\dot{x}}{c} + \frac{x^3}{3} - x, \tag{3.5}$$

can be rewritten in the following way:

$$\begin{aligned} \epsilon\dot{x} &= x - \frac{x^3}{3} - y \\ \dot{y} &= -x. \end{aligned} \tag{3.6}$$

The parameter ϵ controls the difference of the time-scales between both variables. The only fixed point of this system is located at $x_u^* = 0$, $y_u^* = 0$, which is an unstable one.

3.3.2 The Hodgkin–Huxley model

The FitzHugh–Nagumo model was first introduced in 1955 [51], as a simplified version of the Hodgkin–Huxley nerve model [43]. The latter was introduced to model the firing dynamics observed in the gigantic axon of squids. This firing is common to many neuron and nerve cells [68]. The axon is a long cylinder which extends from the neuron centre, and electric signals propagate along its outer membrane. The electrical pulses appear because this membrane is permeable to different ions [3] . The permeability depends on the actual membrane potential $V(t)$, on the ion concentration and also on the current –originated, for example, in local depolarisation relative to the rest state– present. The most important ions are potassium and sodium, (K^+ and Na^+). The difference in the concentration of K^+ ions between the inner and outer axon membrane, causes a potential difference of about $v_0 \approx 70$mV. The dynamical variable measured in the experiments is the deviation of the membrane potential with respect to this rest state.

Due to the spatial extension of the axon, the potential varies along its extension. We will now, however, concentrate on the homogeneous case, where the membrane potential V is constant along the axon.

Let I_a be the applied current across the membrane. It has two contributions: I_i, originated in the ions that pass the membrane; there will be another source of current, which is the time-variation in the transmembrane potential,

$$I_a = I_i + C\frac{dV}{dt}, \tag{3.7}$$

where C is the capacitance of the membrane. Hodgkin and Huxley [43] wrote

$$\begin{aligned} I_i &= I_{\mathrm{K}} + I_{\mathrm{Na}} + I_L \\ &= g_{\mathrm{K}} n^4 (V - V_{\mathrm{K}}) + g_{\mathrm{Na}} m^3 h (V - V_{\mathrm{Na}}) + g_L (V - V_L) \end{aligned}$$

The currents I_{K}, I_{Na} and I_L are, respectively, the potassium, sodium and "leakage" current: the sum of all other ions currents. V_{K}, V_{Na} and V_L are the equilibrium potentials; g_i are constant values such that $g_{\mathrm{K}} n^4$, $g_{\mathrm{Na}} m^3 h$ and g_L are the associated conductances. The values of m, n and h depend on time, verifying

$$\begin{aligned} \dot{n} &= \alpha_n(V)(1-n) - \beta_n(V) n, \\ \dot{m} &= \alpha_m(V)(1-m) - \beta_m(V) m, \\ \dot{h} &= \alpha_h(V)(1-h) - \beta_h(V) h. \end{aligned} \tag{3.8}$$

The functions $\alpha_i(V)$ and $\beta_i(V)$ were determined experimentally; α_n, α_m and α_h, are sigmoidal-like: for $V \to \infty$ they saturate in 1 (the first two), and in 0 (the latter). The variables n, m and h are restricted to the interval $[0, 1]$.

The full expression for the membrane potential dynamics, is then

$$C\frac{dV}{dt} = -g_{\rm K} n^4 (V - V_{\rm K}) - g_{\rm Na} m^3 h (V - V_{\rm Na}) - g_L (V - V_L) + I_a. \quad (3.9)$$

The set of equations (3.8) and (3.9) consitute the model that Hodgkin and Huxley solved numerically and found in good agreemens with the experiments.

In this model, by varying the parameter I_a –which is the easiest to control experimentally–, it is found that for $I_a = 0$, the system is excitable; but for currents above a given threshold I_a^*, the system becomes oscillatory, and the neuron steadily fires.

Depending on the parameter values, this model displays many dynamical behaviours, in addition to excitable and oscillatory dynamics, it also exhibits *bursting*: a high-frequency, continuous, firing.

3.3.3 FitzHugh derivation

The Hodgkin–Huxley model is very complicated and several models appeared as simplifications of it, trying to capture the basic ingredients of the phenomenology that arises from it. A particularly successful model is the one proposed by R. FitzHugh [44], and later confirmed experimentally by J. Nagumo *et al.* [69]. FitzHugh noticed that the variables V and m, represent rapidly changing variables, representing excitability. The other two variables, n and h, are recovery variables, slow compared to the former two variables. He demonstrated that many of the dynamical properties of the Hodgkin–Huxley model remain if the system is simplified. He tried to idealise the shape of the nullclines, in order to simplify the mathematical formulation. Interestingly, he found that a slight modification to the van der Pol model, allowed for a cartoon of the Hodgkin–Huxley one. He proposed, then, the following dynamical system

$$\begin{aligned} \epsilon \dot{x} &= x - \frac{x^3}{3} + y + I \\ \dot{y} &= -x + a + b\, y. \end{aligned} \quad (3.10)$$

He named this system BVP (for Bonhoeffer–van der Pol). It must be verified that $1 - 2b/3 < a < 1$, $0 < b < 1$ and $b < c^2$. The parameters a, b, ϵ are fixed constants, I represents an injected current. It was left in the x variable only for analogy to the Hodgkin–Huxley model. In general, the results are independent on which variable the signal is applied to [70]. The (small) value of ϵ fixes the separation of the time-scales between the fast (excitatory) x variable and the y slow recovery (inhibitory) one. Typical values of this separation are around $\epsilon \in [10^{-4}, 10^{-2}]$. The sign of the variables x and y can be inverted (given the fact that all the terms correspond to odd powers) and the dynamical properties will remain unchanged.

Qualitatively, the dynamics of the FitzHugh–Nagumo model is similar to the phenomenology captured by the Hodgkin–Huxley model. It exhibits oscillatory and excitable regimes, not exhibiting bursting, though. The functional form of the forces acting on the x and y variables, was selected only for simplicity, and to allow for some theoretical treatment –which would be much harder to perform in the Hodgkin–Huxley model–. In fact, there are further simplifications to this model. For example, taking linear piece-wise interpolations of the cubic term in the equation for x. The main dynamic properties of the system remain unchanged.

Without loss of generality, and very useful for some applications, one can take $b = 0$. It is common to assume that the noise term enters in the injected current, so in absence of another sources, the model reads

$$\begin{aligned} \epsilon \dot{x} &= x - \frac{x^3}{3} + y + \sqrt{D}\xi(t) \\ \dot{y} &= -x + a, \end{aligned} \tag{3.11}$$

where D is the noise intensity of the noise source $\xi(t)$.

3.3.4 Dynamical properties

Linear Analysis

The system (3.11) has only one fixed point: $x^* = a$, $y^* = a - a^3/3$. The linear analysis indicates that the Jacobian matrix is given by

$$\mathbb{J}(x, y) = \begin{pmatrix} \frac{1}{\epsilon}(1 - x^2) & \frac{1}{\epsilon} \\ -1 & 0 \end{pmatrix}.$$

At the fixed point the eigenvalues are

$$\lambda_{1,2} = \frac{1 - a^2 \pm \sqrt{(a^2 - 1)^2 - 4\epsilon}}{2\epsilon}. \tag{3.12}$$

As ϵ is a positive real constant, it can be seen that there is an interval

$$a^2 < 2\sqrt{\epsilon} + 1, \tag{3.13}$$

such that the eigenvalues are complex conjugates. This implies an oscillatory dynamics around the fixed point. Furthermore, if $a^2 < 1$, the real part of the eigenvalues is positive, and then the fixed point is unstable (see 3.3, first column). For $a^2 > 1$, the fixed point is stable, there is a region $|a| > 1$ (whose size depends on the value of ϵ), such that the behaviour is oscillatory. Thus, there is a bifurcation at $|a| = 1$ between an oscillatory behaviour (for $|a| < 1$) and an excitable one ($|a| \geq 1$). Note, however, that equation (3.13) implies that the region where there are complex eigenvalues in the excitable regime, vanishes in the limit $\epsilon \to 0$, which is the region of relevance in the context in which this model is used.

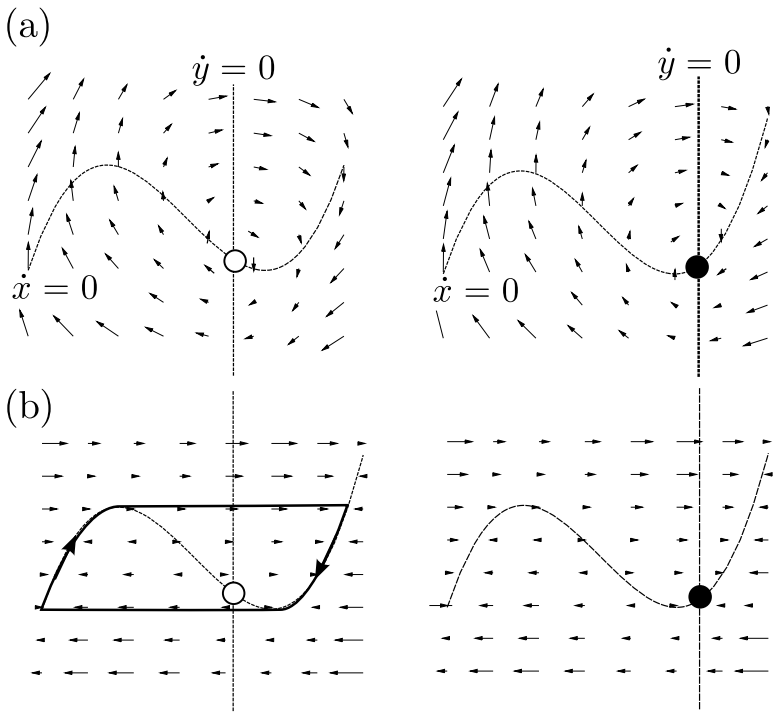

Figure 3.3: It is shown a schematic representation of the phase space for the FitzHugh–Nagumo model. The first column of both panels, depict the oscillatory regime, where the control parameter is $a = 0.5$, in which a unstable fixed point appears. The second column represents the phase space in the excitable regime ($a = 1.3$), in which there is a stable fixed point. The panel (a), shows $\epsilon = 1$, in order to make visible velocity field in both directions. For smaller values of ϵ –see panel (b), where $\epsilon = 10^{-2}$–, the magnitude of the force in x direction is much larger, carrying very fast the system to the nullcline x.

A final note is that the branches of the x-nullcline are attractors of the dynamics, and the system evolves approaching them: they behave as a limit cycle –see figure 3.3(b)–, such behaviour is more apparent for vanishing values of ϵ .

We will now show an approximation of the time to perform a cycle, valid for small values of ϵ.

Analytic derivation of the oscillation time

For small enough values of the time-scale parameter ϵ, the dynamics in the x variable occurs very fast, and the system relaxes quasi-instantly to the branches of the cubic x-nullcline: The relaxation time is much faster than

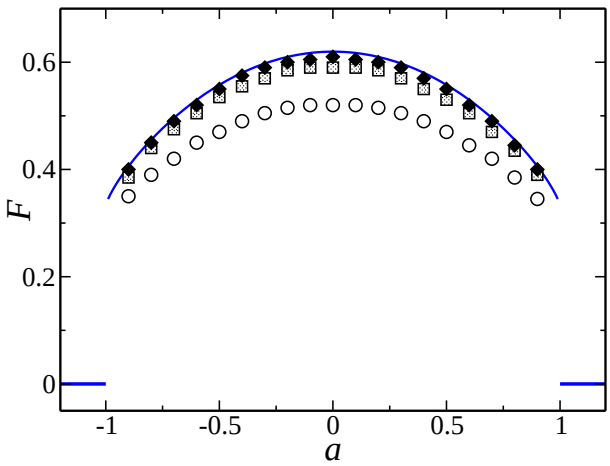

Figure 3.4: We plot the frequency of the oscillations for the FitzHugh–Nagumo model as a function of the control parameter a. The symbols correspond to the numerical results for three different values of the parameter ϵ, which controls the time-scale separation of the variables, namely: $\epsilon = 10^{-2}$ (white circles), $\epsilon = 10^{-3}$ (gray squares) and $\epsilon = 10^{-4}$ (black diamonds). The solid line corresponds to the analytical approximation given by equation (3.19).

any other time-scale of the system, for example the oscillation time. Along this section, we will restrict to the case ϵ very small.

As the system, starting from any initial condition, rapidly reaches the nullclines of the x variable –see figure 3.3(b) for the associated velocity field–, we can consider that all the dynamics of the system during the cycle occurs in these nullclines. Furthermore, we can neglect the jump time from one branch to the other. Formally stated, we can put

$$\epsilon\,\dot{x} = x - x^3 + y = 0. \tag{3.14}$$

This can be associated to the fact that $\epsilon = 0$. Then, we have

$$y = x - x^3, \tag{3.15}$$

and taking the time-derivative, we get,

$$\dot{y} = \dot{x}(1 - x^2). \tag{3.16}$$

From the definition of the model, we also know that the recovery variable dynamics follows (see equation (3.10))

$$\dot{y} = x - a. \tag{3.17}$$

So, if we equate the expressions (3.16) and (3.17), and solving for the time derivative $\dot{x}$, we get

$$\dot{x} = \frac{1 - x^2}{x - a}, \tag{3.18}$$

In order to compute the oscillation period, we must integrate the above equation along the trajectory performed on the limit cycle (see figure 3.3), i.e.: for the right branch the integration limits are, $x \in [1, 2]$, whilst for the left branch $x \in [-2, -1]$:

$$\begin{aligned} T &= \int_{-1}^{-2} dx \, \frac{1 - x^2}{x - a} + \int_{1}^{2} dx \, \frac{1 - x^2}{x - a} \\ &= 3 + (a^2 - 1) \ln \left(\frac{4 - a^2}{1 - a^2} \right). \end{aligned} \tag{3.19}$$

From it, the frequency of the oscillations is readily given as $f = T^{-1}$. The agreement of this approximation with the actual values of frequency is shown in figure 3.4. It is observed that the approximation is better, for vanishing ϵ, as the approximation implies. For $|a| > 1$ the frequency is zero, and the system is excitable.

It is useful to compare these results in figure 3.4 with those observed in figure 3.1, panel (b). It can seen that the frequency of oscillations follow the same overall behaviour and, thus, this system behaves as a type II excitable system.

The effect of noise

In the excitable regime, qualitatively, the dynamics does not depend on to which variable the noise is applied [70]. From now on, and without loss of generality, we will consider the noise acting on the slow variable. Also, when an external signal is applied, in general it is considered that it is applied on the recovery variable.

The excitable behaviour of the FitzHugh–Nagumo model changes depending on the separation of time scales of the variables. This can be seen in figure 3.5. This figure shows the dynamics of the FitzHugh–Nagumo model for low separation in the time-scales of both variables (signalled by a large value of ϵ). For very small values of the noise intensity, the dynamics is basically oscillatory around the stable fixed point –remember that in this case the eigenvalues of the Jacobian matrix are complex–. For larger noise intensities, it is observed that there are firings whose amplitude varies considerably. Furthermore, as it is apparent in the time-evolution of the x variable –second row of panel (a)–, for some noise intensities, there are subthreshold oscillations before a large excursion: this fact is related to the existence of *canard orbits* [71].

A very different kind of dynamics appears when the value of ϵ is much smaller (see figure 3.6). In this case, the dynamics occurs mostly on the

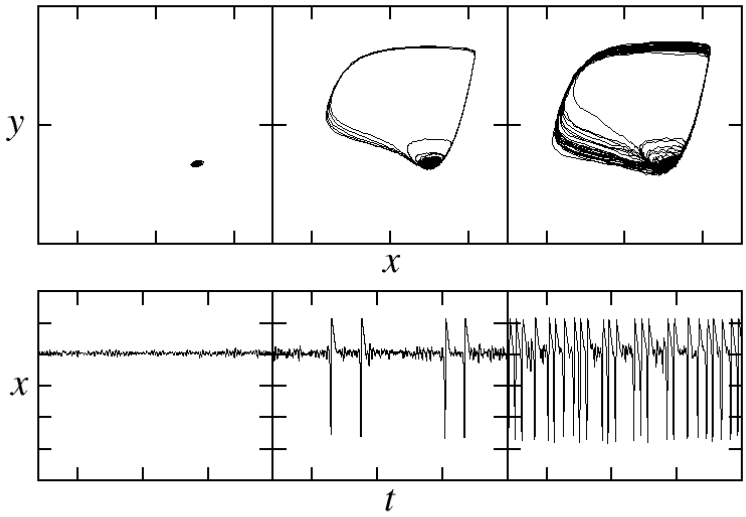

Figure 3.5: We depict the dynamics of the FitzHugh–Nagumo model for $a = 1.1$, and $\epsilon = 10^{-1}$. In the first row, we plot trajectories of the in the phase space; while in the second row, the corresponding time evolution of the x variable is represented. The intensity of noise varies in the panels (a) $D = 10^{-2}$, (b) $D = 4 \times 10^{-2}$ and (c) $D = 0.5$.

$x-$nullcline. Even for larger noise intensities, the motion remains confined to coordinates close to that *locus*. This implies that a phase oscillator, or a phase representation of this system is a very good approximation in that limit. Since the limit cycle is centred around the origin, one can simply consider the phase representation $\phi = \arctan(y/x)$. In can be demonstrated [72, 42], that a system whose dynamics is governed by

$$\dot{\phi} = -\frac{dV(\phi)}{d\phi} + \omega + \sqrt{D}\xi(t), \tag{3.20}$$

where

$$V(\phi) = \frac{\Delta}{\lambda} \mathrm{e}^{\lambda(\cos(\phi)-1)}, \tag{3.21}$$

can exhibit dynamics akin to that of a FitzHugh–Nagumo model.

In [73], it was shown that this system displays the phenomenon of stochastic resonance. However, the mechanism underlying the phenomenon is different to that of the bistable system shown in 2.2.2. In bistable systems, there is a matching between the Kramers' time and the signal period. In the FitzHugh–Nagumo case, the signal lowers the excitability threshold, and intermediate noise intensities are able to perturb the system just beyond the

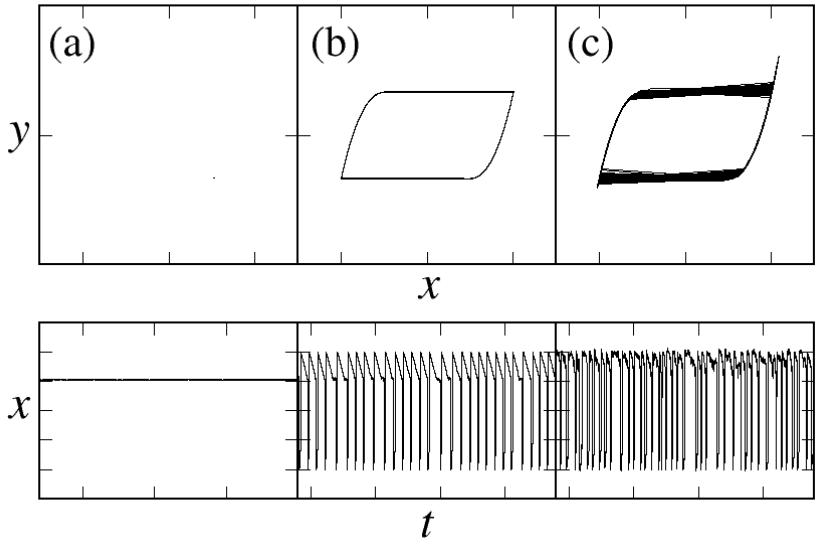

Figure 3.6: We depict the dynamics of the FitzHugh–Nagumo model for $a = 1.1$, and for $\epsilon = 10^{-4}$. In the first row, we plot trajectories of the in the phase space; while in the second row corresponds to the time evolution of the x variable. From left to right, the strength of the noise is: $D = 10^{-2}, 2 \times 10^{-2}, 0.5$. It can be seen that for smaller values of the time-scale separation ϵ, the dynamics approach very fast the nullclines of the x variable.

linear response, and then a firing is produced. Furthermore, the system will be able to respond to a periodic modulation if its period is larger than the excitable system's refractory time. Thus, for these systems, the dependence of the response with frequency is highly non-trivial. For large noise intensities, the dynamics is ruled by the stochastic terms, and the phenomenon disappears. On the other hand, a very small noise intensity makes the system respond linearly to it, and the system remains near the fixed point. It is of no surprise that signals with periodicities lower than the refractory time are not amplified –at least not in a trivial way–.

3.4 Coherence Resonance

In 1997, in reference [74], it was unveiled for the first time the phenomenon of *coherence resonance*. It is related to that of stochastic resonance in the sense that noise plays also a constructive role in the dynamics of the system. Its typical footprint is that the regularity of the firings in an excitable system is maximum for intermediate noise intensities. If the noise is too large or

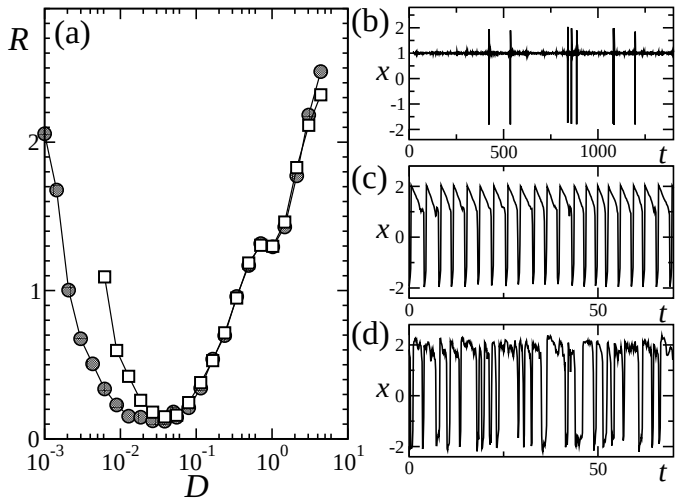

Figure 3.7: We show the basic footprints of the coherence resonance phenomenon in the FitzHugh–Nagumo model. The large panel (a) shows the Jitter as a function of noise intensity. Each curve corresponds to different values of the bifurcation parameter a: The circles correspond to $a = 1$, exactly in the bifurcation point and the squares to $a = 1.02$. A clear minimum for intermediate noise intensities, signalling a more regular spiking can be observed. The same can be seen in panels (b), (c) and (d), that show the time-evolution of the x variable for different noise intensities: $D = 10^{-3}$, 5×10^{-2} and $D = 1$, respectively. In all the panels, we fixed $\epsilon = 10^{-2}$.

too small, this regularity is lost.

A typical measure for this phenomenon is that of the jitter, R. Let $t_1, t_2, \ldots, t_N$ be the times between consecutive firings. The jitter is computed as

$$R = \frac{\sqrt{\langle (t_i - \langle t_i \rangle)^2 \rangle}}{\langle t_i \rangle}, \tag{3.22}$$

where $\langle t_i \rangle$ is the mean time between spikes and $\langle (t_i - \langle t_i \rangle)^2 \rangle$ is the second moment of the interspike distribution. In case of a perfectly periodic state, the jitter vanishes, increasing as the spiking become more irregular events.

We consider a single FitzHugh–Nagumo unit under the effect of noise, described by equation (3.11). If one plots the jitter as a function of noise intensity D (see panel (a) in figure 3.7), it is observed that a minimum of this measure appears for intermediate noise intensities. This indicates that the regularity of the pulses has an maximum value for some optimum value of noise strength. This is also shown in panels (b)-(d) of figure 3.7, where for the optimum noise intensity the spikes are almost periodic.

3.4.1 Mechanism of the phenomenon.

The mechanism behind coherence resonance can be understood via a simple qualitative argument.

The interspike time interval has two main contributions, $t^{(a)}$ (the activation time) and $t^{(e)}$ (the excursion time). The former is the time needed for the system to escape from the fixed point. The latter, corresponds to the interval the system spends in the excursion.

The distribution of these times is rather different: on one hand the activation time follows basically a Poissonian distribution that strongly depends on the noise intensity. On the other hand, the excursion time displays a much weaker dependence on the noise intensity as the dynamics during the excursion is almost independent on the perturbations.

Assuming that both times are independent, we can split the computation of the jitter in the two contributions [75], and then

$$R^2 = \frac{\langle (t_i - \langle t_i \rangle)^2 \rangle}{\langle t_i \rangle^2} \approx \frac{\langle (t_i^{(a)} - \langle t_i^{(a)} \rangle)^2 \rangle \langle t_i^{(a)} \rangle^2}{\langle t_i^{(a)} \rangle^2 \langle t_i \rangle^2} + \frac{\langle (t_i^{(e)} - \langle t_i^{(e)} \rangle)^2 \rangle \langle t_i^{(e)} \rangle^2}{\langle t_i^{(e)} \rangle^2 \langle t_i \rangle^2}. \tag{3.23}$$

By defining the corresponding jitters R_a and R_e of the activation and excursion times respectively, we can rewrite equation (3.23) as

$$R^2 = R_a^2 \left(\frac{\langle t_i^{(a)} \rangle}{\langle t_i \rangle} \right)^2 + R_e^2 \left(\frac{\langle t_i^{(e)} \rangle}{\langle t_i \rangle} \right)^2 \tag{3.24}$$

If we assume a Poissonian process for the times $t^{(a)}$, $R_a^2 = 1$ and the constribution of the first term will be the given by the ratio of the activation time to the interspike interval. For increasing noise intensity this term rapidly decreases from one to zero. The second term, on the other hand, increases with noise mainly due to the increase of $\langle t_i^{(e)} \rangle / \langle t_i \rangle$. Then, the squared value of the jitter has a minimum as a function of noise intensity.

This prediction can be confirmed by inspection of figure 3.7, where a clear minimum in the jitter is observed for intermediate noise strengths. The dynamical trajectories, also, exhibit a more periodic behaviour (see panel (c) in the same figure).

Another measure used for the coherence resonance phenomenon is the self-correlation function of the dynamical variables, that maximises for the most regular (i.e. periodic) dynamics.

Chapter 4

Synchronisation of dynamical systems

In this chapter, we will briefly introduce the concept of synchronisation of interacting dynamical systems. This subject has become a major field of research in the last years, and then we do not intend to give a detailed explanation of the many interesting phenomena related to it. We will summarise the results that are relevant for our results, in the following sections. The interested reader is invited to read one of the introductory books on the subject [76, 77].

Laxly defined, synchronisation refers to the adjustment of rhythms in coupled oscillators. However, synchronisation phenomena appears not only when the coupling strength is the only relevant term in the dynamics of the system. Synchronised units might exhibit a rich coherent behaviour.

We, in the following section, will make a brief historical introduction to the synchronisation phenomenon. Next, in section 4.2, we will define some concepts involved in the description of the synchronisation phenomenon. In the last section, we describe the Kuramoto framework for synchronisation, that will be useful if the forthcoming chapters. We will present the theoretical treatment of this model under the effect of noise and diversity, and we will briefly discuss the similarities between them.

4.1 Historical notes

The first description and understanding of a synchronisation phenomenon, was presented in the XVIIth century, by Christiaan Huygens. He observed that two pendulum clocks, after some period of time, would oscillate with the same pace. Furthermore, they did it in an anti-phase fashion: whenever one pendulum reached the leftmost position, the other one was in the rightmost position. Interestingly, this phenomenon would happen regardless the clocks being non-identical: separately, they would delay or advance the time in

different ways. He discovered that such a behaviour would only happen if the pendula were hung from hooks hanging from in the same wooden beam. Huygens, for the first time, discovered that the subtle interaction through the wooden beam would give raise to a collective, *synchronised* behaviour.

One of the most interesting examples of synchronisation is that of the flashing fireflies in Malaysia: Large amount of male fireflies –placed for hundreds of meters– flash synchronously at dusk. This fact was known since the beginning of the XXth century, although no satisfactory explanation of the phenomenon was given until the 1960's. When isolated, each firefly flashes at a pace that is different between individuals. But only when they are in visual contact, they pulse synchronously.

The understanding on how a synchronised behaviour can emerge in coupled dynamical systems was not obtained until the pioneer works by A.T. Winfree [78, 79] and Y. Kuramoto [55, 7] and the conditions under which coupled systems finally synchronise was identified by R. Mirollo and S.H. Strogatz [59]. Furthermore, it was found that even chaotic systems can synchronise [80]. In many cases, studying synchronisation in continuous-time dynamical systems is intractable from an analytical point of view; thus, as simplified models, the understanding of synchronisation in maps [81, 82] is of particular relevance.

The first person to propose a tractable mechanism showing synchronisation was A.T. Winfree [78], who recognised that in some cases the dynamics of the system would relax fast to a limit cycle, and then it could be reduced to a simple description. He also noticed that the interplay between coupling and diversity among the units could cause a collective synchronised behaviour.

In the last decades, the interest on this phenomenon increased continuously. Its pervasiveness in a broad range of dynamical systems makes it relevant for different disciplines. In Biology, for example, neurons -which strongly interact with many others- fire synchronously under certain conditions, for example during an epileptic seizure. Also the cardiac tissue shows a synchronised firing of thousands of nerve cells during a beat. In Astronomy, it is common the synchronisation of translation and rotation periods (this phenomenon is persistent in many planets). In Electronics, chaotic synchronisation is used for securing transmitions, and a long etcetera.

4.2 Definitions

An oscillatory dynamical system is one whose trajectory in the phase space approaches a limit cycle. It means that, basically independently of the initial condition, the time evolution of the system in the phase space tends to some definite closed trajectories. Also, if the system is perturbed by some means, it relaxes very fast to this limit cycle. In these situations, the dynamics of

the system can be assimilated by the motion in the limit cycle. Thus, the motion can be considered isomorph to a motion in a circle.

Oscillatory systems must be autonomous: the oscillations do not fade out (due, for example, to friction forces). Instead, there is some source that keeps the oscillatory behaviour. This kind of dynamical systems, thus, have an *intrinsic rhythm*: the recurrence time for the unit to return back to the original point.

The generalised concept of *phase* is that of a coordinate defined to represent in which position of the system in limit cycle. Then, two units will have the same phase if located in the same position of the limit cycle, regardless the amount of complete cycles they have performed.

Synchronisation is a phenomenon that occurs in interacting dynamical systems. It happens when the units adjust their rhythms, even if they are different when uncoupled. This does not necessarily imply that as result of the interaction the rhythms should become equal (which is a particular case of synchronisation), but only that some trivial relation appears among them. It is important to remark that if the coupling strength does not not allow the interacting units to be considered as independent (for example the units are rigidly binded), this should not be considered as synchronisation.

In this thesis, we will use the term *entrained* to describe a situation in which the interacting units are located at the same point, but their dynamics is trivial. For example, a situation in which interacting units stay confined in a fixed point of the dynamics, is an entrained state.

Abusing a little bit of language, it is possible to talk about *synchronisation by an external force*, if a system behaves in a synchronous way with the external force. Then, one can describe the stochastic resonance phenomenon as a region in which the system is synchronised with the external stimulus. The synchronisation in this case is, however, not perfect.

4.3 Kuramoto Model

4.3.1 Description

As stated in section 1.3, the simplest model that can describe an oscillatory behaviour is a dynamical system defined in a circle. The model originally proposed by Kuramoto [55, 83, 84] to study coupled oscillators was one such that a single unit would oscillate with a constant angular velocity ω_i. The units are coupled through a function $\Gamma(\phi)$ which is a $2\pi-$periodic function on the phase difference, i.e.

$$\dot{\phi}_i = \omega_i + \sum_{j=1}^{N} \Gamma(\phi_j - \phi_i) + \sqrt{D}\xi_i(t). \tag{4.1}$$

It is usual to take simply $\Gamma(\phi) \propto \sin(\phi)$. In this case, and for small phase difference, it behaves like a linear interaction.

If an oscillator has a set Υ_i of N_i neighbors, it is common to normalise the coupling, in order to ensure well defined behaviour in the thermodynamic limit. The dynamics is given by

$$\dot{\phi}_i = \omega_i + \frac{C}{N_i} \sum_{j \in \Upsilon_i} \sin(\phi_j - \phi_i) + \sqrt{D}\xi_i(t). \tag{4.2}$$

In this expression the values of the frequencies ω_i are distributed according to a probability distribution function $g(\omega)$, whose first two moments are $\langle \omega \rangle = \Omega$ and $\langle (\omega - \Omega)^2 \rangle = \sigma^2$. The $\xi_i(t)$ is a Gaussian white noise, of zero mean and $\langle \xi(t)\xi'(t) \rangle = \delta(t - t')$.

The parameter C determines the coupling strength. In the particular case of mean-field coupling, in which every unit is coupled with all the others, we get

$$\dot{\phi}_i = \omega_i + \frac{C}{N} \sum_{j=1}^{N} \sin(\phi_j - \phi_i) + \sqrt{D}\xi_i(t), \tag{4.3}$$

We can think of the system as particles moving around a circle of radius one in the complex plane. Then, to study its collective behaviour, it is useful to compute the complex *time-dependent Kuramoto order parameter*,

$$\rho(t)\, \mathrm{e}^{\imath \Psi(t)} = \frac{1}{N} \sum_{i=1}^{N} \mathrm{e}^{\imath \phi_i}. \tag{4.4}$$

This parameter is the position of the centre of mass of all the units. Its modulus, $\rho(t)$, is the distance between the origin of the complex plane and the position of the baricenter. If all the units have the same phase, then $\rho = 1$ and this is –in the Kuramoto framework– considered to be a fully synchronised state. On the other hand, if the units are uniformly distributed around the circle, $\rho = 0$ which indicates an incoherent state. Between these two extreme cases, some degree of synchronisation is present in the system. It is usual to define $\rho \equiv \langle \rho(t) \rangle$ as the *Kuramoto order parameter*, as it determines a phase transition between synchronised and desynchronised states.

The argument of the complex Kuramoto order parameter, $\Psi(t)$, the angular position of the centre of mass, is usually called *global phase*.

We can rewrite the definition (4.4), as the set of equations

$$\rho(t)\cos(\Psi(t)) = \frac{1}{N} \sum_{i=1}^{N} \cos(\phi_i) \qquad \rho(t)\sin(\Psi(t)) = \frac{1}{N} \sum_{i=1}^{N} \sin(\phi_i). \tag{4.5}$$

The interaction term in equation (4.3) can be rewritten as

$$\begin{aligned} \frac{1}{N}\sum_{i=1}^{N}\sin(\phi_i-\phi_j) &= \frac{1}{N}\sum_{i=1}^{N}[\sin(\phi_i)\cos(\phi_j)-\cos(\phi_i)\sin(\phi_j)] \\ &= \rho(t)\cos(\Psi(t))\sin(\phi_j)-\rho(t)\sin(\Psi(t))\sin(\phi_j). \end{aligned} \tag{4.6}$$

It is then possible to express conveniently the dynamics of the individual units (in equation (4.3)) in terms of the global order parameter (or conversely, it can be understood as interaction with the mean-field),

$$\dot{\phi}_i = \omega_i + C\,\rho\,\sin(\Psi-\phi_i) + \sqrt{D}\xi_i(t). \tag{4.7}$$

This formulation allows to perform analytical calculations, and write efficient computer codes to perform numerical simulations of models with this kind of coupling.

It is worth noting that for the Kuramoto model, and without loss of generality, it is possible to change the coordinate system to a rotating frame moving with velocity Ω: i.e., $\phi - \Omega\,t \to \phi$, $\langle\omega\rangle = 0$. This does not alter the results, and simplifies the calculations. In this coordinate system, the value of the global phase is irrelevant, and we can set it to $\Psi = 0$.

4.3.2 Synchronisation transition of diverse units

In the deterministic case, in which the noise intensity is $D = 0$, the expression (4.7) admits to be written in potential form, $\dot{\phi}_i = -\partial V_i/\partial\phi_i$ with

$$V_i(\phi) = -\omega_i\phi + C\,\rho\,\cos(\Psi-\phi). \tag{4.8}$$

Depending on the frequency ω_i, there will be two possible behaviours for the oscillators. On one hand, if $\omega_i \leq |C\,\rho|$, there is a stable fixed point, located at

$$\phi_i^* = \arcsin\left(\frac{\omega_i}{C\,\rho}\right), \tag{4.9}$$

such that the unit will get *locked*. On the other hand, if $\omega_i > |C\,\rho|$, there will be no fixed points for the unit, and it will *drift* apart.

Kuramoto assumption was that the drifting oscillators do not contribute to the final value of ρ as they are supposed to be equally distributed in the circle. The locked oscillators are assumed to have a stationary distribution $p(\phi)$. In such situation, it must be given by

$$p(\phi) = \frac{\mathcal{N}}{\dot{\phi}} = \frac{\mathcal{N}}{|\omega_i - C\,\rho\,\sin(\phi_i)|}. \tag{4.10}$$

Here, $\mathcal{N}$ is a normalising constant, such that $\int_{-\pi}^{\pi} d\phi\, p(\phi) = 1$, which yields

$$\mathcal{N} = \frac{1}{2\pi}\sqrt{\omega^2 - (C\,\rho)^2}. \tag{4.11}$$

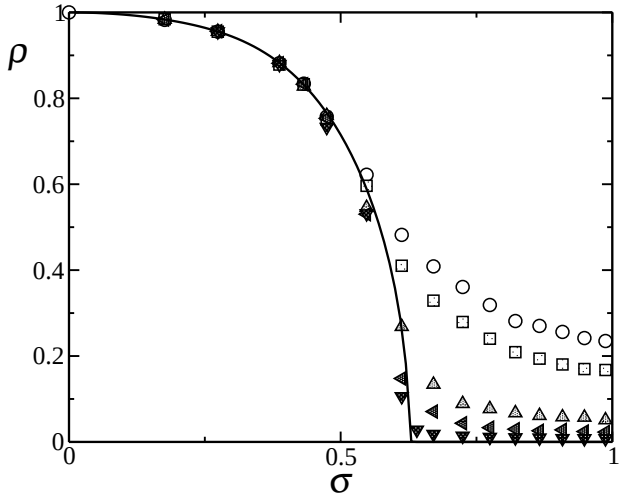

Figure 4.1: In this plot we show the original result by Kuramoto (see equation (4.15)) for the degree of synchronisation of a globally coupled set of oscillators. The distribution of natural frequencies, $g(\omega)$ is a Gaussian distribution, of $\langle\omega_i\rangle$, $\langle\omega_i^2\rangle = \sigma^2$. The different symbols represent different system sizes: $N = 50, 100, 500, 5\times10^3, 5\times10^4$, from top to bottom in the right end of the panel. The solid line represents the theoretical prediction (see text for details).

The order parameter can be computed by

$$\rho e^{\imath\Psi} = \langle\cos(\phi)\rangle + \imath\langle\sin(\phi)\rangle. \tag{4.12}$$

If the distribution $g(\omega)$ is an even function, in the thermodynamic limit, the distribution $p(\phi)$ is symmetric around zero, and then, the term $\langle\sin(\phi)\rangle$, vanishes. The expression for the contribution of the locked oscillators to the global variable is

$$\rho e^{\imath\Psi} = \int_{-C\rho}^{C\rho} d\omega\ \cos(\phi(\omega))g(\omega). \tag{4.13}$$

Where $\phi(\omega) = \arcsin(\omega/C\rho)$. By performing a change of variables -and recalling that the global phase was set to zero-, we can rewrite the former expression as

$$\rho = C\rho\int_{-\pi/2}^{\pi/2} d\phi\ \cos^2(\phi)\ g(C\rho\cos^2\phi). \tag{4.14}$$

This self-consistent relation allows us to identify that the incoherent solution (all the oscillators uniformly distributed in the circle) is always a trivial solution of this equation. So, the state $\rho = 0$ is always present.

The other solution is simply given by the integral relation

$$1 = C \int_{-\pi/2}^{\pi/2} d\phi \, \cos^2(\phi) \; g(C\rho \sin(\phi)). \tag{4.15}$$

The limit $\rho \to 0^+$, shows that this equation bifurcates continuously for $g(0) < g^*(0)$, at a point

$$g^*(0) = \frac{2}{\pi C}. \tag{4.16}$$

This is the result that Kuramoto proved in his first paper on this subject. It can be shown [83] that the bifurcation is supercritical (subcritical) if $g''(0) < 0$ (respectively, $g''(0) > 0$).

For example, if $g(\phi)$ is a Gaussian distribution with standard deviation σ, $g^*(0) = 1/\sigma^*\sqrt{2\pi}$. In figure 4.1, we show the transition to desynchronisation of a globally coupled Kuramoto model. It can be clearly seen a second order phase transition for the order parameter ρ.

This result implies that diversity σ is a factor that worsens the collective behaviour of the system: above a given critical value, the degree of synchronisation is $\mathcal{O}(N^{-1/2})$. A very good agreement between theory and numerical simulations is seen in this figure.

4.3.3 Kuramoto model under the effect of noise

We now consider a set of globally coupled phase rotators, under the effect of noise, i.e. their dynamical evolution is given by

$$\dot{\phi}_i = \omega + \frac{C}{N} \sum_{j=1}^{N} \sin(\phi_j - \phi_i) + \sqrt{D}\xi(t). \tag{4.17}$$

Qualitatively, the effect of noise has some resemblances with that of diversity, i.e. above a critical value the degree of synchronisation vanishes. However, in this case, the route to synchronisation is quite different.

As we are not considering diversity in the natural frequencies, the Kuramoto order parameter can be computed as

$$\rho e^{\imath\Psi} = \int_0^{2\pi} d\phi \, P(\phi, t) \, e^{\imath\phi}, \tag{4.18}$$

where $P(\Psi, t)$ is the probability distribution function obtained by solving the associated Fokker–Planck equation

$$\frac{\partial P(\phi,t)}{\partial t} = C\rho \frac{\partial}{\partial \phi} \left[\sin(\Psi - \phi) P(\phi, t)\right] + \frac{D}{2} \frac{\partial^2}{\partial \phi^2} P(\phi, t). \tag{4.19}$$

Solving the self-consistency relation given by equations (4.18) and (4.19) is not trivial in general. It is possible, however, to solve them in some limiting cases.

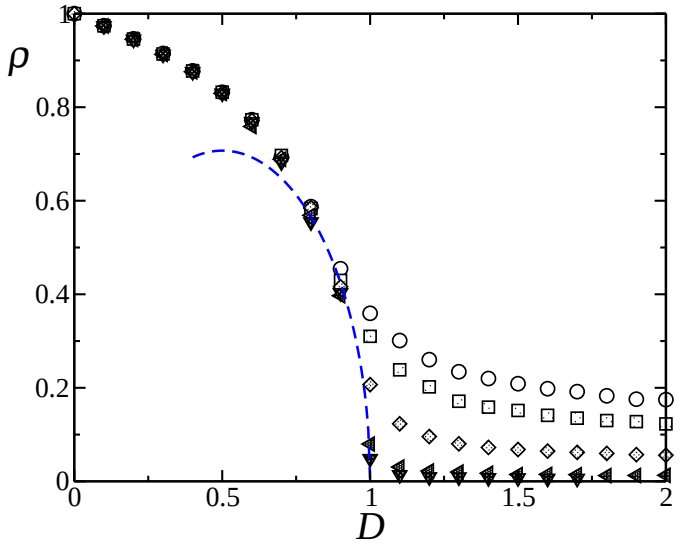

Figure 4.2: We show the results of the Kuramoto order parameter as a function of noise intensity D in a system without diversity. The different symbols represent different system sizes: $N = 50, 100, 10^3, 5\,10^4$, from top to bottom in the right end of the panel. The dotted line correspond to the theoretic computation of ρ, equation (4.24). The coupling strength is set to $C = 1$.

To proceed, we expand $P(\phi, t)$ into a Fourier series

$$P(\phi, t) = \frac{1}{2\pi} \sum_{l \in \mathbb{Z}} P_l(t) \mathrm{e}^{\imath l \phi}. \tag{4.20}$$

From the definition of the Kuramoto order parameter, $P_1 = \rho\, \mathrm{e}^{\imath \Psi}$ and $P_0 = 1$ (due to the normalisation of the probability distribution).

By subsituting equation (4.20) into the expression (4.19), the Fokker–Planck equation reduces to an infinite set of coupled ordinary differential equations,

$$\frac{d\,P_l}{dt} = -\frac{D}{2} l^2 P_l + \frac{lC}{2} \left(P_{l-1} P_l - P_{l+1} P_l^* \right). \tag{4.21}$$

The first three terms read:

$$\begin{aligned} \dot{P}_1 &= \frac{C}{2} \left(P_1 - P_2 P_1^* \right) - \frac{D}{2} P_1 \\ \dot{P}_2 &= C \left(P_1^2 - P_3 P_1^* \right) - 2D P_2 \\ \dot{P}_3 &= \frac{3C}{2} \left(P_2 P_1 - P_4 P_1^* \right) - \frac{9D}{2} P_3. \end{aligned} \tag{4.22}$$

The homogeneous solution (one in which all the rotators are uniformly distributed around the circle), is always a solution of the system. A simple linearisation around this solution, shows that the only mode that can change stability is P_1: In all the others, all the terms are of second order with respect to the displacements from $\rho = 0$. The first order term, P_1, is unstable if $C > D$, and stable otherwise.

By setting $P_3 \approx 0$ and $\dot{P}_2 \approx 0$, we can express the time evolution of the Kuramoto order parameter in the form

$$\frac{d}{dt}\rho e^{\imath\Psi} = \rho e^{\imath\Psi}\left(\frac{C-D}{2} - \frac{C^2}{4D}\rho^2\right). \tag{4.23}$$

This equation in known as the Landau–Stuart, and describes the appearance of a mean field in a population of interacting noisy elements. Its stationary solution can be easily obtained, by equating the term in parenthesis to zero. This treatment, yields for the Kuramoto order parameter the value

$$\rho = \sqrt{C-D}\frac{\sqrt{2D}}{C}. \tag{4.24}$$

This result is valid near the transition to the desynchronised state. The transition point is located at $C = D$. In figure 4.2, it is shown the good agreement near the transition point. Near the transition point, the order parameter grows as the square root of the distance to the bifurcation point, which illustrates the analogy with the mean-field theory of phase transitions.

The results from this section and the previous one show a somehow predictable behaviour of disordering agents: as their influence grows, there is a point above which the synchronised behaviour is lost. It is remarkable, however, that this does not happen continuously, but rather through a genuine phase transition.

Part II

Results: The role of disorder

Chapter 5

Collective firing in excitable media

5.1 Introduction

In coupled excitable systems, macroscopic firing (a significatively large fraction of the units fires simultaneously) excited by noise has been observed in chemical excitable media [85, 86], neuron dynamics [87] and electronic systems [88], and it has been described through several theoretical approaches [89, 90, 91]. This synchronised firing can be considered as a constructive effect induced by the noise. Other examples in which noise actually helps to obtain a more ordered behaviour are stochastic resonance [17], stochastic coherence (or coherence resonance) [74], and noise-induced phase transitions [92].

Diversity, the fact that not all units are identical, is an important ingredient in realistic modelling of coupled systems. Ensembles of coupled oscillators with diversity have been paradigmised [7] and largely studied [83, 5], with the result that synchronised behaviour can appear once the disorder induced by the diversity is overcome by the entraining effect of the coupling. In particular, refs. [93, 84] show an analytical study of the active rotator model in the regime of large frequencies. The results are valid only in the strongly oscillatory regime and they also characterise the transition from full synchronisation to desynchronisation. It has been shown that in a purely deterministic excitable system diversity may induce collective firing [94] if a fraction of the elements are above the oscillatory bifurcation. So, diversity and noise might be expected to play a similar role.

In this work, we develop an analytical understanding for the emergence of collective firing in coupled excitable systems in presence of disorder, either noise or diversity. We show that three different dynamical regimes are possible: sub-threshold motion, where all elements remain confined near the fixed point; coherent pulsations, where a macroscopic fraction fire simulta-

neously; and incoherent pulsations, where units fire in a disordered fashion. Remarkably, the coherent behaviour appears through a genuine phase transition when the noise intensity, the coupling or the diversity cross a critical value. A second phase transition to the disordered (incoherent) phase is recovered for large enough noise intensity or diversity, or small enough coupling. The mechanism for collective firing is the degradation of entrainment which can be originated either by noise or diversity. This is generic and opens a new scenario for experimental observations.

This chapter is organised as follows: in the next section 5.2, we present the model and the relevant order parameters. Then, in section 5.3, we introduce a general theoretical treatment to understand the mechanism behind the emergence of collective firings in this system. In section 5.4 we compare the results of numerical simulations with the theory previously introduced. Then, in section 5.5, we show specialise the theoretical treatment in the case of diverse units. In the final section, the conclusions are drawn.

5.2 Model and order parameters

We consider as a prototypical model an ensemble of globally coupled *active-rotators* $\phi_j(t)$, $j = 1, \ldots, N$, whose dynamics is given by [55]

$$\dot{\phi}_j = \omega_j - \sin\phi_j + \frac{C}{N}\sum_{k=1}^{N}\sin\left(\phi_k - \phi_j\right) + \sqrt{D}\xi_j. \tag{5.1}$$

The natural frequencies ω_j are distributed according to a probability density function $g(\omega_j)$, with mean value ω and variance σ^2. Notice that $\omega_j < 1$ (resp. $\omega_j > 1$) corresponds to an excitable (resp. oscillatory) behaviour of the solitary rotator j. In the oscillatory case, it is worthwhile remember to remember that, in this case, the actual frequency is $\sqrt{\omega^2 - 1}$. Throughout the chapter we consider the case $\omega < 1$. D is the intensity of the Gaussian noises ξ_j of zero mean and correlations $\langle \xi_j(t)\xi_k(t)\rangle = \delta(t - t')\delta_{jk}$, and C is the coupling intensity.

To characterise collective behaviour we use the time-dependent global amplitude, $\rho(t)$, and phase, $\Psi(t)$ [7, 56].

$$\rho(t)e^{i\Psi(t)} = \frac{1}{N}\sum_{k=1}^{N} e^{i\phi_k(t)}. \tag{5.2}$$

The Kuramoto order parameter $\rho \equiv \langle\rho(t)\rangle$, where $\langle\cdot\rangle$ denotes the time average, is known to be a good measure of collective synchronisation in coupled oscillators systems, i.e. $\rho = 1$ when oscillators synchronise $\phi_j(t) = \phi_k(t)$, $\forall j, k$, and $\rho \to 0$ for desynchronised behaviour. Notice, however, that the Kuramoto parameter adopts a non-zero value even when all the variables ϕ_j, being equal to each other, are at rest. In the excitable regime

there are two different dynamical regimes that could give raise to a value $\rho = 1$, a dynamical one in which the units fire pulses synchronously (this situation would correspond to full synchronisation). And a static one, in which all the units rest in the stable fixed point. To discriminate between this static entrainment from the dynamic entrainment of excitable systems when all units fire synchronously, we use the order parameter introduced by Shinomoto and Kuramoto [56]

$$\zeta = \left\langle \left| \rho(t) e^{i\Psi(t)} - \left\langle \rho(t)\, e^{i\Psi(t)} \right\rangle \right| \right\rangle , \tag{5.3}$$

which differs from zero only in the case of synchronous firing. Finally, a measure for the activity of the units, widely used in problems of stochastic transport in non-symmetric potentials is the current

$$J = \frac{1}{N} \sum_{k=1}^{N} \left\langle \dot{\phi}_k(t) \right\rangle . \tag{5.4}$$

A non-zero current J describes a situation in which the systems are firing (not necessarily synchronised).

5.3 Theoretical approach

We now provide an analytical theory to understand the behaviour of ρ, ζ and J as a function of the control parameters, C, D and σ. The theory proceeds in three steps. First, under the assumption of entrainment, we derive a dynamical equation for the global phase Ψ, depending on the value of the Kuramoto parameter ρ. Second, using the solution of that equation, we obtain expressions for ζ and J which depend on ρ. Finally, we calculate self-consistently the value of ρ.

5.3.1 Global phase dynamics

Averaging equation (5.1) over the whole ensemble and using the definition of global amplitude and phase of equation (5.2) we have

$$\frac{1}{N} \sum_{k=1}^{N} \dot{\phi}_j = \omega - \rho(t) \sin \Psi(t) + \sqrt{\frac{D}{N}} \xi(t). \tag{5.5}$$

where $\xi(t)$ is a Gaussian noise of zero mean and correlations $\langle \xi(t)\xi(t') \rangle = \delta(t - t')$. In order to perform an approximation for equation (5.5), we take the time-derivative of equation (5.2), obtaining

$$\frac{d}{dt} \left(\rho\, \mathrm{e}^{\imath\Psi} \right) = \dot{\rho}(t)\, \mathrm{e}^{\imath\Psi(t)} + \imath \dot{\Psi}\, \rho(t) \mathrm{e}^{\imath\Psi}(t) = \frac{\imath}{N} \sum_{k=1}^{N} \dot{\phi}_k \mathrm{e}^{\imath\phi_k}. \tag{5.6}$$

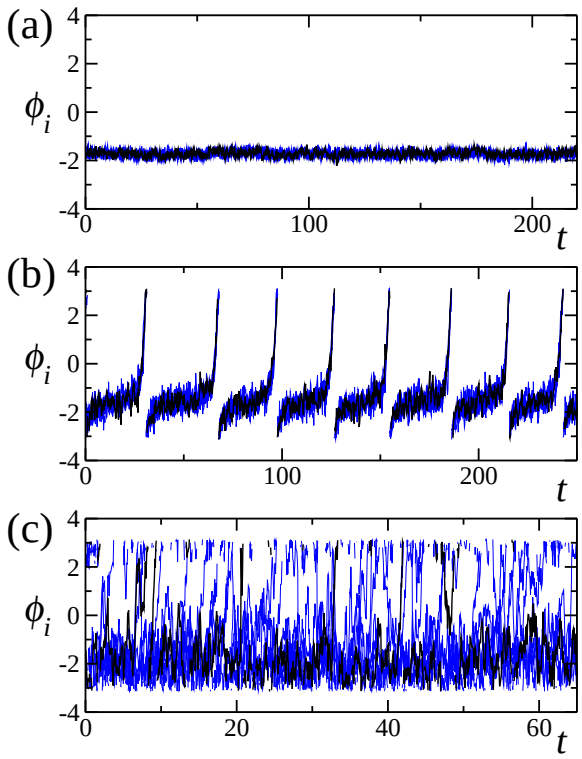

Figure 5.1: Dynamical trajectories for 10 typical units in a system of $N = 400$ with $\omega = 0.98$ and $C = 4$. Each row depicts different noise intensities (and no diversity): $D = 0.1$ (panel a, regime I, no firing), $D = 0.65$ (panel b, regime II, synchronised firing) and $D = 4.0$ (panel c, regime III, desynchronised firing).

If we now rewrite the previous equation in terms of the phase difference with respect to the global phase, i.e. $\phi_j(t) = \Psi(t) + \delta_j(t)$, we can rewrite the last equation as

$$\dot{\rho}(t) + \imath\, \rho(t)\dot{\Psi}(t) = \frac{\imath}{N}\sum_{k=1}^{N} \dot{\phi}_k e^{\imath\delta_k(t)}. \tag{5.7}$$

We consider now that the rotators are *entrained* in the sense that $\delta_j(t) \ll 1$. Under this assumption, we substitute the expansion $e^{i\delta_k} = 1 + i\delta_k + \mathcal{O}(\delta_k^2)$ in the previous expression. Equating real and imaginary parts, we obtain

$$\rho(t)\dot{\Psi}(t) = \frac{1}{N}\sum_{k=1}^{N} \dot{\phi}_k + \mathcal{O}(\delta_k^2). \tag{5.8}$$

The definition of δ_i leads to $\rho(t) = N^{-1}\sum_k e^{i\delta_k}$. Hence $\dot{\rho}(t) = \mathcal{O}(\delta_k^2)$ and, consistently with the order of the approximation, we can replace in equation

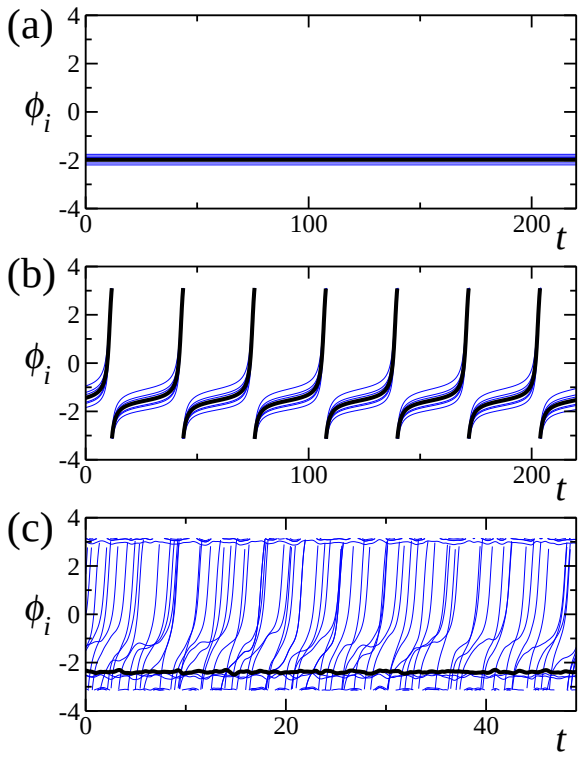

Figure 5.2: Dynamical trajectories for 10 typical units in a system of $N = 400$ with $\omega = 0.95$ and $C = 4$, without noise $D = 0$, and different diversities: $\sigma = 0.63$ (top, regime I, no firing), $\sigma = 1.73$ (middle, regime II, collective firing) and $\sigma = 3.0$ (bottom, regime III, desynchronised firing).

(5.8) the time dependent $\rho(t)$ by the constant value ρ. Therefore, equation (5.5) can be approximated by

$$\rho\dot{\Psi}(t) = \omega - \rho \sin \Psi(t) + \sqrt{\frac{D}{N}}\xi(t), \tag{5.9}$$

which in the limit $N \to \infty$, reduces to

$$\dot{\Psi}(t) = \frac{\omega}{\rho} - \sin \Psi(t). \tag{5.10}$$

It is remarkable that the global phase obeys the same dynamics than the individual units but with a natural frequency scaled with ρ, the Kuramoto parameter measuring the entrainment degree. Therefore, a decrease in the entrainment lowers the collective threshold from $\omega = 1$ to $\omega = \rho$ and the system can start firing synchronously. The effect can be understood as a broadening of the distribution of the phases ϕ, so that a fraction of the rotators crosses over the threshold and, if the coupling is large enough,

they pull a macroscopic fraction of the oscillators. Thus degradation of the entrainment has the paradoxical effect of increasing the coherent firing. It is essential to realize that equation (5.10) depends only on the value of ρ and not in the specific way the degradation of ρ is achieved, so that similar effects can be achieved either increasing the noise, either decreasing the coupling, or increasing the diversity in the natural frequencies; a significantly insightful result not previously understood nor discussed.

5.3.2 Computation of the order parameters

We now turn our attention to the computation of the probability distribution $P(\Psi, \rho)$. As shown previously, ρ is approximately constant for small δ_i, and then the probability density associated to the macroscopic equation (5.9), is

$$P(\Psi; \rho, \omega) = Z^{-1} e^{-2N\,U(\Psi;\rho,\omega)/D} \int_0^{2\pi} d\Psi'\, e^{2\,NU(\Psi'+\Psi;\rho,\omega)/D}, \tag{5.11}$$

with Z is a normalising constant. The associated potential is given by

$$U(\Psi; \rho, \omega) = -\frac{\omega}{\rho}\Psi - \cos(\Psi), \tag{5.12}$$

In the thermodynamic limit, the expression in equation (5.9) reduces to eq. (5.10), the distribution function gets simplified, and then it is given by

$$P(\Psi; \rho) = \begin{cases} \frac{1}{2\pi}\sqrt{\omega^2 - \rho^2}/(\omega - \rho \sin\Psi) & \text{for } \rho < \omega \\ \delta(\Psi - \arcsin(\omega/\rho)) & \text{for } \rho \geq \omega \end{cases}.$$

Another interesting result of our approach, is that it allows us to express ζ and J as a function of the Kuramoto order parameter ρ. Without loss of generality, we can arbitrarily take as initial condition $\Psi(t=0) = -\pi/2$, irrelevant when taking the time average. In the case $\rho < \omega$, the solution of equation (5.10) is given by

$$\omega - \rho \sin\Psi(t) = \frac{\omega^2 - \rho^2}{\omega - \rho\cos\Omega t}, \tag{5.13}$$

where $\Omega = \sqrt{(\omega/\rho)^2 - 1}$ is the frequency of the global phase oscillations. The current is obtained from eq. (5.5), $J = \omega - \langle \rho \sin(\Psi)\rangle$. Time averages are computed over a period $T = 2\pi/\Omega$ using eq. (5.13),

$$J = \frac{\omega^2 - \rho^2}{T} \int_0^T \frac{dt}{\omega - \rho\cos\Omega t} = \sqrt{\omega^2 - \rho^2}. \tag{5.14}$$

For $\rho > \omega$, $J = 0$.

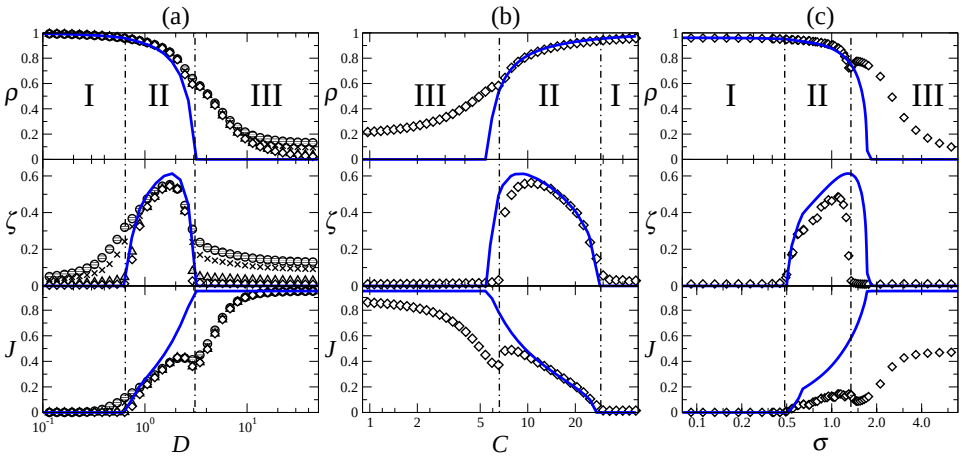

Figure 5.3: Symbols represent ρ, ζ and J as obtained numerically from eqs. (5.1). Solid lines are the theoretical results. Panel (a) shows the variation with respect to the noise intensity D in absence of diversity, $\sigma = 0$, for a natural frequency $\omega = 0.95$, coupling strength $C = 4$, and different system sizes: $N = 50$ ($\circ$), $N = 10^2$ ($\times$), $N = 10^3$ ($\triangle$), $N = 10^4$ ($\diamond$). Panel (b) displays the same results as a function of C for $D = 1.0$. Panel (c) shows the variation with respect to diversity σ for $D = 0.3$, $C = 4$ and $g(\omega_j)$ being a uniform distribution. In all cases there are three regimes: (I) no firing, (II) synchronised firing and (III) desynchronised firing.

Approximating again $\rho(t)$ by a constant value, the Shinomoto–Kuramoto parameter $\zeta \cong \rho \left\langle \left| e^{\mathrm{i}\Psi(t)} - \left\langle e^{\mathrm{i}\Psi(t)} \right\rangle \right| \right\rangle$ can be computed for $\rho < \omega$ performing the time averages over a period T using eq. (5.13):

$$\zeta = \frac{2}{\pi} \sqrt{2(\omega - \sqrt{\omega^2 - \rho^2})(\omega + \rho)} K\left(\frac{2\rho}{\rho - \omega}\right), \tag{5.15}$$

where $K(m)$ is the complete elliptic integral of the first kind [95]. If $\rho > \omega$ we get $\zeta = 0$.

As a final step, we derive a equation for ρ using a self-consistent, Weiss-like, mean field approximation, which assumes constant values for the global magnitudes and then averages over their probability distribution [92, 7]. For our particular case, we start by rewriting equation (5.1) as

$$\dot{\phi}_i(t) = -\frac{dV(\phi_i; \Psi, \rho, \omega_i)}{d\phi_i} + \sqrt{D}\,\xi_i(t), \tag{5.16}$$

where we have defined the *potential*

$$V(\phi; \Psi, \rho, \omega) = -\omega\phi - \cos(\phi) - C\rho\cos(\Psi - \phi). \tag{5.17}$$

Note that the coupling appears only through the global parameters ρ and Ψ. For fixed ρ and Ψ, the stationary probability distribution function reads [10]

$$P_{\mathrm{st}}(\phi;\Psi,\rho,\omega) = Z^{-1} e^{-2V(\phi)/D} \int_0^{2\pi} d\phi'\, e^{2V(\phi'+\phi)/D}, \tag{5.18}$$

where Z is a normalising constant. From its definition, we have

$$\rho = \frac{1}{N}\sum_{k=1}^{N} \langle \cos(\phi_k - \Psi)\rangle\,, \tag{5.19}$$

and we obtain

$$\rho = \int d\omega g(\omega) \int_0^{2\pi} d\Psi P(\Psi;\rho) \int_0^{2\pi} d\phi P_{\mathrm{st}}(\phi;\Psi,\rho,\omega)\cos(\phi-\Psi) \tag{5.20}$$

where we have performed a triple average: with respect to the distribution function (5.18), with respect to the distribution $g(\omega)$ of natural frequencies and with respect to the distribution $P(\Psi;\rho)$ of the global phase which is inversely proportional to the instantaneous velocity given by eq. (5.11). The self-consistent equation (5.20) for ρ needs to be solved numerically. In section 5.5, we will show a simplified expression in the case when only diversity is considered.

5.4 Numerical results and discussion

In the following, we discuss the theoretical results and compare them with the numerical results obtained from a numerical integration of equations (5.1). Typical trajectories showing the three dynamical regimes are displayed in figures 5.1 and 5.2 while the corresponding order parameters are plotted in figure 5.3. Figure 5.3(a) shows ρ, ζ and J as function of the noise intensity D in absence of diversity. The solid lines correspond to the theoretical results while symbols show the numerical results for different system sizes. In this figure, we can observe the three aforementioned behaviours: For small noise intensity (regime I) each rotator fluctuates around its fixed point. Although for un-coupled rotators noise would eventually excite some spontaneous random firings, the coupling of a large number of units suppresses these individual firings. The Kuramoto parameter ρ is close to 1 and the deviations from unity are due to the small dispersion induced by noise. Region I is, in fact, characterised by $\rho > \omega$ for which our theory predicts that the Shinomoto–Kuramoto parameter ζ and the current J vanish which physically reflects the nonexistence of collective movement. In this region, the numerical results for ρ, ζ and J are in excellent agreement with the theoretical predictions.

Our theory predicts that a transition to a dynamical state characterised by synchronised firing behaviour (regime II) takes place when $\rho = \omega$, in

very good agreement with the numerical results. This transition is clearly signalled by non-vanishing values of ζ and J. The prediction of ρ is good for a large part of region II (up to values of $\rho = 0.7$). Later it underestimates its value.

For very large noise intensity, the rotators desynchronise while keeping a non-zero current value (regime III). Hence, the synchronised activity, as measured by ζ goes though a maximum as noise amplitude increases. Our theory predicts that the transition between regions II and III occurs for $\rho = 0$ where $\zeta = 0$ and the current takes the maximum possible value $J = \omega$. This limit for the very large disorder, can be understood by inspection of eq. (5.5), for vanishing ρ and taking into account that a time average of the noise, makes this term to vanish. The existence of this transition is somewhat expected: as in this transition an increasing disorder (either noise or diversity or a decreasing coupling strength) causes a loss of entrainment in the units, characterised by the fact that $\zeta = 0$.

Surprisingly, since the small values of ρ in this transition are beyond the assumptions of the theory, the location of the second transition is also well predicted. Moreover, the whole shape of the Shinomoto–Kuramoto parameter ζ is well reproduced over the whole range. The maximum of eq. (5.15) occurs for $\rho \approx 0.821\omega$, which is well confirmed by the numerical results. The theoretically predicted current J fits the numerical values in the same range than ρ. Note, however, the numerical simulations show a local maximum for the current J which indicates a local increasing in the total transport due to the coherent dynamics in the regime II. This local maximum is not present in the theoretical approximation.

Some of these states were already described by Kuramoto and Shinomoto [56]. By looking at the probability distribution of ϕ_i, these authors identify two regions in parameter space: the *time-periodic regime* (P) and the *stationary regime* (S). Region P corresponds to our regime II where the order parameter ζ is different from zero and there is collective motion of the oscillators. Our findings allow us to split region S of these authors in our distinct regions I and III: while region I is a fluctuating regime around the steady state, region III has a high activity as characterised by a non-zero current J. In refs. [89, 90], a semi-analytical approach was used to analyse the existence of these three phases. However, a physical description on why these regimes appear, and the finding of general mechanisms that could trigger the collective behaviour in these systems, was lacking.

These results indicate that noise acts in two antagonistic ways: while a given noise intensity can excite the sub-threshold units, forcing a synchronised firing, large amplitude noise deteriorates the synchronisation properties of the ensemble. This scenario resembles the so called noise induced phase transitions [92] in which a transition to an ordered ferromagnetic-like state is induced by increasing the noise intensity; the order is destroyed again for large enough noise. Here, the transition is towards an organised

collective motion of the active rotators.

The reverse scenario can be observed varying the coupling strength C, see figure 5.3(b). The Kuramoto parameter ρ increases with C (notice, however, the existence of a small bump in the numerical results), indicating that the degree of synchronisation increases with coupling, as expected. A large coupling suppresses noise-induced firings, and the system is macroscopically at rest, regime I, as indicated by the vanishing of ζ and J. For weak coupling the noise induces desynchronised individual firings (regime III) characterised by a macroscopic current J and again a zero value for ζ. For intermediate values of the coupling (regime II) the interplay of noise and coupling leads to the largest degree of synchronised firing with a large value for ζ.

Finally figure 5.3c shows ρ, ζ and J as a function of the diversity σ. It is clear in the figure the existence of the same three regimes that were obtained by varying the noise intensity or the coupling. Altogether figure 5.3 clearly illustrates the fact that similar effects can be achieved increasing the noise, decreasing the coupling or increasing the diversity in the natural frequencies as theoretically predicted.

The full dependence of the order parameters with respect to noise intensity and coupling strength is presented in figure 5.4. In these plots, we show a compariso between the theory presented and the numerical simulations. It is seen a very good agreement between both for the region of large coupling strengths (i.e. $C > 1$).

5.5 Order parameters for diverse units

In the particular case of noiseless units, i.e. where diversity is the only disordering factor, equation (5.1) can be expressed as

$$\dot{\phi}_i = \omega + \eta_i - \sin\phi_i + \frac{C}{N}\sum_{j=1}^{N}\sin\left(\phi_j - \phi_i\right). \tag{5.21}$$

The parameter $\omega_i = \omega + \eta_i$ is the natural frequency of the $j-$th unit. The values of the natural frequencies are drawn from a probability distribution function $g(\eta_i)$, of mean $\langle\eta_i\rangle = 0$ and correlations $\langle\eta_i\eta_j\rangle = \sigma^2\delta_{ij}$. We will stick to the case $\omega < 1$, such that when $\sigma = 0$, all the systems are in the excitable regime and, in the absence of perturbations, they will all stay in perfect order at the stable equilibrium point. This order is degradated by the presence of diversity that makes each unit act differently from the others. We first study how the order decreases with diversity.

We now show how to compute ρ in this particular case. A straightforward algebra leads to dynamical equations for the angles ϕ_i in which the coupling between units appears only through the global variables, ρ, Ψ, as:

$$\dot{\phi}_i = \omega_i - R\sin(\phi_i - \alpha). \tag{5.22}$$

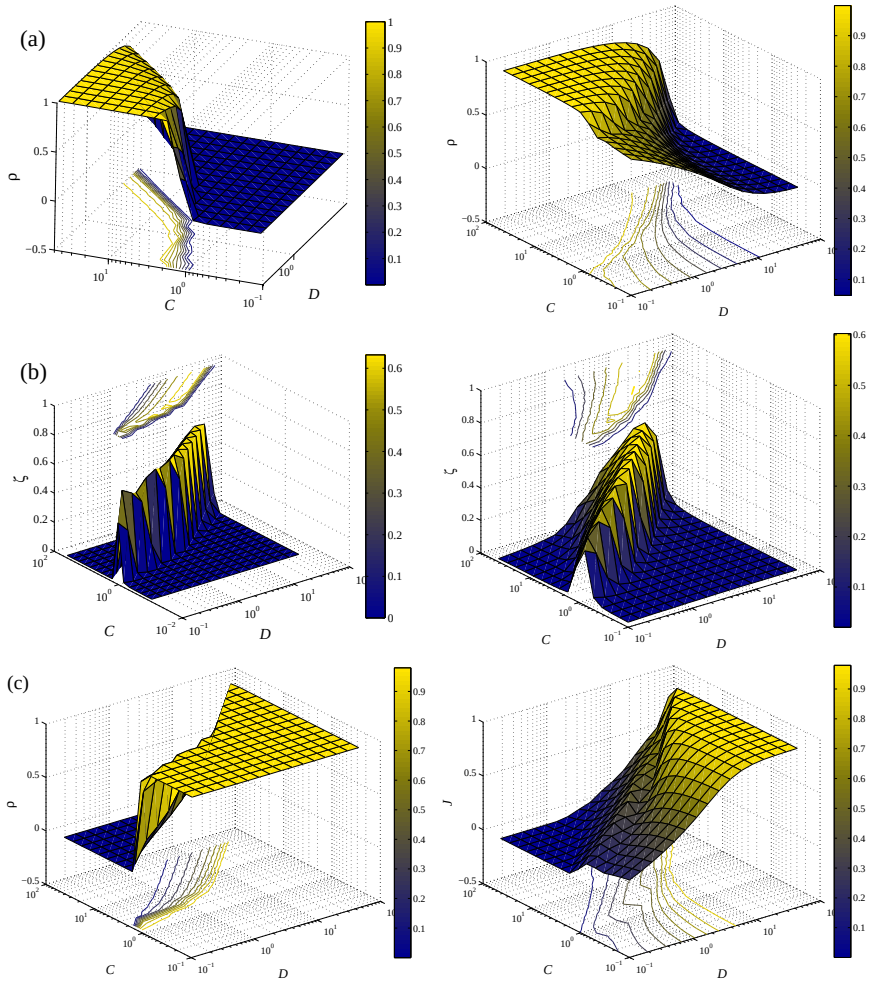

Figure 5.4: Relevant order parameters as a function of noise intensity and coupling strength. The left column shows the results of the simple theory presented in section 5.3.2. The right column, shows the results for direct numerical simulations. A good agreement between both can be observed for intermediate to large couplings. We have fixed the natural frequency to $\omega = 0.98$ and the system size to $N = 10^3$.

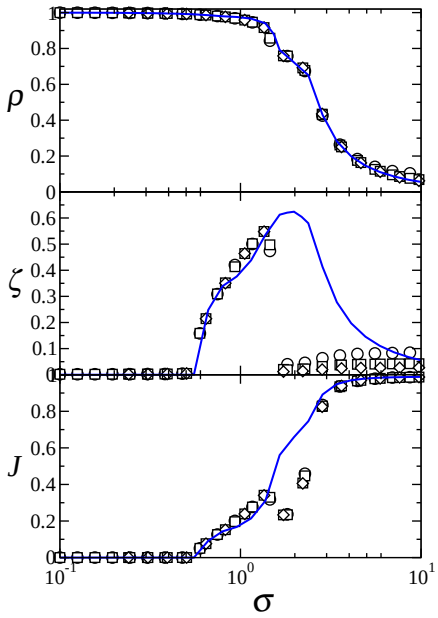

Figure 5.5: Common firing in the active-rotator model in presence of diversity. In panel (a) we show the Kuramoto order parameter ρ as a function of the diversity σ for the active-rotator model with quenched disorder defined in eq. (5.1). The parameters are $\omega = 0.99$, $C = 4$, $N = 100, 400, 10^3$. The values of η_i are taken from a Uniform distribution of zero mean and variance σ^2. The line is the mean-field prediction obtained by solving the self-consistent equation (5.25) and the dots are the results of numerical simulations of the dynamical equations (5.1). Second row, plots the Shinomoto–Kuramoto orderparameter ζ as a function of diversity. A transition to a state in which the units pulse synchronously can be observed by the non-zero value of ζ starting around $\sigma \approx 0.56$. The line is the theoretical prediction and the symbols depict the numerical simulations.

where

$$R = (1 + 2C\rho\cos\Psi + c^2\rho^2)^{1/2} \qquad \text{and,} \qquad \tan\alpha = \frac{c\rho\sin\Psi}{1 + c\rho\cos\Psi}.$$

We now make the approximation of constant values for ρ and Ψ. According to this equation, the rotators split in two categories: (i) those for who the natural frequency satisfies $|\omega_i| < R$ are in the excitable regime and the probability density function of the angle distribution is a delta function centred around the stable angle $f(\phi_i) = \delta(\phi_i - \phi_i*)$ with $\phi_i^* = \arcsin(\omega_i)/R$; (ii) those for which $|\omega_i| > R$ are in the oscillatory regime and the probability distribution is inversely proportional to the angular velocity $f(\phi_i) \propto |\dot{\phi}_i|^{-1}$.

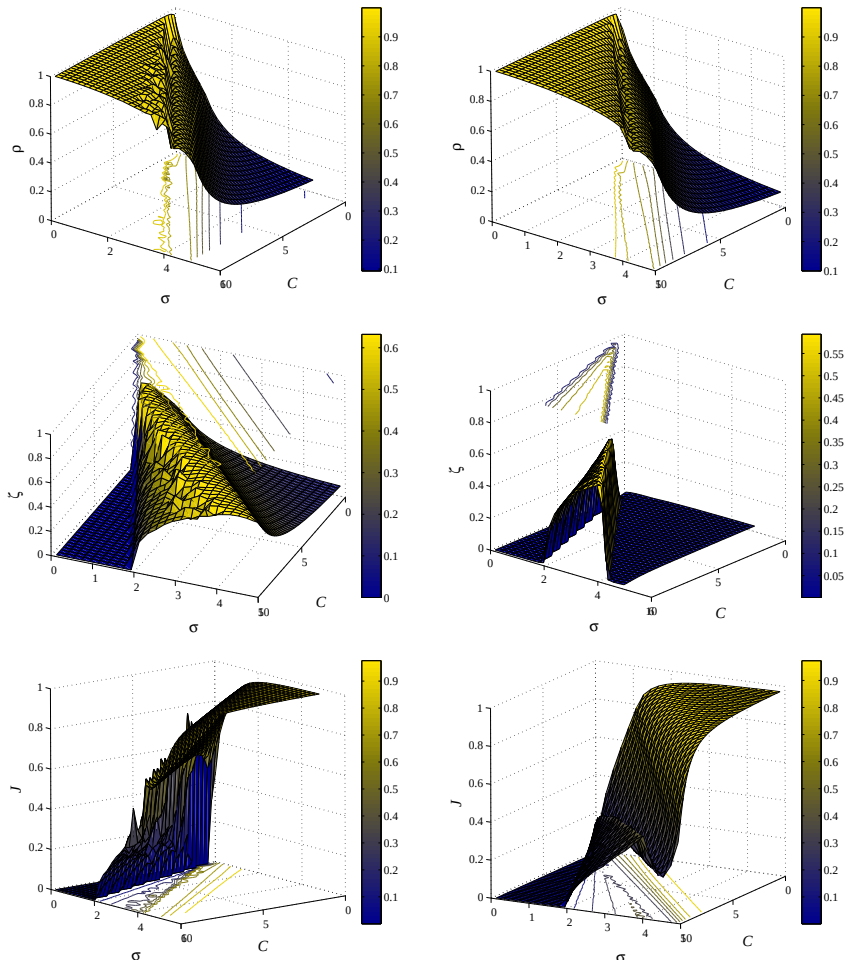

Figure 5.6: Surfaces of the order parameters as a function of diversity, σ, and coupling strength. The plots located in the left column, show the results for the theoretical treatment introduced in section 5.5; the right column, the results for the numerical simulations. The mean natural frequency is $\omega = 0.99$, and for the simulations the system size is $N = 10^3$.

Computing the normalisation constant we have:

$$f(\phi_i) = \begin{cases} \delta(\phi - \phi_i^*) & |\omega_i| < R \\ \frac{\sqrt{\omega_i^2 - R^2}}{2\pi} \frac{1}{\omega_i - R\sin(\phi_i - \alpha)} & \omega_i > R \\ \frac{\sqrt{\omega_i^2 - R^2}}{2\pi} \frac{1}{-\omega_i + R\sin(\phi_i - \alpha)} & \omega_i < -R \end{cases} \tag{5.23}$$

This, in turn, allows to find the average value that appears in the definition of the Kuramoto order parameter as $\langle \mathrm{e}^{i\phi_i} \rangle = F(\eta_i, \rho, \Psi)$, with

$$F(\eta_i, \rho, \Psi) = \mathrm{e}^{\imath\alpha} \times \begin{cases} \sqrt{1 - \frac{\omega_i^2}{R^2}} + \imath \frac{\omega_i}{R} & |\omega_i| < R \\ \imath \left(\frac{\omega_i}{R} - \sqrt{\frac{\omega_i^2}{R^2} - 1} \right) & \omega_i > R \\ \imath \left(\frac{\omega_i}{R} + \sqrt{\frac{\omega_i^2}{R^2} - 1} \right) & \omega_i < -R \end{cases} \tag{5.24}$$

Finally, the order parameter is found by solving the consistency equation (the subindex i is now dropped from the notation):

$$\rho \mathrm{e}^{\imath\Psi} = \left\langle e^{\imath\phi} \right\rangle = \int d\eta \, g(\eta) F(\eta, \rho, \Psi) \tag{5.25}$$

This equation has to be solved numerically. In figure 5.5(a) we plot ρ versus the diversity σ in the case of a Gaussian distribution for $g(\eta)$ and the values $\omega = 0.95$, $C = 1$ together with the results of numerical simulations of the dynamical equations (5.1). It can be seen that the order parameter decreases monotonically as the diversity increases, although there is no sharp phase transition to a state of $\rho = 0$. This second regime, however, is analogous to the one it plays in models such as in Kuramoto studies. Finally, in figure 5.6, we compare the numerical simulations with the theoretical treatment introduced in this section in the $(C - \sigma)-$plane. A good agreement is also observed.

5.6 Conclusions

In summary, we have developed a theory for the emergence of collective firing in a paradigmatic ensemble of sub-threshold excitable units, containing coupling and a source of disorder as generic ingredients. The collective behaviour emerges as a phase transition whose underground mechanism is the degradation of entrainment originated by the competing effects of disorder and coupling. Paradoxically, this degradation results in establishing a lower effective threshold for collective firing, and thus inducing a somehow ordered state. Our theory clearly establishes that it does not matter the specific source of disorder, either noise or diversity will lead to similar results. This mechanism is not restricted to the model we considered, it will

exist in any physical, chemical or biological excitable system with the aforementioned basic generic ingredients. Our results are likely to be relevant also for non-globally coupled systems, such as extended systems with local couplings and complex networks.

In extended systems the macroscopic fraction of units firing collectively are typically localised in a region of the space, leading to the propagation of an excited wave. Waves induced by parametric noise in chemical excitable systems has been reported [85, 86]. It has been argued in [89] that the transition between I and II would be triggered by changes in the excitability of the neurons, if one assumes that noise intensity is a constant. In this chapter we have presented a more plausible scenario by which biological systems can trigger such transition by adjusting the level of diversity among the neurons. We expect that our results will stimulate further experiments on systems with different sources of disorder.

Chapter 6

Synchronisation of coupled FitzHugh–Nagumo systems

6.1 Model studied

In the last years, the phenomenon of synchronisation in coupled limit cycle oscillators has been extensively investigated [7, 76]. However, not such a thorough study has been carried out for excitable systems, despite the fact that many features of the dynamics of biologically relevant systems, for example, neurons, can be described by simple excitable models. For example, it is found that epileptic crises are characterised by a particularly large amount of neurons firing simultaneously [96].

It is the goal of this chapter to delve into some aspects of the synchronisation properties of coupled excitable systems under the presence of noise or diversity. Although we do not have any specific applications in mind, we believe that our results are quite general, since we use a prototypical model of excitable dynamics. It is known that in those systems noise can induce phenomena such as stochastic resonance [30] (under the presence of an external forcing) or coherence resonance [74, 97, 98]. The latter is a mechanism by which an unforced excitable system shows a maximum degree of regularity in the period between emitted pulses in the presence of the right amount of noise. We focus here on the stationary synchronisation properties of the common firings [99], and a more detailed study including the coherence resonance aspects is left for future work. We find that there is a non-equilibrium phase transition between synchronised and desynchronised states. We discuss the proper order parameter to characterise this transition and obtain numerically the phase diagram.

In this chapter, we extend the previous results shown in chapter 5, where we considered the active-rotator model. However, that model provides an example of type I excitability. We now consider the FitzHugh–Nagumo model which provides a prototypical model for studying type II excitability

(see chapter 3 for more details). This model has been also widely used as a model for spiking neurons as well as for cardiac cells [100, 101]. The mathematical model is defined in terms of activation x and inhibition y variables, as follows:

$$\epsilon \dot{x} = x - \frac{1}{3}x^3 - y \tag{6.1}$$

$$\dot{y} = x + a + \sqrt{D}\xi(t) \tag{6.2}$$

where, following reference [74], a Gaussian white noise $\xi(t)$ of zero mean and correlations $\langle \xi(t)\xi(t')\rangle = \delta(t-t')$ has been added to the slow variable y. D will be called the noise intensity. The difference in the time scales of x and y is measured by ϵ, a small number. We work exclusively in the so-called excitable regime, characterised by $|a| > 1$.

There is a single stable fixed point (x_0, y_0) which, in the absence of any external perturbation, $D = 0$, is reached independently of the initial condition. When random perturbations are present, the trajectories eventually exit the basin of attraction of the stable fixed point and return to it after making an excursion in phase space, i.e. a pulse.

The next step is to consider an ensemble of N globally coupled systems:

$$\epsilon \dot{x_i} = x_i - \frac{1}{3}x_i^3 - y_i + \frac{C}{N}\sum_{j=1}^{N}(x_j - x_i) \tag{6.3}$$

$$\dot{y_i} = x_i + a_i + \sqrt{D}\xi_i(t), \qquad i = 1, \ldots, N \tag{6.4}$$

with independent noises, $\langle \xi_i(t)\xi_j(t')\rangle = \delta_{ij}\delta(t-t')$. The systems are globally coupled by a gap-junctional form, as indicated by the last term of equation (6.3), where C is the coupling strength. The values of a_i are drawn from a probability distribution $g(a)$, with mean $\langle a_i \rangle = a$, and standard deviation σ. The results that will be shown in this chapter are robust against changes in ϵ; we will fix its value to $\epsilon = 10^{-2}$.

Numerical simulations of this coupled system of equations[1] show that, for some range of parameter values, the different units fire pulses at the same times. Notice that, although some amount of noise is needed in order to induce firings and hence observe synchronised behaviour, too a large noise finally degrades the quality of the synchronised state. A general framework to study such synchronisation phenomena is given by the work by Kuramoto [7]. He considers coupled phase variables $\phi_i(t)$ following a stochastic dynamics and discusses the existence of a synchronised regime in terms of the coupling strength and the noise intensity. It turns out that the Kuramoto model displays a genuine phase-transition in which synchronisation disappears if the noise surpasses a given critical value. We will show that the same behaviour can be observed in our model.

[1] The numerical integration of eqs. (6.3-6.4) use a stochastic Runge-Kutta method (known as the Heun's method [12]) with a time step $h = 10^{-4}$.

The first step consists in defining phase-like variables ϕ_i for our model. They should satisfy the condition that their variation between 0 and 2π represents the pulse movement starting from the fixed point, travelling through all the cycle, and ending again at the fixed point. Several different approaches have been taken in order to evaluate the phases ϕ_i. The most naive, definition is based upon the fact that the limit cycles in which the variables (x_i, y_i) evolve are approximately centred around the origin. Then, the easiest choice is

$$\phi_i = \arctan\left(\frac{y_i}{x_i}\right). \tag{6.5}$$

However, this choice is only valid for particular cases of the parameters of the FitzHugh–Nagumo model. For large noise intensities, for example, the pulses are not so clearly entered around the origin. A definition of more general validity uses the so-called Hilbert transform [76]. Let us consider the variable $x_i(t)$. From it we can construct the so-called "analytic signal", $s_i(t) = x_i(t) + \imath\, \hat{x}_i(t)$, where $\hat{x}_i(t)$ denotes the Hilbert transform of the function $x_i(t)$. For a general function, $g(t)$, such a transform is defined as

$$\hat{g}(t) = -\frac{1}{\pi}\mathsf{PV}\int_{-\infty}^{\infty}\frac{g(\tau)}{t-\tau}d\tau \tag{6.6}$$

where PV denotes the principal value of the integral. The phase is defined as the argument of $s_i(t)$, i.e.

$$\phi_i(t) = \arctan\left(\frac{\hat{x}_i}{x_i}\right). \tag{6.7}$$

From a computational point of view, it is very costly to perform the convolution involved in the Hilbert transform. We will show now that the same phase can be obtained by a much more efficient procedure. This is based upon the equality

$$g(t) + \imath\hat{g}(t) = 2\mathcal{F}^{-1}\left[\mathcal{F}\left[g(t)\right]\cdot\Theta(\omega)\right] \tag{6.8}$$

involving the Fourier transform operator $\mathcal{F}$. Here $\Theta(\omega)$ is the Heaviside function: $\Theta(\omega) = 0$ for $\theta < 0$, $\Theta(\omega) = 1$ for $\theta \geq 0$ defined in the Fourier space ω.

This relation can be proved by replacing

$$g(t) = \int_{-\infty}^{\infty} g(t_0)\delta(t-t_0)dt_0, \tag{6.9}$$

in the right hand side of equation (6.8):

$$2\quad \mathcal{F}^{-1}\left[\mathcal{F}\left[\int_{-\infty}^{\infty} g(t_0)\delta(t-t_0)dt_0\right]\cdot\Theta(\omega)\right] \tag{6.10}$$

$$
\begin{aligned}
&= 2\int_{-\infty}^{\infty} \mathcal{F}^{-1}\left[\mathcal{F}\left[g(t_0)\delta(t-t_0)\right]\cdot\Theta(\omega)\right] dt_0 \\
&= 2\int_{-\infty}^{\infty} \mathcal{F}^{-1}\left[g(t_0)\delta(t-t_0)\frac{\mathrm{e}^{\imath t_0\omega}}{\sqrt{2\pi}}\cdot\Theta(\omega)\right] dt_0 \\
&= 2\int_{-\infty}^{\infty} \left(\frac{1}{2}g(t_0)\delta(t-t_0) + \frac{\imath}{2\pi}\frac{g(t_0)}{t_0-t}\right) dt_0 \\
&= g(t) + \imath\hat{g}(t)
\end{aligned}
$$

Thus one can achieve the calculation of the Hilbert transform by using two Fourier transforms. This leads to a very efficient numerical algorithm since the use of the fast Fourier transform involves a computer time of order $\mathcal{O}(T\,\log T)$ instead of $\mathcal{O}(T^2)$ which would be the case if one evaluates directly the convolution that defines the Hilbert transform (T is the length of the time series considered).

6.2 Synchronisation properties

We define an order parameter that allows us to measure the degree of synchronisation in the coupled system. In order to follow the Kuramoto scheme, we use the phases ϕ_i introduced before in terms of the Hilbert transform, eq. (6.7). Time-dependent collective amplitude, $\rho(t)$, and phase, $\Psi(t)$, are defined as in section 5.3. Once again, we will compute the order parameter ρ introduced by Kuramoto is defined as the time average $\rho \equiv \langle\rho(t)\rangle_t$.

6.2.1 Effect of noise

First of all, we study the transition to collective pulses in absence of diversity. In figure 6.1(a) we plot ρ as a function of the noise intensity D for different number of coupled systems. It turns out that the order parameter continuously decreases with increasing D, thus showing that the quality of the synchronisation worsens for large noise intensity. The dependence of the order parameter ρ for relatively small system size ($N > 100$) disappears, showing that finite size effects are very small for these systems sizes. Figure 6.1, panel (a), also shows that the Kuramoto order parameter for this coupled FitzHugh–Nagumo model does not decay to zero with increasing noise intensity. This is due to the fact that for an excitable system, most of the time all the units oscillate near the fixed point. Hence, the order parameter ρ is different from zero, even in the case in which all the units are uncoupled and fire unsynchronously. Since we are interested in measuring the deviations from this desynchronised state, we use the Shinomoto–Kuramoto order parameter, ζ, first introduced in reference [56], which only gives non-zero values in the case in which a macroscopic fraction of units fires synchronously (see chapter 5 for a complete discussion).

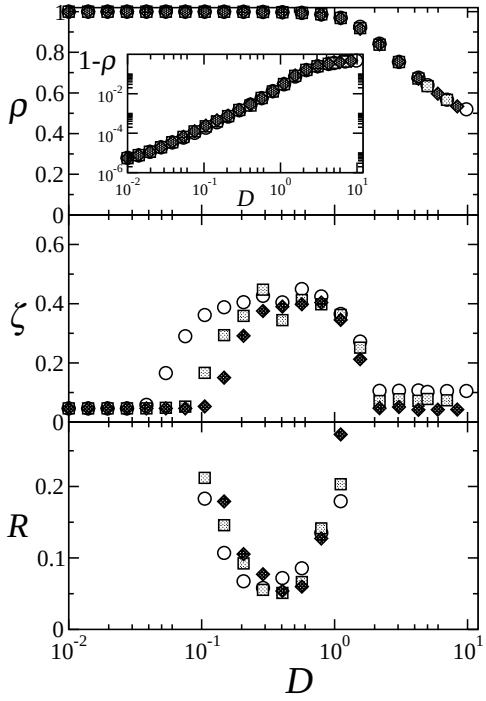

Figure 6.1: In this figure we show the order parameters ρ, ζ and the jitter R, for various system sizes, from $N = 100, 400, 10^3$. The other parameters for the simulations were $a = 1.01$ and $k = 2$. The inset in the first panel shows the increase of the disorder with increasing noise (in the plot, signalled by a decrease in the Kuramoto order parameter).

In figure 6.1, panel (b), we plot the order parameter ζ, for the same values of the parameters as in the previous figure. In this case, we notice the vanishing of the order parameter, indicating clearly the existence of a phase transition at a critical noise value D separating the regime of synchronisation/desynchronisation. Note that the location of this transition could not be easily derived from the data in figure 6.1. In the case of complete desynchronisation, ζ is almost constant except for finite system-size fluctuations (see the panel (a) in figure 6.1). Thus, it is possible also in this system to identify the region of collective pulses by recourse of the Shinomoto–Kuramoto order parameter, by defining the phase through the Hilbert transform.

In panel (a) of figure 6.1, we show a decrease of the value of ρ for increasing noise intensities. In view of our results with the active rotators, it is possible to understand this phenomenon also in terms of the disordering of the positions.

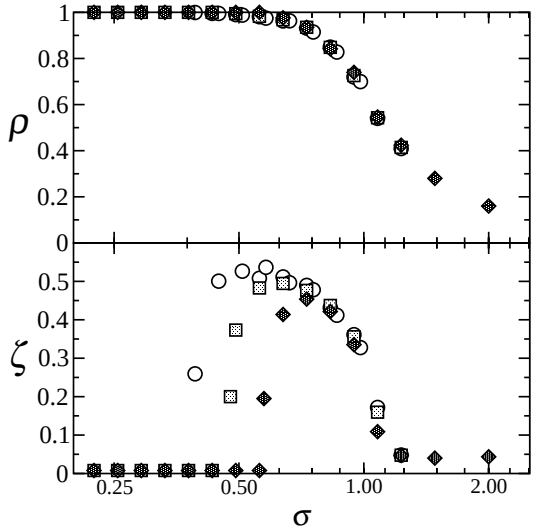

Figure 6.2: In this figure we show the order parameters ρ and ζ for a FitzHugh–Nagumo system composed by diverse units. The distribution $g(a)$ is a uniform of mean $\langle a \rangle = 1.01, 1.02, 1.05$ and standard deviation σ, the coupling strength is $C = 2$ and the system size is $N = 400$. It is noticeable a maximum in the value of the Shinomoto–Kuramoto order parameter, for intermediate values of σ, displaying the system a more regular behaviour.

In panel (c) we plot the jitter, (see 3 for further details), defined as

$$R = \frac{\sqrt{\langle (t_i - \langle t_i \rangle)^2 \rangle}}{\langle t_i \rangle}, \tag{6.11}$$

where $\langle t_i \rangle$ is the mean time between spikes and $\langle (t_i - \langle t_i \rangle)^2 \rangle$ is the second moment of the interspike distribution. In case of a perfectly periodic state, the jitter vanishes, increasing as the spiking become more irregular. It is seen that for this model, the phenomenon of Coherence Resonance appears, as expected, in the phase of collective firings: a clear minimum in R is noticeable. These results are equivalent to those found in the active rotator model.

6.2.2 Effect of diversity

We now turn our attention to the case of diverse units. In figure 6.2, panels (a) and (b), we show that the region of collective firings appear also in presence of diversity: the fact that some units become oscillatory (i.e. $a_1 < 1$), suffices to drive all the units into an oscillatory behaviour. This region of collective firings as a function of the diversity σ, is narrower for larger values

of the mean parameter a. Also, the region of coherent behaviour appears also for larger values of σ.

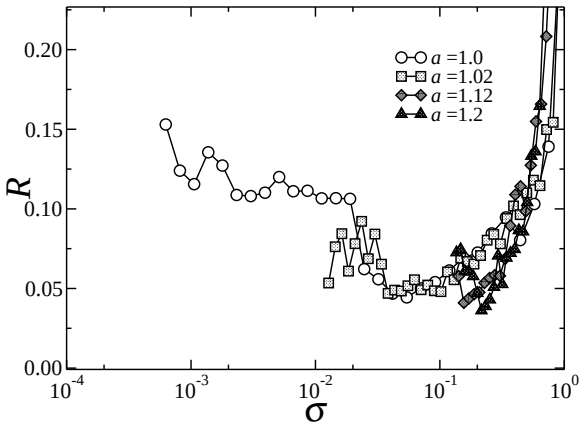

Figure 6.3: We show the jitter for different values of the average value a, in a system composed by diverse units in absence of noise. The values of a_i are drawn from a Gaussian distribution. The coupling strength is $C = 1$, the system size is $N = 400$. It is noticeable a maximum in the value of the Shinomoto–Kuramoto order parameter, for intermediate values of the diversity σ, a more regular behaviour is found.

Finally, we investigate how does the jitter depend on the value of diversity. The results are shown in figure 6.3. Interestingly, a phenomenon associated to that of coherence resonance appears also in a system composed by diverse units. This result is unexpected, as the disorder is static. The reason for this phenomenon to occur is involved, and will be discussed in more detail in the next chapter. Basically stated, diversity causes a change in the shape of the nullclines, driving away the global dynamics from the excitable regime, to the oscillatory region. However, the mechanism that causes the pulses to be more regular is not quite well understood yet.

6.3 Conclusions

In summary, we have shown that an ensemble of globally coupled FitzHugh–Nagumo excitable systems subjected to independent noises (or conversely, a system composed by many diverse units) experience a loss of synchronisation for increasing noise intensity. Paradoxically, it is noise what initially induces the firings and sets the possibility of observing synchronised pulses.

The synchronisation/desynchronisation transition requires a proper definition of the order parameter for its characterisation, since the usual measures used in coupled oscillators do not properly identify the transition point.

We have found that a modified definition of the usual Kuramoto order parameter clearly displays such a transition. This order parameter is obtained from phase-like variables defined through the use of the Hilbert transform and we have given details of a numerically efficient method to compute the phase variables. Further work will aim to characterise this non-equilibrium transition and its universality class. Preliminary results show that the transition is present in locally coupled systems in $d = 2$ dimensions, but not in $d = 1$.

The same phenomenon holds in presence of diversity, and we even found a phenomenon related to that of coherence resonance, but in presence of diversity instead of noise.

As stated before, we do not have any specific applications in mind, but since the FitzHugh–Nagumo equations have been widely used to model some biological systems, we believe that our results can be relevant when analysing the collective response of such systems in a noisy environment.

Chapter 7

Global firing induced by network disorder

7.1 Introduction

In chapter 5 we have shown that in a system composed by coupled excitable units, *any* source of disorder can trigger a coherent collective firing of the system. It is of interest, then, to investigate possible sources of disorder that can induce the same collective phenomenon.

So far, we have only considered a very simple case of interaction: an all-to-all, global coupling. In many cases, this allows for analytical calculations, as shown in chapter 5. But in some cases, such as neurons in brain [68], the interaction between units is not only composed by attractive (activator) couplings, as we previously considered. Neurons, have also inhibitory synapsis. In the case of very simple dynamic phase models, this can be modelled as pair-wise interactions whose strength is negative [102].

The simultaneous presence of attractive and repulsive links in dynamical systems was first addressed by Daido [103, 104, 105]. He focused, in the case where the number of attractive and repulsive links, and their relative strength, is the same on average. In ref. [106], Zanette studied the effect of the presence of repulsive links on the dynamical properties of a set of Kuramoto phase oscillators. He analysed how the stability of the fully synchronised solution, depends on the fraction of repulsive links present in the system. Furthermore, and at difference to what happens in presence of disorder, we found that in finite-size systems, where the network of repulsive interactions is fully random [107], the transition from a fully-synchronised state to desynchronised one has a finite width that vanishes for infinite systems.

In this chapter we study a set of active rotators coupled through a network that contains both attractive and repulsive links. We will isolate these interactions as the only source of disorder for the units, and investigate its

role on the emergence of a collective behaviour. This chapter is organised as follows: in the next section we present the model and the relevant order parameters; also we show that the same framework presented in chapter 5 is also valid in a very generic set of systems where the effects considered in this chapter are of relevance. Later, section 7.3 shows that a coherent firing can be induced if some repulsive random links are added to the studied model. In section 7.4 we show the influence of network topology on these systems. The final section draws some conclusions.

7.2 Model studied and order parameters

7.2.1 Model

We consider an ensemble of coupled *active rotators* [56] $\phi_j(t)$, $j = 1, \ldots, N$, whose dynamics is given by

$$\dot{\phi_j} = \omega - \sin\phi_j + \frac{C}{N}\sum_{k=1}^{N} W_{kj}\sin\left(\phi_k - \phi_j\right) \tag{7.1}$$

The natural frequencies ω are equal for all the oscillators. Notice that $\omega < 1$, (resp. $\omega > 1$) corresponds to an excitable (resp. oscillatory) behaviour of a solitary rotator. Also, in the oscillatory case, note that actual frequency (for a single unit) is given by $\sqrt{\omega^2 - 1}$. Throughout this chapter we will consider only the case $\omega < 1$. The coupling strength is given by the parameter C. The terms W_{ij} are symmetric weighting terms of the coupling, i.e. $W_{kj} = W_{jk}$. In order to isolate the effects of network links, in the studied system there is not noise in the system, nor diversity in the natural frequencies.

First, we will study a particular construction for the network of repulsive links, name a fully-random network, also known as Erdős-Rényi [108, 107, 109]. It is simply constructed in the following way: for each pair of nodes (i, j), the link between them becomes repulsive with probability p_d. The network in this way created has, on average, $p_d\, N(N-1)/2$ repulsive links. Later, we will study the phenomenon in presence of other network topologies, that we will describe in the corresponding section. For this particular network, the values for the matrix W_{ij} are chosen at random as

$$W_{ij} = \begin{cases} 1 & \text{with probability } 1 - p_d \\ -\kappa & \text{with probability } p_d, \end{cases}$$

i.e., with probability p_d, a link is repulsive. The relative strength of the repulsive links is given by the parameter κ.

It is useful to rewrite equation (7.1) as

$$\dot{\phi_j} = \omega - \sin\phi_j + C\rho\,\sin(\Psi - \phi_j) - \frac{C(1+\kappa)}{N}\sum_{k\in\mathcal{N}_j}\sin\left(\phi_k - \phi_j\right), \tag{7.2}$$

which allows for a more efficient development of a numerical scheme to simulate the system. Below we detail how this is helpful, in order to reduce this system in a similar way to what was done in chapter 5.

7.2.2 Order parameters

For this system, we will refer to the *completely synchronised* state, as the one where all the elements are located in the same position of the circle, i.e. $\phi_i = \phi^* = \arcsin(\omega)$, $\forall i$. This corresponds to a resting state, where all the units remain located in the (common) fixed point of the dynamics. Furthermore, this is the only state compatible with $\rho = 1$, as all the units are excitable.

The fully synchronised state always exists. However, depending on the network of repulsive links, $\mathcal{N}$ this state can become unstable. This is very clear, for example, in the limiting case where $p_d = 1$, i.e. all the links are repulsive.

From now on, it is essential to remind that not all possible network realizations break the stability of the fully synchronised state. For a fixed set of parameters, there will be a set of network realizations compatible with them, and the stability of the synchronised state may change from one network realization to another. In order to investigate this changes, we will first compute the fraction of network realizations such that the complete synchronised state becomes unstable, f_d.

The relevant order parameters to describe the dynamical properties of this system, are the same used in the previous chapters 5 and 6, that we will repeat succinctly here: We first compute the time-averaged Kuramoto order parameter ρ, which is known to be a good measure of collective synchronisation in coupled oscillators systems. However, for these systems, being excitable, the Kuramoto order parameter adopts a non-zero value even when all the units are at rest. To discriminate between this static entrainment from the dynamic entrainment, we make use of the Shinomoto–Kuramoto order parameter ζ. Finally, as a measure of the activity of the units, we compute the current J.

7.3 Fully random networks

7.3.1 Stability of the fully synchronised state

From a qualitative point of view, it is interesting to know why the fully synchronised state becomes unstable: starting from the fully synchronised state ($\rho = 1$), let us consider the unit j^*, that the largest number of repulsive links (i.e. $N_{j^*} \geq N_i, \forall i$). There will exist a critical value p_d^*, such that if we keep adding repulsive links (i.e. increasing p_d) up to a point where $p_d > p_d^*$, then for the j^*-th unit the fully synchronised state is unstable, and the

same holds then for the whole system. Any small perturbation, will drive the system apart from the fully synchronised state.

This explains qualitatively that there is a set of units that separate from the central cluster when enough negative links are added. For fully random networks, by construction, the amount of repulsive links each unit has is distributed uniformly along the nodes (see ref. [106]) and its degree distribution is given by a binomial distribution. Thus, all the oscillators become *frustrated* for the same p_d, and thus, the fully-synchronised phase disappears as a first-order phase transition in the thermodynamic limit.

For small systems, the degree distribution is broad: relatively, the variations in the node degree make some units to become frustrated before the others, and thus there is a smooth transition from the fully synchronised state to a fully frustrated one. This simple argumentation implies that there should be some *heterogeneity* in the degree distribution in order to observe a smooth transition between these two states.

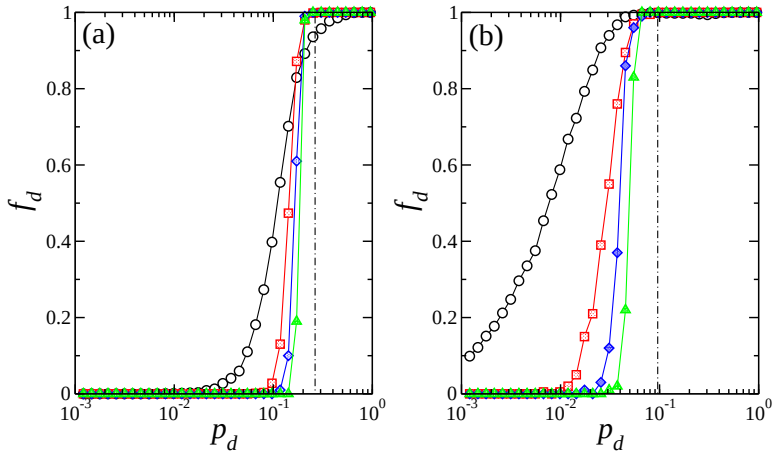

Figure 7.1: We plot the fraction of network realizations such that the fully synchronised state is unstable as a function of the density of repulsive links, p_d. The different symbols correspond to different system sizes: $N = 10, 50, 100, 200$ for increasing sharpness. The system parameters are $\omega = 0.98$, $C = 4$, $\kappa = 3$ (left panel) and $\kappa = 10$ (right column). The value of f_d is averaged over 1000 realizations. The corresponding values for p_d^* in the infinite size limit are, respectively: $p_d^* = 0.2624373429638\ldots$ (left column) and $p_d^* = 0.095431761077\ldots$ (right column), represented with vertical lines.

The computation of the stability of the fully synchronised state can be simply done by linearising the equation (7.2) around the fixed point $\phi^* = \arcsin(\omega)$. Let $\vec{\delta} = \{\delta_1, \delta_2, \cdots, \delta_N\}$ be a vector whose components are the displacements with respect to the fixed point of the units $\phi_j = \phi^* + \delta_j$.

Then, the linearisation process yields:

$$\dot{\delta}_j = -\sqrt{1-\omega^2}\,\delta_j - C\rho\delta_j + \frac{C(\kappa+1)}{N}\sum_{k\in\mathcal{N}_j}(\delta_k - \delta_j). \tag{7.3}$$

Near the transition to the fully synchronised state, $\rho = 1-\mathcal{O}(\delta^2)$, so (keeping the terms up to first order in δ) it can be approximated to 1. This expression can be further reduced by writing it down in a matrix form

$$d\frac{\vec{\delta}}{dt} = \mathbb{J}\times\vec{\delta} = -\left[(\sqrt{1-\omega^2}+C)\mathbb{I} - \frac{C(\kappa+1)}{N}(\mathbb{M}-\mathbb{N})\right]\vec{\delta}. \tag{7.4}$$

Here, the matrix $\mathbb{M}$, is the adjacency matrix of the network of repulsive links; $\mathbb{N}$ is a diagonal matrix where $\mathbb{N}_{ii}$ is the number of repulsive links for the node i. Finally, $\mathbb{I}$ is the identity matrix.

Then, one proceeds in the following way: For a parameter set, and given a network realization of repulsive links, one determines the real part of the maximum eigenvalue $\Re(\lambda_0)$ of the matrix $\mathbb{J}$. This procedure is repeated for several network realizations, and then f_d is computed as the amount of times $\Re(\lambda_0)$ is positive. In figure 7.1 we plot the fraction of network realizations such that the fully synchronised state is unstable as a function of p_d. It is seen that the value of p_d such that the stability is lost, increases for larger N.

There is a critical value for the density of repulsive links p_d^*, such that the fully synchronised state becomes unstable. If the system is large enough, and the only considered displacements are those in unit i, this approximation yields

$$\frac{C(\kappa+1)}{N}\sum_{k\in\mathcal{N}_j}(\delta_k-\delta_j) \cong Cp_d(\kappa+1). \tag{7.5}$$

By putting this expression into equation (7.3), one gets an expression for the limiting value of p_d such that the synchronised state is stable,

$$p_d^* = \frac{1+\sqrt{1-\omega^2}/C}{1+\kappa}. \tag{7.6}$$

For the parameters in figure 7.1, the corresponding values were computed, verifying that this approximation is in good agreement with the results. One can define $p_d^*(N)$, the value of wiring probability such that one half of the network realizations have an unstable fully synchronised state. It is observed that $p_d^*(N)$ approaches logarithmically to p_d^*.

7.3.2 Theory

In the previous section, we have shown that the fully synchronised state becomes unstable for increasing values of p_d. It is then foreseeable that

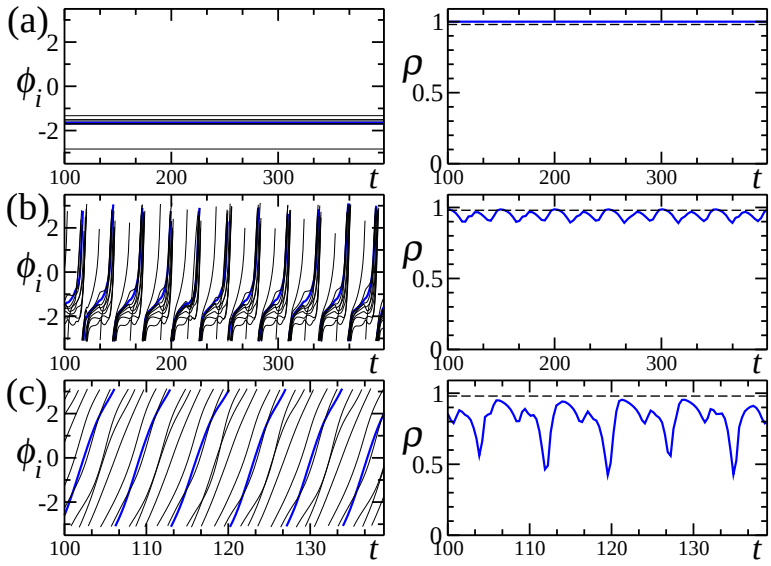

Figure 7.2: In each panel, we plot the dynamical results for different values of p_d, the probability of establishing a link. The left panels show the dynamics of the global phase (blue thick line), and 10 representative units (black, thin lines). In the right plots of each panel, we show the time-dependence of the Kuramoto order parameter ρ for the corresponding values of p_d. It is observed that for the system being oscillatory, a worsening in ρ is needed such that it becomes $\rho < \omega$ (the oscillatory threshold is shown in black dotted lines). The values for p_d are: (a) $p_d = 0.1$, (b) $p_d = 0.15$, (c) $p_d = 0.42$. The other parameter values are set to: $C = 4$, $\kappa = 3$, $\omega = 0.98$, and $N = 50$.

this would imply a decrease in the value of ρ. In this section, we follow the general guidelines given in chapter 5 in order to derive an approximate theory to predict the global behaviour of a coupled set of active rotators with repulsive links. Let us now give some details of this computation.

By direct averaging equation (7.2) over the whole system and using the definition of global amplitude and phase of eq. (5.2) we have

$$\frac{1}{N}\sum_{k=1}^{N}\dot{\phi}_j = \omega - \rho(t)\sin\Psi(t). \tag{7.7}$$

This expression is exact, as all the coupling terms are symmetric, the two contributions from the coupling in equation (7.2) wash out. Taking the time-derivative in eq. (5.2) and introducing $\delta_j(t) = \phi_j(t) - \Psi(t)$, we obtain:

$$\dot{\rho}(t) + i\,\rho(t)\dot{\Psi}(t) = \frac{i}{N}\sum_{k=1}^{N}\dot{\phi}_k e^{i\delta_k(t)}. \tag{7.8}$$

We consider now that the dispersion of the rotators in the circle is small, i.e. $\delta_j(t) \ll 1$. and substitute the expansion $e^{i\delta_k} = 1 + i\delta_k + \mathcal{O}(\delta_k^2)$ in the previous expression. Once again, equating real and imaginary parts, we obtain

$$\rho(t)\dot{\Psi}(t) = \frac{1}{N}\sum_{k=1}^{N}\dot{\phi}_k + \mathcal{O}(\delta_k^2). \tag{7.9}$$

The definition of δ_i leads to $\rho(t) = N^{-1}\sum_k e^{i\delta_k}$. Hence $\dot{\rho}(t) = \mathcal{O}(\delta_k^2)$ and, consistently with the order of the approximation, we can replace in the previous equation $\rho(t)$ by the constant value ρ. Therefore, eq. (5.5) can be approximated by $\rho\dot{\Psi}(t) = \omega - \rho\sin\Psi(t)$, which can be rewritten as

$$\dot{\Psi}(t) = \frac{\omega}{\rho} - \sin\Psi(t). \tag{7.10}$$

As in chapter 5, we find the same dynamical expression for the time evolution of the global phase. This expression shows that, whenever the relation $\rho < \omega$ holds, the system might globally exhibit coherent global pulsations. This mean-field theoretical prediction is well confirmed by the numerical simulations (see figure 7.2).

7.3.3 Numerical results

In figure 7.3 we show the dependence of the relevant order parameters as a function of the density of repulsive links p_d. The results in such figures confirm the theoretical arguments of previous section: a decrease in the value of the Kuramoto order parameter ρ below the natural frequency ω causes the units to fire at the same time. At difference with the results in previous chapters, however, there is a strong dependence of the size of coherent pulsationson system size: for large enough systems, this region is narrower. It is also worthwile mentioning that for small systems, there is a second regime of collective firings for very large values of p_d (the rightmost part of panels (a) and (b) in figure 7.3).

In is remarkable that the size of the region of collective firings depends on the system size in a different way from what was found in presence of noise nor disorder.

Let us define the quantity

$$R_j(\phi_j, \{\phi_i\}) = C\rho\,\sin(\Psi - \phi_j) - \frac{\kappa(1+C)}{N}\sum_{k\in\mathcal{N}_j}\sin\left(\phi_k - \phi_j\right). \tag{7.11}$$

R_j will be positive if the unit j is coupled attractively to the mean-field, and negative if repelled. The reason for this is found if we compare figure 7.1: for increasing system size, f_d undergoes a sharper transition to an state in which a fully unsynchronised state. For larger systems, the degree

distribution of the repulsive network approaches a delta function located at $k^* = p_d N$. This means that, simultaneously, many oscillators pass from an attractive global interaction to a repulsive one, $R_j < 0$. So, these units are repelled from the position of the mean-field. For small systems, this transition occurs gradually, as few oscillators fulfil this relation just above the transition. Also, it is interesting to mention that for ω closer to the bifurcation point, $\omega = 1$ the region of coherent pulsations is present for systems as large as $N = 10^4$.

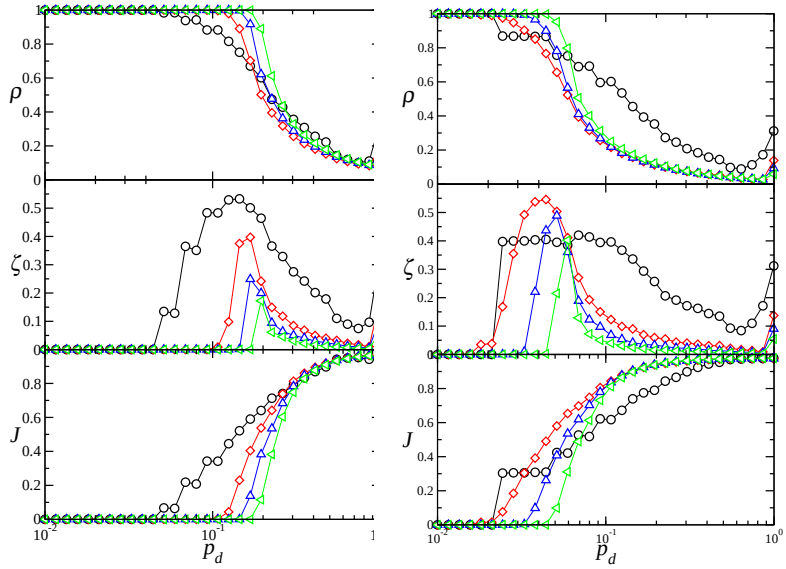

Figure 7.3: In this figure we show the numerical results of the order parameters for 10^3 different network realizations. The left (right) column corresponds to simulations with $N = 10, 50, 100, 200$. The other system parameters are: $\omega = 0.98$, $C = 4$, $\kappa = 3$ ($\kappa = 10$ for the right column). The system parameters are coparable to those presented in figure 7.1.

7.4 Heterogeneous networks

In the previous section, we stated that the reason for the narrowing of the region of collective pulses in the fully-random network is the fact that also the degree distribution gets narrower for larger systems. Then, it implies that a network of repulsive links with a broad degree distribution, could exhibit the phenomenon of collective firings even in the infinite-size limit. We will refer to this network as a *heterogeneous* one: the corresponding degree distribution is *broad*. For fully-random networks, they approach a homogeneous state for larger sizes.

For heterogeneous networks, there will be a fraction of sites for whom $R_j < 0$, and other such that $R_j > 0$. If the distribution of links does not change with system size, these fractions will not depend on size either, and then it is expected that the fraction of units departing from a central cluster will remain fixed, and ρ will be basically independent on system size. Then, increasing the proportion of repulsive links, will not affect the position of the transition, $\rho < \omega$, to coherent firing. A similar argument for the second transition, shows that the position of the transition from coherent pulses to desynchronised firing will remain unchanged too, and then it is expected that heterogeneous networks will have a non vanishing region of synchronous firings.

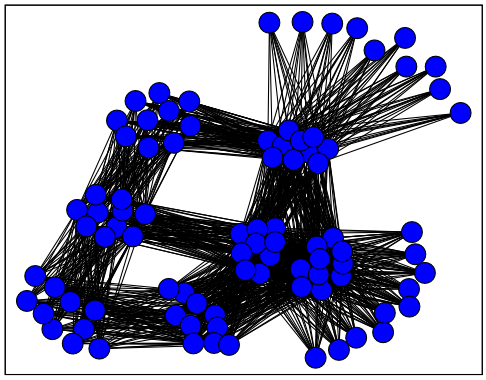

Figure 7.4: An schema of the replicated-random network (right) and the fully randomised version of the network. The parameters are $p_d = 0.3$, $N_0 = 10$ and $N = 100$. Please note that each *cluster* represent a set of *homologous* nodes (see inline text for details).

We will first consider a hierarchical network constructed as follows: We first build a fully random network, whose size is N_0 and wiring probability p_d. The average number of links will be $\mathcal{O}(N_0)$, while its dispersion will be $\mathcal{O}(\sqrt{N_0})$. Let us write $i \in \mathcal{N}_j^0$ the neighbors i of the site j. We then build a $N = M\,N_0$ size network in the following way: for each node l_1, let $l_1' \equiv l_1 \bmod (N_0)$ be an integer number between 1 and N_0, i.e. a node in the seed network; l_2 and l_2' are constructed in the same way. Then, l_1 and l_2 are neighbors if $l_1' \in \mathcal{N}_{l_2'}^0$. It means that if $l_1 \equiv l_2 \bmod (N_0)$, for any l_1 and l_2, they are *homologous* nodes: all their neighbors are the same. A representation of the network constructed in this way is shown in figure 7.4.

The number of links per site is, for the complete network,

$$\bar{k} = p_d\,N_0\,M = p_d N = M\,\bar{k_0},$$

where $\bar{k_0}$ is the average degree of the initial network. However, the standard

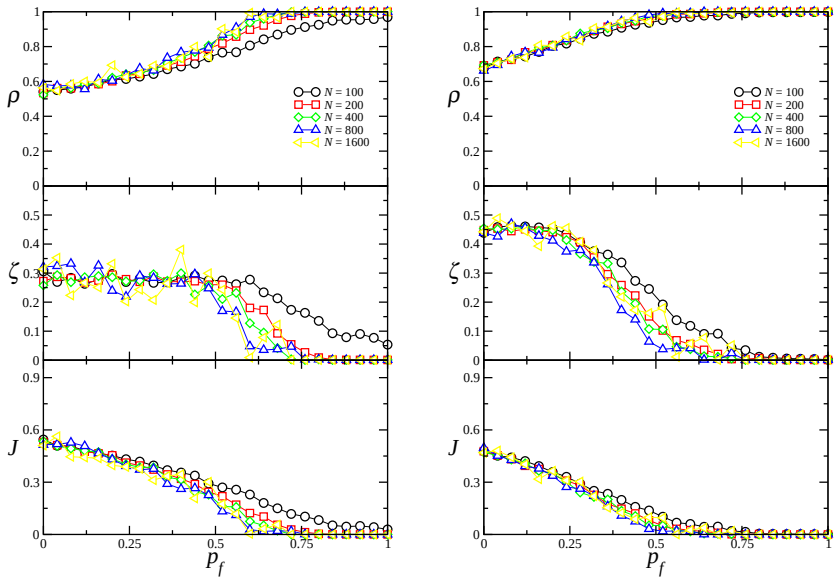

Figure 7.5: In this figure we show the numerical results of the order parameters for a replicated-random network. The plots are as a function of the proportion of randomised links p_f. The system parameters are: $\omega = 0.98$, $C = 4$, $N_0 = 20$,$\kappa = 1, 2$ (left, right columns), $p_d = 0.40, 0.20$, for the left and right columns, respectively. The different symbols correspond to different system sizes $N = 100, 200, 400, 800, 1600$. The shown results were obtained averaging over 10^3 network realizations.

deviation of the degree distribution is given by

$$\sqrt{\langle k_i^2 - \bar{k}\rangle} = M\sqrt{\langle k_i^{0\,2}\rangle - \bar{k_0}^{\,2}} = M\,\sigma_0,$$

where σ_0 is the standard deviation of the seed network whose size is N_0. So, by keeping constant the size of the initial network at N_0, and increasing N by adding homologous nodes, the broadness of the degree distribution will grow linearly with system size.

Let l^0 be a node of the initial network. Then all its homologous nodes l' in the final network will preserve the sign, i.e. $\mathrm{sign}(R_{l^0}) = \mathrm{sign}(R_{l'})$, due to the fact that the second term in the definition of R is remains constant (it is divided and multiplied by M).

This network is not a purely random one (in fact it has a very large clustering coefficient [109], and is self-similar). This fact, however is of no influence to the considerations we will perform in the forthcoming discussion: The only relevant feature for the emergence of a collective behaviour is the stationary density of sites whose overall coupling to the other units is

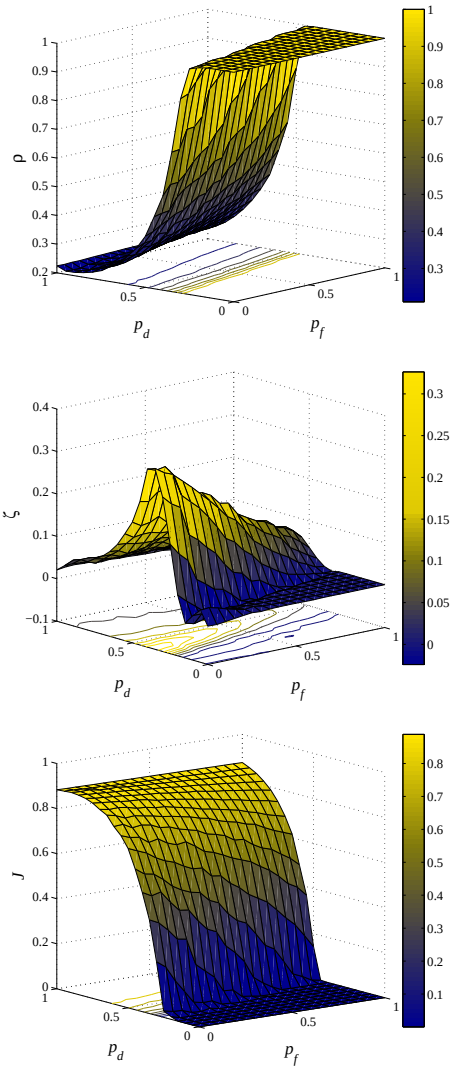

Figure 7.6: Numerical results of the relevant order parameters for the replicated-random network. The surfaces are shown as a function of the proportion of randomised links p_f and the probability of establishing links in the base network, p_d. The system parameters are: $\omega = 0.98$, $C = 4$, $N_0 = 20$,$\kappa = 2$, the system size was fixed in 400The results shown, were obtained with 100 network realizations.

negative, as we discussed above. In fact, one could rewire a given fraction of the sites in order to obtain a random network [110]. We will call p_f the probability of modifying the end node of a link and picking another site at random. For $p_f = 1$, the fully random network is recovered. It

is worth mentioning that this randomisation does not preserve the degree distribution.

It is interesting to determine how the eigenvalues of the adjacency matrix $\mathbb{M}$ look like for $p_f = 0$. Let λ_i^0 be the eigenvalue of the initial network. The complete network has N_0 eigenvalues given by $\lambda_i^0 M$. Note that, for fixed N_0, the eigenvalues scale as M, instead of $\sqrt{M}$, which is the "semi-circle law" [111, 112] for random matrices. The other $(M-1)N_0$ eigenvalues, are equal to zero.

In figure 7.5 we show the results of the relevant order parameters as a function of p_f, the ratio of randomly rewired edges. For some values of p_d (those selected in the figures), a coherent global behaviour is found -signalled by the non zero value of ζ-. The role of increasing p_f, is that of turning more *entrained* the solutions of the system: ρ grows up to unity, and the collective firing disappears. Also, the current J, decreases, vanishing for very large p_f, i.e. for more random networks.

It is also very interesting that the results are basically independent on system size: for a fixed value of N_0, if the system size is increased by adding replicas, all the relevant order parameters remain unchanged. Then, the region of collective firings remain present even for infinite-size systems.

Finally, figure 7.6 shows the full dependence of the relevant order parameters with respect to the probabilities p_d (of establishing a link in the base random network) and p_f (the fraction of randomised links). It is noticeable that for increasing p_f, the value of ρ decreases, independently of the value of p_d. The reason is that this procedure homogenises the degree distribution of the network. On the other hand, there is an intermediate range of values of p_d such that the network behaves more coherently (signalled by an increase of the order parameter ζ).

7.5 Conclusions

We have shown that a set of purely excitable coupled units can exhibit a global firing if some repulsive links are present in the system. These repelling interactions have the role of decreasing the entrainment of the units. Thus (in a similar fashion to what was shown in chapter 5), this decreasing of the entrainment causes the whole system to undergo a bifurcation to an oscillatory behaviour.

We also demonstrated the important role that the *heterogeneity* of the network (understood as broadness of the degree distribution) has on the dynamical properties of this system. We found that when all the units have the same amount of repulsive links, there is no region of collective firings. Broad degree distributions, on the other hand, ensure that some of the units will drift apart from the central cluster, decreasing entrainment. It is this mechanism, combined with the fact than most of the units remain close to

the mean-field, what causes the same theoretical prediction of the previous chapter to be valid.

These results are not only valid in this theoretical model, but instead we think they are of broad applicability, as we only considered the influence of very generic ingredients. As will be discussed in chapter 10, for example nervous and neural systems interact not only through attractive (in the context of the model studied in this chapter, they are called *activator*) interactions, but also through repulsive (*inhibitor*) couplings. Thus, these connections would be enough to trigger a coherent firing when the neurons are slightly perturbed.

Chapter 8

Diversity-induced resonance

8.1 Introduction

Noise induced, or stochastic, resonance emerged in the early eighties as a proposal to explain the periodicity observed in the Earth ice ages [23, 25]. The mechanism is such that an external forcing acting upon a nonlinear system can be conveniently amplified under the presence of the right amount of noise. This innovative proposal led many researchers to look for a similar *constructive* role of noise in physical, chemical, biological, and many other kinds of systems [113, 17, 42, 114]. While initially the studies focused on simple, low–dimension, dynamical systems, more recent work [115, 92] has considered the constructive role of noise in extended systems composed of many coupled identical units. The assumption of identical units, while being mathematically convenient, is not very realistic for many of the applications since it is clear that in some natural systems, specially in biology, the units composing the ensemble present a disparity in the values of some characteristic parameters. Among other consequences, this natural diversity makes each isolated system respond differently to an external forcing; it is an open question to investigate the effect that diversity has on the global response of the collective system.

This problem has received some recent attention. For instance, Hong [116] analyses the locking behaviour of an ensemble of coupled oscillators with different internal frequencies subject to a periodic external forcing. He finds that the quenched disorder helps a small fraction of the oscillators to lock to the external frequency. However, he does not observe a collective behaviour in which the whole ensemble benefits form the diversity in the internal frequencies. In this chapter we give evidence that the right amount of diversity, in the form of quenched noise, might help an extended system to respond globally in a more coherent way to an external stimulus.

As in the case of stochastic resonance, we believe that the results reported here are very general. For the sake of concreteness, however, we have

considered two prototypical nonlinear systems: one bistable and another excitable. In both cases, we show that there is a resonance effect in the global response as a function of the diversity.

8.2 Model studied

We consider first an ensemble of N coupled bistable systems. They correspond to the ϕ^4 model (also called Ginzburg–Landau or "model A"). This is one of the basic models in equilibrium statistical mechanics and has been used to model many physical situations, although the simplest application is to describe the paramagnetic-ferromagnetic transition that occurs as a function of the temperature. In this model, a set of real variables $x_i(t)$, $i = 1, \ldots, N$ are located in the sites of a regular d-dimensional lattice.

$$\frac{dx_i}{dt} = ax_i - x_i^3 + \frac{C}{N_i} \sum_{j \in \mathcal{N}_i} (x_j - x_i) + \eta_i \tag{8.1}$$

here $\mathcal{N}_i$ denotes the set of neighboring sites with which site i interacts, and N_i is the number of such neighboring sites. C is the coupling constant. An usual version of this model includes in $\mathcal{N}_i$ only the $2d$ nearest neighbors of i. In this paper, we will be considering the mean-field or all-to-all coupling version in which all sites interact with the same strength. Hence $\mathcal{N}_i$ contains all the lattice sites and $N_i = N$. The disorder η_i is usually considered to be a white noise of intensity proportional to the temperature. The model then displays a phase transition from an ordered (ferromagnetic) phase to a disordered (paramagnetic) phase at a critical temperature T_c[117]. This is the generic behaviour when $a > 0$ and $C > 0$, the only cases considered in this paper.

As we stated in the introduction, we are interested in analysing the role of diversity in the units x_i. To this end, we neglect the thermal noise. Instead, the diversity appears as quenched noise, i.e. the values η_i (with $i = 1, \ldots, N$) do not depend on time, and are independently drawn from a probability distribution $g(\eta)$. At this moment we only assume a symmetric distribution $g(\eta) = g(-\eta)$. The mean value of the distribution is $\langle \eta_i \rangle = 0$ and the correlations are $\langle \eta_i \eta_j \rangle = \sigma^2 \delta_{ij}$. The root-mean-square σ is a measure of the diversity.

Furthermore, we will consider that the system is also subjected to an external periodic forcing, of intensity A and frequency $\Omega = 2\pi/T$. Thus, equation 8.1 becomes

$$\frac{dx_i}{dt} = ax_i - x_i^3 + \frac{C}{N} \sum_{j=1}^{N} (x_j - x_i) + \eta_i + A \sin(\Omega t). \tag{8.2}$$

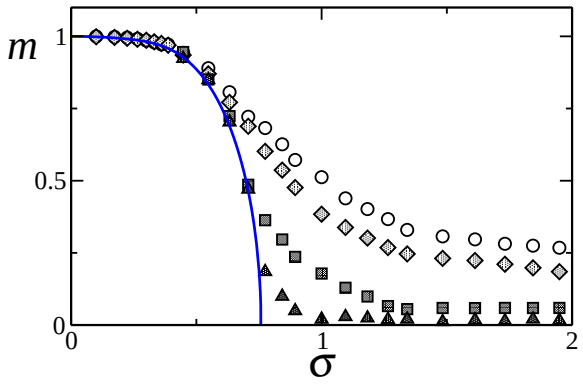

Figure 8.1: Disordering effect of diversity in the ϕ^4 model. We show the magnetisation m as a function of the diversity σ for the ϕ^4 model with quenched disorder defined in eq. 8.1. The parameters are $a = 1$, $C = 1$ and the values of η_i are taken from a Gaussian distribution $g(\eta)$ of zero mean and variance σ^2. The line is the prediction of the mean-field theory and the symbols are the results of numerical simulations of the dynamical equations (8.1) for system sizes $N = 50, 10^2, 10^3, 10^4$ (the transition sharpens as N increases).

8.2.1 The disordering role of diversity

In this section we review the disordering effect that diversity has on the ϕ^4 model defined above in absence of an external signal (see eq. 8.1). We use the all-to-all coupling where a full analytical understanding is possible. The all-to-all coupling assumption simplifies the problem and allows one to reduce it to a one variable. This is basically the Weiss mean-field treatment which is exact in the case of global coupling. Let us introduce the global variable $m(t)$ as:

$$m(t) = \frac{1}{N}\sum_{i=1}^{N} x_i(t) \tag{8.3}$$

The "magnetisation" is defined as the time average of this global variable:

$$m = \langle m(t) \rangle. \tag{8.4}$$

The coupling between the x_i variables appears only through this collective variable:

$$\frac{dx_i}{dt} = (a - C)x_i - x_i^3 + Cm + \eta_i \tag{8.5}$$

This can be interpreted as a relaxational dynamics $\frac{dx_i}{dt} = -\frac{\partial V(x_i)}{\partial x_i}$ with a potential:

$$V(x_i) = \frac{C - a}{2}x_i^2 + \frac{1}{4}x_i^4 - (Cm + \eta_i)x_i \tag{8.6}$$

In the limit $t \to \infty$ the variable x_i will tend to one of the minima of $V(x_i)$. We restrict ourselves from now on to the case $C \geq a$ for which the potential $V(x_i)$ has a single minimum, hence avoiding the possible metastable states that could occur otherwise. For fixed values of m and η_i the variable x_i will tend to the unique solution of the cubic equation:

$$x_i^3 + (C-a)x_i = Cm + \eta_i \tag{8.7}$$

The explicit solution is $x_i(\eta_i, m) = -\frac{\gamma}{u_i} + u_i$ with the notation

$$u_i = \sqrt[3]{\alpha_i + \sqrt{\gamma^3 + \alpha_i^2}}$$

and $\gamma = (C-a)/3$, $\alpha_i = (Cm + \eta_i)/2$. To determine the value of the mean-field variable m we use the self-consistency relation (the subindex i is now dropped from the notation):

$$m = \langle x \rangle = \int d\eta \, g(\eta) \, x(\eta, m) \tag{8.8}$$

where, assuming self-averaging, we have replaced the sum over variables by an average over the realizations of the diversity variables η. Using the symmetry property of the distribution $g(\eta)$ the self-consistency relation can be expanded for small m:

$$m = F_1 m + F_3 m^3 \tag{8.9}$$

where F_1, $F_3 > 0$ are coefficients that depend of a, C and σ. As in the standard Weiss theory, this equation can have one or three solutions depending on the value of F_1. If $F_1 > 1$ then the only solution corresponds to the disordered phase $m = 0$. For $F_1 < 1$ there are two additional solutions $m = \pm m_0$, which correspond to the ordered phase. A detailed analysis shows that for fixed a and C the ordered solution $m \neq 0$ appears for a diversity σ smaller than a critical value σ_c, while a diversity $\sigma > \sigma_c$ only admits the disordered solution $m = 0$. In this sense, diversity has a similar role to noise since a large diversity destroys the ordered state. The phase diagram is plotted in figure 8.1, in the case of a Gaussian distribution for $g(\eta)$ and $a = 1$, $C = 1$. In this case, the critical point can be computed as $\sigma_c = \left[\frac{\Gamma(1/6)}{2^{1/3} 3 \pi^{1/2}}\right]^{3/2} = 0.7573428\ldots$.

8.3 Disorder-induced resonance in the ϕ^4 model

8.3.1 Qualitative description

We now focus in the system subjected to an external periodic signal. The global response is quantified by the average position of the units $m(t) =$

$\frac{1}{N}\sum_i x_i(t)$ for which we now derive an evolution equation. By averaging the previous equation over the whole population, we obtain in the limit of large N:

$$\frac{dm}{dt} = am - \frac{1}{N}\sum_i x_i^3 + A\,\sin(\Omega t). \tag{8.10}$$

Following reference [118], let us introduce δ_i, such that $x_i = m + \delta_i$. We additionally introduce $\frac{1}{N}\sum_i \delta_i^2 = \Delta$. Notice that $\Delta(t)$ is a function of time as it depends on the distribution of $\delta_i(t)$, furthermore $\Delta \geq 0$. Under the assumption of δ_i being distributed according to an even distribution[1] we get,

$$\frac{dm}{dt} = m(a - 3\Delta) - m^3 + A\,\sin(\Omega t). \tag{8.11}$$

with $\Delta = \frac{1}{N}\sum_i \delta_i^2$. Hence, in the absence of forcing, $m(t)$ follows a relaxational dynamics if an effective potential:

$$V(m) = \frac{3\Delta - a}{2}m^2 + \frac{1}{4}m^4 \tag{8.12}$$

Here and henceforth averages with respect to the variables η_i are replaced with averages with respect to the distribution $g(a)$.

The unforced system is bistable with equilibrium points at

$$m_\pm = \pm\sqrt{1 - 3\Delta}.$$

For $\sigma = 0$, Δ vanishes after an initial transient to wash out the effect of the possibly different initial conditions for the x_i's. A weak, subthreshold, forcing (namely $A \lesssim 0.3$ for the range of frequencies used in this work), will not suffice to have the global variable $m(t)$ jump from one stable point to the other as it will simply make small oscillations around one of the equilibrium points. As the diversity increases, Δ increases with a twofold effect: first, the stable points approach each other and, second, the height of the barrier separating them decreases. It might be possible that the weak external forcing is now able to overcome the reduced barrier and the global variable m exhibits wide oscillations between the two fixed points following the external forcing. If the diversity increases even further, leading to $\Delta > 1/3$, the barrier disappears, the two fixed points merge at $m_0 = 0$ and the global variable makes small oscillations around this new fixed point. We then predict a resonance effect for intermediate values of the diversity for which the amplitude of the oscillations of m will be maximum.

[1] Alternatively, one could simply neglect the third moment of the distribution of δ_i, an assumption valid for small δ_i.

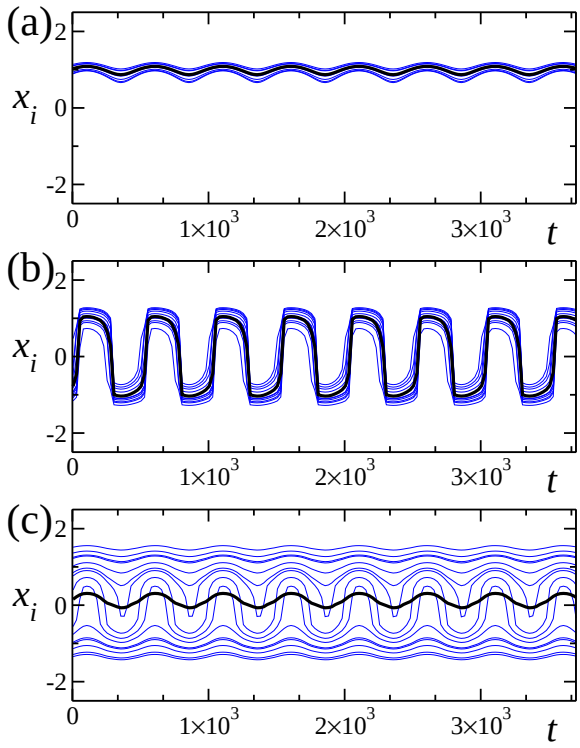

Figure 8.2: For the bistable model we show some representative trajectories $x_i(t)$ (thin, blue lines) and the average trajectory $m(t)$ (thick, black line) in the case of $\sigma = 0.20$ (panel a), $\sigma = 0.54$ (panel b) and $\sigma = 2.0$ (panel c); The system parameters are $a = 1$, $C = 1$, $T = 500$, $A = 0.2$ and $N = 400$. Note the wide variations of $m(t)$ in panel (b), corresponding to the optimal response to the external forcing.

8.3.2 Theoretical approximation

It should be clear now what the mechanism is leading to the resonance. In the homogeneous case, when all systems have $a_i = 0$, the subthreshold forcing can not overcome the potential barrier for any of them. As the diversity increases, there will be a number of units for which the value of a_i is such that the forcing is now suprathreshold for them and the barrier can be overcome in one direction. These units are able, through the coupling term, to pull the other units and hence produce a collective, macroscopic, movement following the variation of the external forcing. For too large diversity, however, some of the units to be pulled offer too much resistance to follow the external force and this effect can not be overcome by the favourable units.

Before we present the numerical results sustaining this diversity-induced

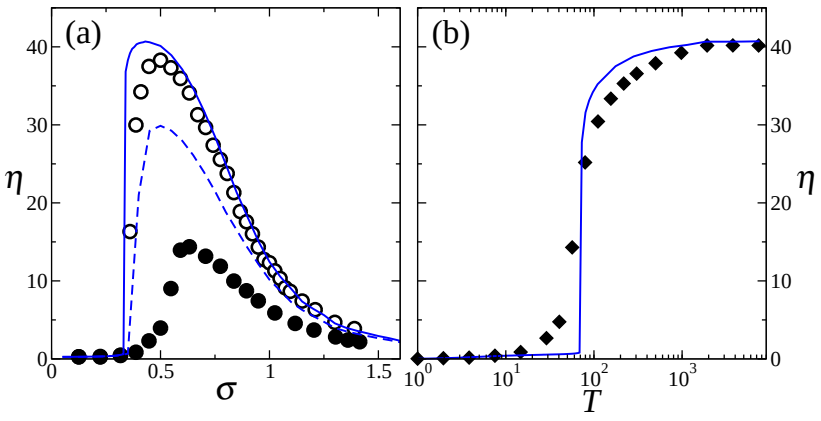

Figure 8.3: Spectral amplification factor, η, of the globally-coupled bistable model, eqs. (8.2). The values of the a_i's are drawn from a Gaussian distribution of zero mean and variance σ^2. Some system parameters, are: $N = 10^3$, $C = 1$, $a = 1$ $A = 0.20$. In the panel (a) we observe that the amplification factor exhibits a maximum as a function of the diversity both in the case of a period $T = 50$ (black circles) and $T = 10^3$ (open circles) of the external forcing. The panel (b) the spectral amplification factor as a function of the period of the forcing (the diversity is fixed at $\sigma = 0.55$). In both plots, symbols correspond to numerical simulations and the lines are the corresponding theoretical predictions of a simplified theory (see the text for details).

resonance, let us present a simplified treatment that allows us to reproduce the aforementioned effect. The main problem to solve numerically eq. 8.11 to determine the time evolution of the global variable $m(t)$ is to find the variation in time of the second moment $\Delta(t)$. The classical treatment of reference [118] consists in writing down a hierarchy of equations which is truncated under some Gaussian approximations for the moments. We follow here an alternative approach. Using an ensemble average, we can write

$$\Delta(t) = \int dag(a) \left[x(t;a) - m(t)\right]^2 , \tag{8.13}$$

where a is distributed according to the distribution $g(a)$ and $x(t,a)$ is the position at time t of a particle whose diversity parameter takes the value a. This integral is performed numerically using a Gaussian quadrature scheme for which we need to compute the necessary values of the function $x(t,a)$. This calculation is done in a regime of "slow forcing", where the period of the forcing signal is large enough such that, given a value of $m(t)$, $x(t,a)$ can be considered as the rest point given by the minimum of the local potential, $V(x;t,a,m)$ or the root of $dV/dx = 0$. This cubic equation can have either one or three real roots: in the latter case, we selected the root with the lowest

potential value[2]. Once $\Delta(t)$ has been computed in this way, the right hand side of eq. 8.3 is fully determined and we can proceed with its numerical integration to find the time evolution of $m(t)$. We quantify the resonance effect by the spectral amplification factor [119], $\eta = 4A^{-2}\left|\langle e^{i\Omega t} m(t)\rangle\right|^2$, and $\langle \ldots \rangle$ denotes a time average (see section 2.2.4 for a detailed definition).

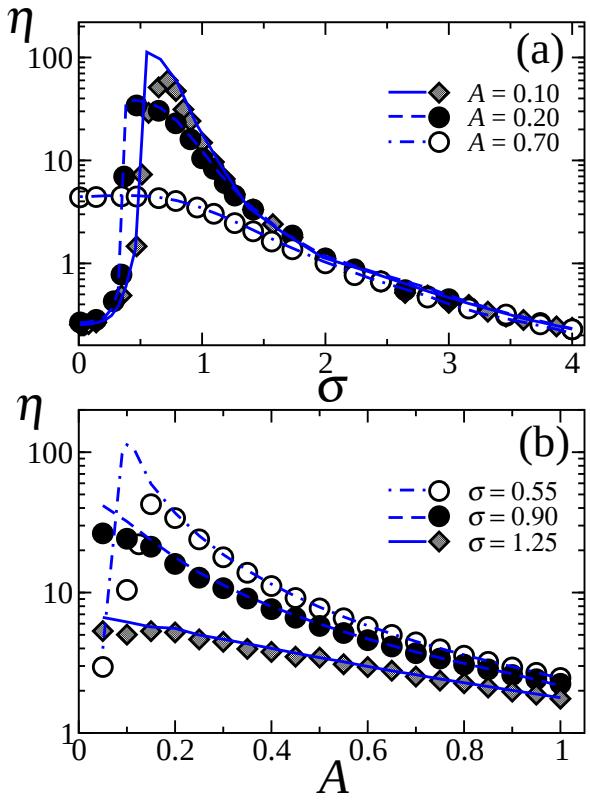

Figure 8.4: (a) Spectral amplification factor, η, of the globally coupled bistable model, eqs. (8.2) as a function of diversity for different values of the amplitude A of the forcing. (b) Dependence of η on the forcing amplitude for fixed values of diversity. Both figures use a period $T = 200$ and other parameters as in fig. 8.3. Symbols represent the results coming from a numerical simulation of the system's equations and the blue lines are the corresponding theoretical predictions.

[2]As a consistency check, we have verified that the ensemble average $\int dag(a)x(t;a)$ is equal to $m(t)$ with sufficient numerical precision.

8.4 Results

In the right panel of figure 8.2 we plot some representative trajectories for the individual units as well as the mean trajectory $m(t)$. In the case of small diversity, it can be seen that the units execute small oscillations around the same minimum following the external forcing (panel a). As the diversity increases over a critical value, the amplitude suddenly increases (panel b). Finally, for too large diversity, each unit now executes small oscillations, but each one oscillates around a different location and, hence, the amplitude of the oscillations of the global variable $m(t)$ decreases (panel c), in agreement with the previous discussion.

In fig. 8.3(a), we plot the amplification factor η versus the diversity σ, for different values of the period T of the external forcing for an amplitude A below the threshold value. As predicted, there is an optimum value of the diversity for maximum amplification, the main result of this chapter. Notice that our approximate treatment agrees rather well with the results coming from a direct numerical integration of the original set of equations (8.2), when the signal is slow.

We now analyse how the system responds to different modulation periods of the external forcing while the amplitude is kept fixed. In the panel (b) of fig. 8.3 we plot the amplification factor as a function of the period of the external forcing for fixed diversity. It can be seen that for large T the amplification factor reaches a constant value, while η vanishes for small T. Both regimes are well described by the theoretical approximation. For large T the agreement is due to the validity of our approximate picture of the dynamics in that limit. For small T, the individual units are not able to follow the fast external forcing and consequently $\dot{x}_i \approx 0$ which leads to the same condition to determine x_i as a function of a_i and m as in the large T limit. It is worth mentioning that the shape of the curve in the inset of fig. 8.3 differs from what appears in stochastic resonance where a maximum at intermediate values of T is observed[17]. This difference is due to the absence in the diversity-induced resonance case of a matching between two time scales which in stochastic resonance are the Kramers' time and the forcing period.

In fig. 8.4(a), we study the effect of the amplitude of the forcing on the system response. As in stochastic resonance [17], a maximum in the response appears only for subthreshold forcing and the height of this maximum increases with decreasing amplitude. However, for suprathreshold forcing (the case $A = 0.7$) the linear regime is recovered and the amplification factor steadily decreases with increasing diversity. Fig. 8.4(b) shows that the spectral amplification factor has a maximum for a well defined value of the amplitude of the external forcing. It is also observed that the theoretical prediction agrees rather well both qualitatively and quantitatively with the numerical results. However, for faster signals the qualitative agree-

ment disappears. In panel (a) of fig. 8.5 it can be seen that the theoretical approximation is valid for very large or vanishing diversities. For intermediate diversities, however, a higher response is predicted for small signal amplitudes, while a lower value is found in numerical simulations.

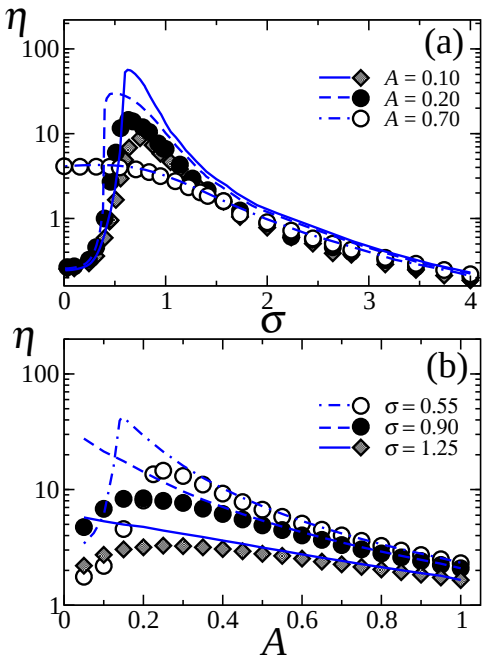

Figure 8.5: (a) Spectral amplification factor, η, of the globally coupled bistable model, eqs. (8.2) as a function of diversity for different values of the amplitude A of the forcing. (b) Dependence of η on the forcing amplitude for fixed values of diversity. Both figures use a period $T = 50$ and other parameters as in fig. 8.3. Symbols represent the results coming from a numerical simulation of the system's equations and the blue lines are the corresponding theoretical predictions.

8.5 Diverse excitable systems

We now turn our attention to excitable systems. As a paradigmatic model of interest in many biological applications, we consider a globally coupled ensemble of excitable units described by the FitzHugh–Nagumo equations:

$$\begin{aligned} \epsilon \dot{x}_i &= x_i - \frac{1}{3}x_i^3 - y_i + \frac{C}{N}\sum_{j=1}^{N}(x_j - x_i), \\ \dot{y}_i &= x_i + a_i + A\sin(\Omega t)\,. \end{aligned} \tag{8.14}$$

The coupling between units is taken into account through the activator variable x with a coupling strength C. Each unit has a parameter a_i, representing the diversity, drawn from a probability distribution $g(a)$ of mean $\langle a_i \rangle = a$ and correlations $\langle (a_i - a)(a_j - a) \rangle = \delta_{ij}\sigma^2$. When $|a_i| < 1$ system i is in the oscillatory regime, while for $|a_i| \geq 1$ it is in the excitable one. As in the double well case, the system is subjected to a periodic forcing of intensity A and frequency Ω and we do not consider explicit noise terms. The combined effect of diversity and noise was considered in reference [120] in the context of coherence resonance. Specifically, the authors of this reference found that in the unforced case, $A = 0$, and in the presence of noise, there was a systematic increase of the coherence factor for increasing inhomogeneity. We focus in this chapter on the forced case, $A \neq 0$ where we will show a resonance effect with respect to the diversity.

The theoretical analysis follows the lines of the double-well system. With the definitions $m = \frac{1}{N}\sum_i x_i$, $Y = \frac{1}{N}\sum_i y_i$ and $\Delta = \frac{1}{N}\sum_i (x_i - m)^2$ we arrive at

$$\begin{aligned} \epsilon \dot{m} &= m(1-\Delta) - \frac{m^3}{3} - Y, \\ \dot{Y} &= m + a + A\sin(\Omega t)\,. \end{aligned} \tag{8.15}$$

We conclude that in this model an increase in the diversity, hence an increase in Δ, induces a change in the shape of the nullclines of the dynamics of the global variables. As in the double well system, in the homogeneous case, $a_i = a$, and $|a| > 1$ all units are in the excitable regime and we consider the case where the weak external forcing is not enough to overcome their excitability threshold. As the diversity increases, some units will have their excitability threshold lowered (they could even become oscillatory) and the forcing is now suprathreshold for them. Those units pull the others, so producing the observed collective behaviour. The actual description of the collective behaviour is somewhat more involved, since Δ exhibits a periodic variation with time and it has a maximum value when the collective variables m and Y are near the fixed point. In the limit of large Δ the nullclines are modified such that the limit cycle disappears altogether.

In fig. 8.6(a) we plot the amplification factor η of the global m variable as a function of the diversity σ for different values of the external time period T and a fixed value of the amplitude A close to threshold, where we can observe the resonance effect. This plot shows some differences with the double well system studied before, namely the presence of several resonances at different values of the diversity. We speculate that this behaviour has its origin in the existence of a well defined refractory time in the dynamics of an isolated unit. Several resonance maxima can also be observed when plotting the amplification factor as a function of the period of the forcing for fixed diversity, see fig. 8.6(b). A similar effect has been also reported for

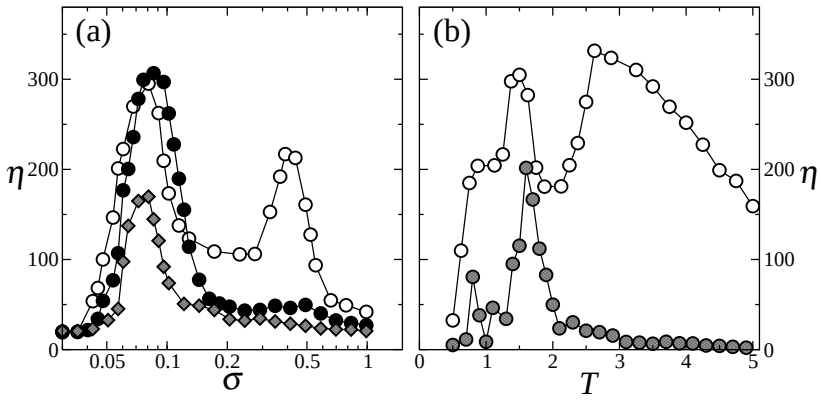

Figure 8.6: Spectral amplification factor, η, of the globally-coupled FitzHugh–Nagumo model, eqs. (8.14), where the a_i's have been drawn from a Gaussian distribution of mean a and variance σ^2. Some system parameters, are: $N = 10^3$, $\epsilon = 10^{-2}$, $a = 1.12$, $C = 1$, $A = 0.05$. (a) Plot of η as a function of the diversity σ for different periods of the external forcing. (b) Plot of η as a function of the period T for different values of the diversity σ. In both cases the symbols represent the results coming from a numerical simulation of the system's equations (the solid line is a guide to the eye).

a single FitzHugh–Nagumo system in the presence of noise and it is known as frequency-dependent stochastic resonance [121].

8.6 Conclusions

In conclusion, we have given evidence that diversity, in the form of quenched noise, can enhance and lead to a resonant effect for the response of an extended system to an external periodic forcing. The evidence has been given for two prototype systems, paradigmatic of bistable and excitable behaviour and, hence, we believe that the same resonance will appear in other more complicated systems. The mechanism of the phenomenon is particularly simple: at a given time a fraction of the units are able to respond to the external forcing; those units, through the coupling terms, are able to pull the others into the direction of the force. For too large diversity, the favourable units can not overcome the effect of the adverse ones. This resonance mechanism is very general and it could appear in many fields.

A final remark is relevant here. Note that in equation (8.11) for the global variable m the effect of the diversity appears only through the variable Δ measuring the dispersion in the behaviour of the dynamics of the individual units x_i. Therefore, the existence of a resonance effect for the

optimal amplification of weak signals *does not depend on the source of the disorder*. The same effect could also be obtained in the presence of disorder induced by noise (stochastic resonance), by a non-regular network of connectivities, inhibitory couplings, etc.

The idea that different sources of diversity can produce a resonant effect leads us to speculate that the amount of diversity present in some biological systems has an important function. Diversity could have been evolutionary tuned in order to enhance the detection of weak signals. Whether natural systems have taken advantage or not from this diversity related effect is a question that, as in the particular case of stochastic resonance, has not yet a clear answer.

Chapter 9

System size and diversity in an opinion formation model

9.1 Introduction

It is nowadays well established that the stochastic terms (noise) in the equations of motion of a dynamical system can have a constructive effect leading to some sort of order. An example is the appearance of ordered phases in a scalar field theory when the noise intensity is increased [92, 122, 123]. The classical prototype is that of *stochastic resonance* [113, 17, 23, 25] by which an adequate value of the noise intensity helps to synchronise the output of a nonlinear dynamical system with an external forcing. Amongst other examples, that of *coherence resonance* shows again that the proper amount of noise helps to improve the regularity of the output of an excitable [74] or chaotic [124] system. Similar results have been referred to as *stochastic coherence* in [125] or *stochastic resonance without external periodic force* [126, 127]. In these examples, the subtle interaction between the nonlinear terms, the coupling (either internal or with an external source) and the noise produce the desired effect. Most of these previous works have considered the appearance of order as a result of tuning the noise intensity to its proper value, whereas the role of system size has been either neglected, or analysed in terms of standard finite-size theory for phase transitions [128].

A recent line of work, however, considers that the output of a nonlinear stochastic system can have a nontrivial dependence on its size (or number of constituents). Some recent work on biological models [129, 130, 131, 132] consider Hodgkin–Huxley type models to show that the ion concentration along biological cell membranes displays (intrinsic) stochastic resonance as well as coherence resonance as the number of ion channels is varied. These references also discuss the possible biological implications. A similar result [97] shows that in the absence of external forcing, the regularity of the collective output of a set of coupled excitable FitzHugh–Nagumo systems is

optimal for a given value of the number of elements. This is a *system size stochastic coherence* effect.

In social sciences, a usual ingredient that is often neglected is that of diversity: not all the individuals are alike. In view of the results obtained in chapter 8, it is interesting to investigate if an analogous phenomenon to diversity-induced resonance appears also in this system.

In this chapter we present an example of system size stochastic resonance in the field of the dynamics of social systems. Our objective is twofold. First, we want to show that the mechanism for system size stochastic resonance is generic and can appear in systems which are very far away from the original ones. We emphasise that system size in social systems plays an important role . For instance, there are examples which show that these systems may display phase transitions that *disappear* in the thermodynamic limit, instead of the other way around which is the usual effect [133]. Second, we study if diversity can play also a constructive role in this system, replacing the intrinsic randomness of this model.

The rest of the chapter is organised as follows: in the next section 9.2 we explain in some detail the model for opinion formation that we have considered in this work in the presence of randomness. The study of the effective noise intensity and a comparison with bistable systems is done in 9.2.2. Then, in subsection 9.2.3, we study the non-trivial system-size effects in this model. In section 9.3 we introduce a modification of the model in order to study the effects of diversity in this model. In the last section of this chapter presents the main conclusions.

9.2 System size stochastic resonance

In physical systems, *system size resonance* [134] has been found in the Ising model, as well as in a set of globally (or local) coupled generic (ϕ^4-type) bistable systems $(x_1, \ldots, x_N)$ under the influence of an external periodic forcing and uncorrelated Gaussian white-noises $\xi_i(t)$:

$$\dot{x_i} \;=\; x_i - x_i^3 + \frac{C}{N}\sum_{j=1}^{N}(x_j - x_i) + \sqrt{D}\xi_i(t) + A\cos(\Omega t) \qquad (9.1)$$

for $i = 1 \ldots N$. It is possible to understand in this case the origin of the resonance with the system size N, by deriving a closed equation for the collective (macroscopic) variable $m(t) = \frac{1}{N}\sum_{i=1}^{N} x_i$ as:

$$\dot{m} = F(m) + \sqrt{\frac{D}{N}}\xi(t) + A\cos(\Omega t), \qquad (9.2)$$

where $\xi(t)$ is a zero mean Gaussian white noise with correlation function $\langle \xi(t)\xi(t')\rangle = \delta(t-t')$. The rescaling by $N^{-1/2}$ of the noise intensity has a simple origin in the central limit theorem. The function $F(m)$ can be computed by using some approximations based on the strong coupling limit, and it can be shown that it still exhibits bistable behaviour [134, 97].

Equation (9.2) shows that the effective noise intensity, D/N, can be controlled both by varying the noise intensity D or the system size N. Hence, the optimal value of the effective noise intensity needed to observe stochastic resonance in the collective response $m(t)$ can be achieved by changing the system size N. It is then conceivable the following situation: let us start with a single system ($N = 1$) subject to an external perturbation and noise, such that the noise intensity is too large in order to observe any synchrony with the weak external forcing, and the jumps between the two stable states occur randomly. If we now couple together an increasing number N of these units, the effective noise for the global system will decrease as $N^{-1/2}$ and the global response to the external signal will be initially improved. Eventually, for too large N, the effective noise intensity will be very small and the system will be unable to follow globally the forcing. The possibility of having stochastic resonance for an optimal system size opens a wide range of applications in those cases in which it is not possible to tune the intensity of the noise at will, but it might be possible to change the number of coupled elements or the effective connections between them in order to obtain the best response.

9.2.1 Model studied

We have considered the model of opinion formation developed by Kuperman and Zanette [135] based on similar models by Weidlich [136]. In this model, the opinion is considered to be a binary variable, and we consider a set of $i = 1, \ldots, N$ individuals, each one having an opinion $\mu_i(t) = \pm 1$ at time t.

The opinion of an individual is not fixed and it can change due to three effects: (i) the interaction with the rest of the individuals, modeled by a simple majority rule; (ii) the influence of fashion, modeled as the effect of some external time varying agent (such as advertising) and (iii) random changes. The model first establishes the connections between the individuals by enumerating the set $n(i)$ of neighbors of individual i.

In order to better mimic the social relations between the individuals, we assume that they are located in the sites of two particular types of network: First, a small-world network[110], constructed as follows: the $i = 1, \ldots, N$ individuals are regularly spaced in a linear chain such that site i is initially linked to the $2k$ nearest sites (we assume periodic boundary conditions). Each individual is then visited sequentially and with probability p_{sw} one of the links to its set of k_{sw} right near neighbors is randomly replaced by a link with a randomly chosen site. Double and multiple connections are

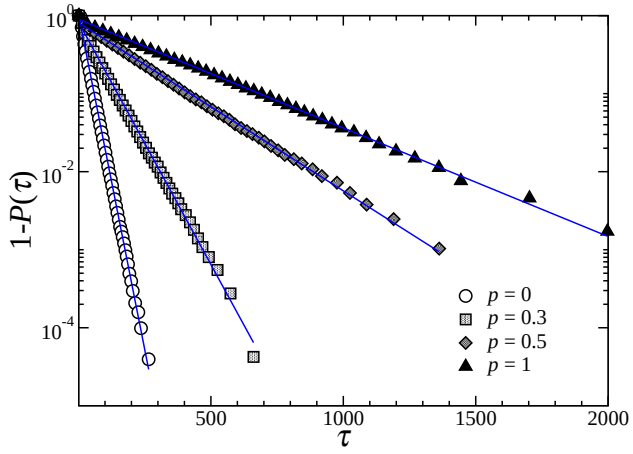

Figure 9.1: Here we plot the complementary of the cumulative probability distribution of residence times. $1 - P(\tau)$, of the opinion formation model. Since it is an exponential, also the residence time distribution $p(\tau)$ is also an exponential. The parameters are $k_{sw} = 2$, $N = 100$ and $\gamma = 0.25$; the different symbols correspond to various rewiring probabilities p_{sw}, ranging from a regular network (circles) to a fully random (triangles).

forbidden, and realizations where the network becomes disconnected are discarded. In this way, the new set of neighbors $n(i)$ of site i, while still keeping an average size of $2k_{sw}$, includes links to very far away sites. The *re-wiring parameter* p_{sw} and the *connectivity parameter* k_{sw} characterise the small-world network.

Beyond the small-world behaviour, another important ingredient of interaction networks is that they often display a scale-free degree distribution. We then also study the results of this model when the topology of interactions is not a regular one, but a scale-free one. As the model for the generation of the network, we use the Barabási–Albert algorithm [137], generated as follows: starting from a fully connected network of size m, at time t a node is added, and attached to m existing nodes, where the probability to be attached to a node is proportional to its degree. This algorithm generates networks with power-law degree distributions with an exponent $\gamma = 3$.

The three effects mentioned above in the evolution of the opinion are precisely implemented as follows: assign at time $t = 0$ random values $\mu_i = \pm 1$ to each individual; then at a given time t the next three steps are applied consecutively:

(i) Select randomly one individual i and let it adopt the majority opinion favoured by the set $n(i)$ of its neighbors, i.e. $\mu_i(t) = \text{sign}\left[\sum_{j\in n(i)} \mu_j(t)\right]$;

if $\sum_{j\in n(i)} \mu_j(t) = 0$ then $\mu_i(t)$ remains unchanged.

(ii) With probability $A|\sin(\Omega t)|$, set $\mu_i(t) = \text{sign}\,[\sin(\Omega t)]$.

(iii) With probability γ, let μ_i adopt randomly a new value ± 1, independently of its present value.

After these three steps have been performed, time increases by a fixed amount $t \to t + 1/N$. This is chosen such that after one unit of time every individual has been updated once on the average.

The parameter A ($0 \leq A \leq 1$) measures the strength of the fashion and Ω its frequency. The last step (iii) introduces noise in the evolution. In order to define a noise intensity D related to the flip rate γ, we consider the model without the effect of fashion (step ii). This is equivalent to setting $A = 0$.

As a measure of the system response to the external stimulus, we compute the spectral amplification factor (for more details, see section 2.2.3), defined as $\eta = 4A^{-2}\left|\langle e^{i\,2\pi t/T} m(t)\rangle\right|^2$, where $m(t)$ is the time-evolution of the average opinion

$$m(t) = \frac{1}{N}\sum_i \mu_i(t) \tag{9.3}$$

and $\langle \ldots \rangle$ denotes a time average. This is known to be a good measure of the response of the system to the forcing signal [119].

9.2.2 Effective noise intensity

In figure 9.5 (panel a) we plot the time dependence of the average opinion $m(t)$. This figure clearly shows that the system behaves as bistable, jumping randomly around the two bistable states which are close to $m = \pm 1$. These random jumps are induced by the noise introduced in step (iii) of the evolution and occur more frequently for large flip rate γ. This picture of a bistable system whose jumps between the stable states are induced by noise is consistent with the fact that, as shown in figure 9.1, the residence time probability in each of the stable states follows the exponential Kramer's law:

$$p(\tau) = \tau_0 e^{-\tau/\tau_0} \tag{9.4}$$

being τ_0 the mean residence time [38]. The dependence of τ_0 in the flip rate γ and the system size N can be seen in figure 9.2.

The next step is to define a noise intensity D by using Kramer's formula, valid for small noise intensity,

$$\tau_0 = \tau' e^{\Delta V/D} \tag{9.5}$$

being ΔV the height of the barrier between the two stable states. As shown in figure 9.2(b), this barrier height increases with the number of individuals

$\Delta V = N\Delta v$ with $\Delta v = \mathcal{O}(N^0)$, as expected. Thus, a simple fitting procedure allows us to obtain the rescaled noise intensity $D^* = D/\Delta v$. This is plotted in figure 9.3 as a function of the flip rate γ.

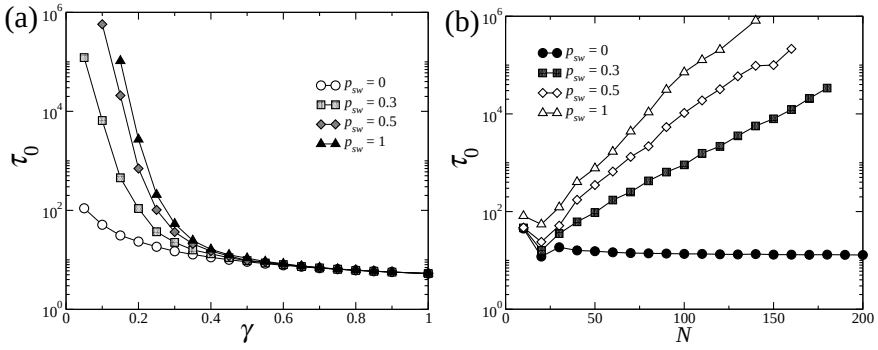

Figure 9.2: (a) Mean residence time τ_0 as a function of the flip rate γ for a system with size $N = 100$ and different values of rewiring probability p_{sw}. (b) Mean residence time τ_0 as a function of system size N for $\gamma = 0.2$ and different values of the rewiring parameter p_{sw}. In both cases, other parameters are $A = 0$, $k_{sw} = 3$.

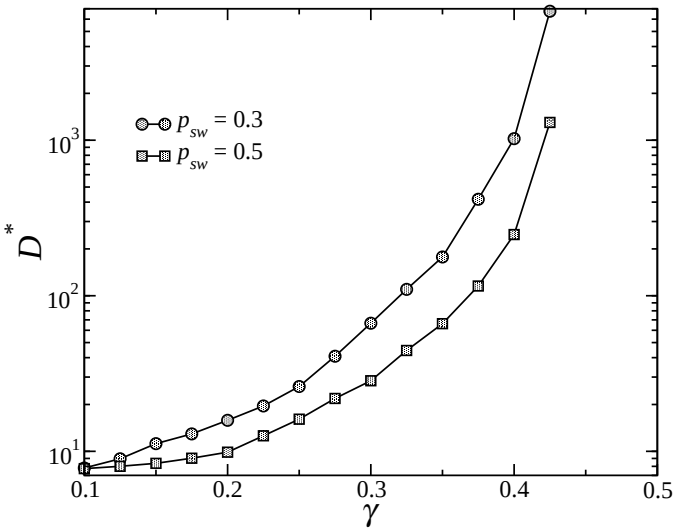

Figure 9.3: The rescaled noise $D^* = D/\Delta v$ (see inline text for details) as a function of flip rate γ for different values of the re-wiring parameter p_{sw} and $k_{sw} = 3$. The functional dependence is found to be faster than an exponential.

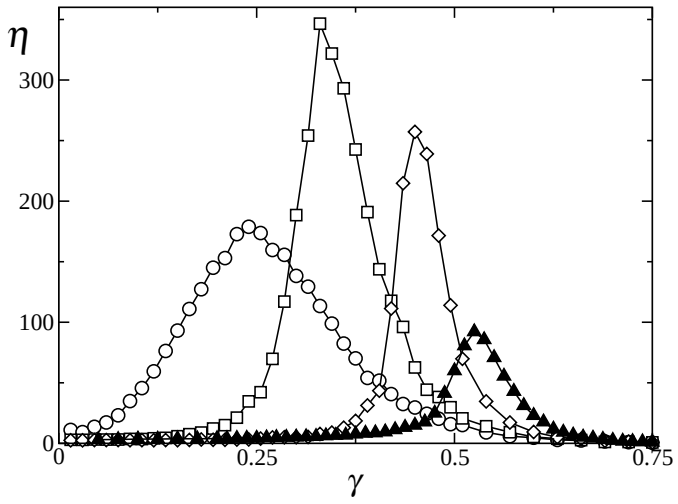

Figure 9.4: We plot the system response (measures through the spectral amplification factor η) for different network topologies in the Kuperman–Zanette model for opinion spreading as a function of the strength of the random term γ. The curves with white symbols correspond to small world networks with $k_{sw} = 3$, and $p_{sw} = 0$ (circles), $p_{sw} = 0.20$ (squares) and $p_{sw} = 1$ (which corresponds to a fully random network, with diamonds). The black triangles correspond to a Barabási–Albert scale free network, with $k_{BA} = 3$. The lines are only a guide for the eyes. The system parameters are $N = 2 \times 10^2$, $T_s = 128$, $\epsilon = 0.02$.

9.2.3 System size effects

In the previous section we have shown that the opinion formation model considered is consistent with the picture of a bistable system with jumps between the two opinion states induced by the noise. In this section we turn our attention to the effect that the fashion, modeled as a periodic external signal, $A > 0$, has on the system. In particular, we ask ourselves the question of on which conditions the average opinion follows the fashion. Since the necessary ingredients are present in this model, it should not come to a surprise that this model displays stochastic resonance, as first shown in [135]. A similar result was also found in [138] for the original Weidlich model. The evidence is given in figures 9.4 which show that, for fixed values of N, the correlation between the majority opinion and the fashion is maximum for the proper value of the flip rate γ. In these figures we plot the signal to noise ratio as a function of the flip rate γ. In order to get a cleaner result, and as in other applications of stochastic resonance [17], we have first filtered the original signal into a binary valued time series $s(t) = \text{sign}\,[m(t)]$. We then

look at the power spectrum $S(\omega)$ of the time series of $s(t)$ and compute the signal to noise ratio in the standard form as the area above the background of $S(\omega)$ at the external frequency value $\omega = \Omega$.

According to the general discussion in the introduction, we expect that the system will display as well stochastic resonance as a function of the number N of individuals. This expectation is evidently fulfilled if one looks at the series of figures 9.5. For small value of N (upper figure), the average opinion $m(t)$ behaves rather erratically and independent of the periodic variation of the fashion. For a very large value of N (lower figure), the average time between jumps is very large and, again, basically independent of the periodic variation of the fashion. It is only for an intermediate value of N (middle figure) that the jumps between the two opinion states are correlated with the fashion. This result is also observed in the set of figures 9.5 which plot the power spectrum $S(\omega)$ coming from the corresponding time series. It is apparent in these figures that the signal to noise ratio first increases and then decreases when the number N grows.

This main result is more clearly shown in figure 9.6 where we plot the signal to noise ratio as a function of the system size N for different values of the flip rate. In each of the cases, it can be seen that there is an optimal value N^* for which the signal to noise ratio takes it maximum value, indicating a maximum correlation between the average opinion and the fashion. Qualitatively, these results are independent of the exact network topology, as can be seen in the same figure, where all the curves show a clear maximum for intermediate system-sizes. Of course, the exact value of the optimal size does depend on the network structure.

For the particular case of the small-world network, the value of N^* is plotted in figure 9.7 as a function of the flip rate γ. It is possible to see the strong dependence of this value with the value of the noise strength η.

9.3 The effects of diversity

9.3.1 Model considered

We now turn our attention into the effects of diversity on this model. From the three rules defining the dynamics of the system, the third rule is assimilable to a noise term: it corresponds to the random changes in the opinion of the individual. In order to isolate the effects of diversity, we will not apply this rule along this section, but only a modified version of the first two.

We will consider that each individual has a tendency to favour one opinion over the other. This is some kind of *preference* to adopt an opinion different to the one is biased to. This tendency, however, is stronger in some individuals with respect to others. Let θ_i, be a constant parameter drawn from a probability distribution $g(\theta)$, verifying $\langle \theta_i \rangle = 0$, $\langle \theta_i \theta_j \rangle = \delta_{ij}\, \sigma^2$. We now define that the dynamics of the model are given by the following rules

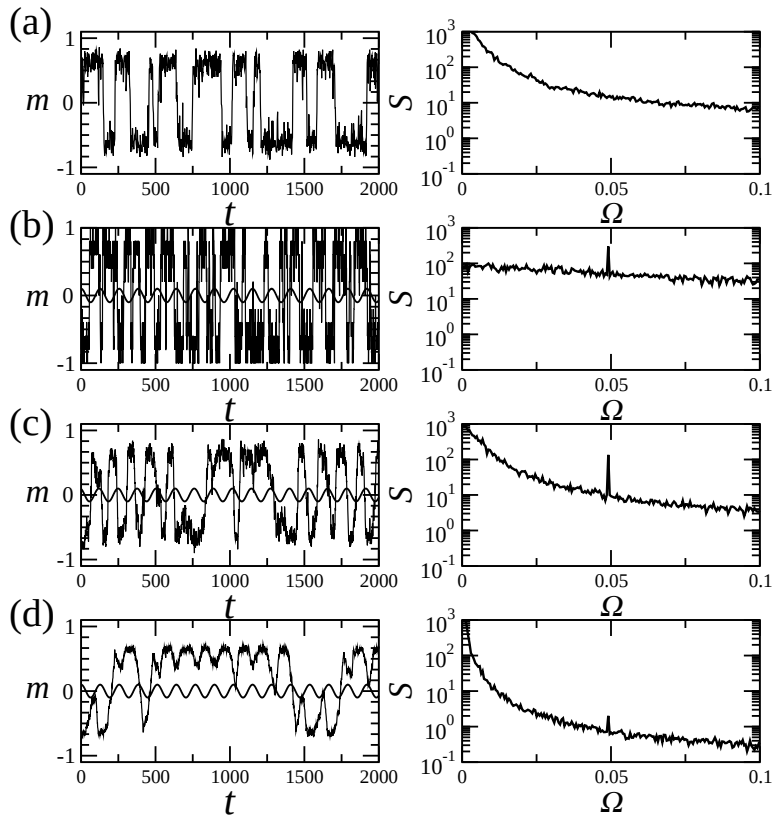

Figure 9.5: We plot the time-evolution of the average opinion as a function of time (left column), and the power spectral density S (right column). The first row (a) shows the dynamics in absence of an external influence $\epsilon = 0$ in the case $N = 100$. The last three rows, shows the results for different system sizes: $N = 10, 100, 1000$ (b, c, and d, respectively). The external signal (the sinusoidal thin line in the evolution plots) has a period $T = 128$. Note that this signal is better followed by a system with an *intermediate* size (panel c). This is also signalled by the largest peak of the spectral density at the driving frequency: $\Omega = 2\pi/128$.

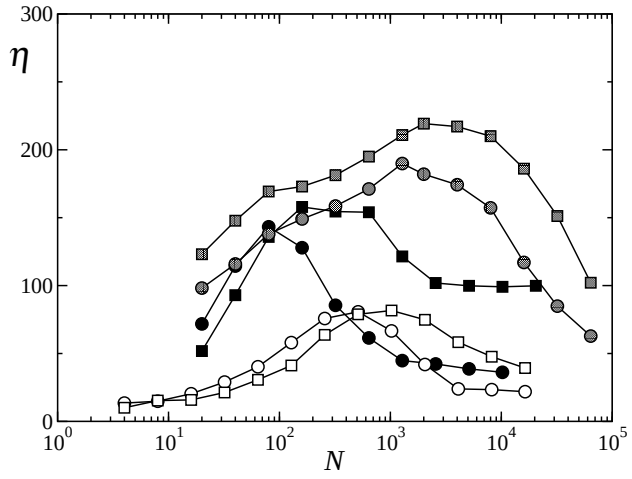

Figure 9.6: Spectral amplification factor as a function of system size, N for different network topologies: gray symbols show the results for a small-world network ($p_{sw} = 0.2$, $k_{sw} = 3$, $\gamma = 0.26, 0.28$), black symbols for a random network (a small world with $p_{sw} = 1$ and $k_{sw} = 3$, $\gamma = 0.40, 0.41$) and white symbols display the results for a Barabási–Albert network ($k_{BA} = 3$, $\gamma = 0.56, 0.57$). In all the plots it is apparent an optimum response for an intermediate system size. The system parameters are as in the previous figures.

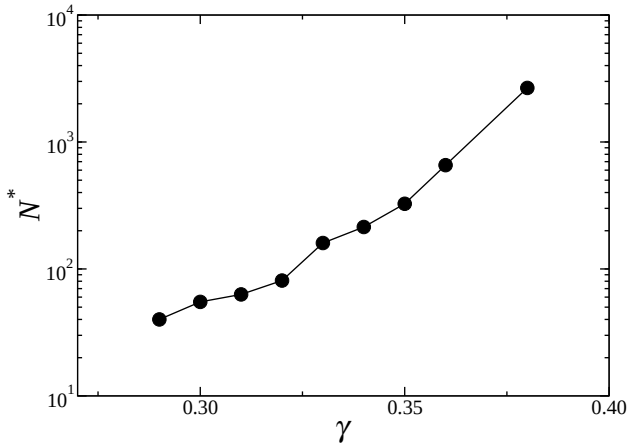

Figure 9.7: The optimum value N^* as a function of the flip rate γ. Same parameters as is figure 9.5. It is observed that the optimum value for system size depends exponentially with the parameter γ.

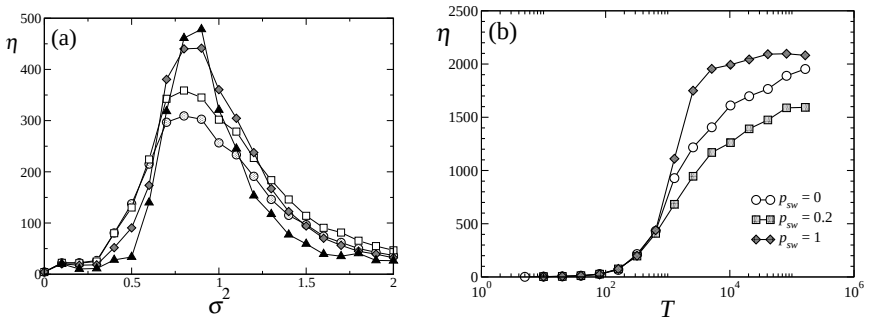

Figure 9.8: (a) Spectral amplification factor as a function of the diversity σ^2 for different values of the parameter α, that measure the relative weight of the preference with respect to the signal. The network topology is kept fixed: all the curves correspond to a small-world network ($p_{sw} = 0.2$, $k_{sw} = 2$). The different symbols represent: $\alpha = 0$ (gray circles), 0.2 (white squares), 1.0 (dark gray diamonds) and 2.0 (black triangles). All the curves show an optimum response for an intermediate value of diversity. (b) System response as a function of time periodicity of the signal, for different network topologies and $\alpha = 1$. In both panels, the signal has an intensity $A = 0.02$, frequency $\Omega = 2\pi/512$; the system size is $N = 10^3$.

(i) Select randomly one individual i, and let it adopt the majority opinion favoured by the set $n(i)$ of its neighbors, if it exceeds his preference θ_i i.e.

$$\mu_i(t) = \text{sign}\left[\sum_{j\in n(i)} \mu_j(t) + \theta_i\right].$$

In case of $\theta_i > 0$ ($\theta_i < 0$), the individual will be more akin to adopt the $+1$ (respectively, -1) opinion. No normalisation is considered when comparing the neighbour's opinion and the individual's tendency.

(ii) With probability $A|\sin(\Omega t) + \alpha\,\theta_i|$, the opinion of the individual is set to $\mu_i(t) = \text{sign}\,[\sin(\Omega t) + \alpha\,\theta_i]$. Note that the preference of the individual acts also in this rule, i.e.: the fashion is taken with more probability if it is the same as its favoured opinion. The parameter α is a scaling factor.

For a given network of connectivities, these two rules define probabilistic dynamics. Once again, the neighbours are drawn from a small-world network, as in the previous sections, although the same results are found for different topologies.

9.3.2 Results

When considering this modified version of the model, there is not an equivalent of the mean first passage time. In absence of the external signal, this model rapidly reaches a steady state, in which the global opinion does not evolve anymore.

Figure 9.8(a) shows the results for the spectral amplification factor η as a function of diversity σ^2, for different values of α, which determines the relative importance that preference has with respect to the external signal. The main result observed in this plot is a clear maximum in the system response for intermediate values of diversity. The reason can be found in the analogy with a system composed by interacting diverse bistable units (studied in chapter 8). In this opinion formation model, each unit is bistable, and the preference θ_i breaks the symmetry with respect to the possibility of choosing one or other opinion. In the same figure, it is apparent that for larger α, the system response becomes larger, but it is also more sensitive to the values of σ^2, shown by the fact that the peak of large system response is sharper.

The system response increases with increasing period of the signal. In this discrete model, this is due to the fact that slower signals allow units with a given bias more akin to adopt its favoured opinion.

With respect to the network topology, the dependence is similar to what was observed in presence of random flippings: For more disordered networks (i.e. for larger values of p_{sw}, closer to a fully random network), the width of the peak in the η versus σ^2 decreases. This is because for smaller values of p_{sw}, it is easier for the system to grow domains of a given opinion in a linear way. Highly random systems respond like in a mean field approach and, for small values of diversity, are not able to make the system jump betweek minima following the external signal.

9.4 Conclusions

In conclusion, we have considered a model for opinion formation. The model incorporates three basic ingredients for the evolution of the opinion held by an individual: imitation, fashion and randomness. We have shown that in the absence of fashion, the model behaves as a bistable system with random jumps between the two stable states with a distribution of times following Kramers' law. We have used this image to compute the noise intensity as a function of the flip rate. Finally we have shown the existence of system size stochastic resonance, by which there is an optimal value for the number of individuals N for which the average opinion follows better the fashion. This result indicates that the response of a social system to an external forcing agent depends in a non trivial manner of the number of constituents, a feature already observed in other different models for social behaviour.

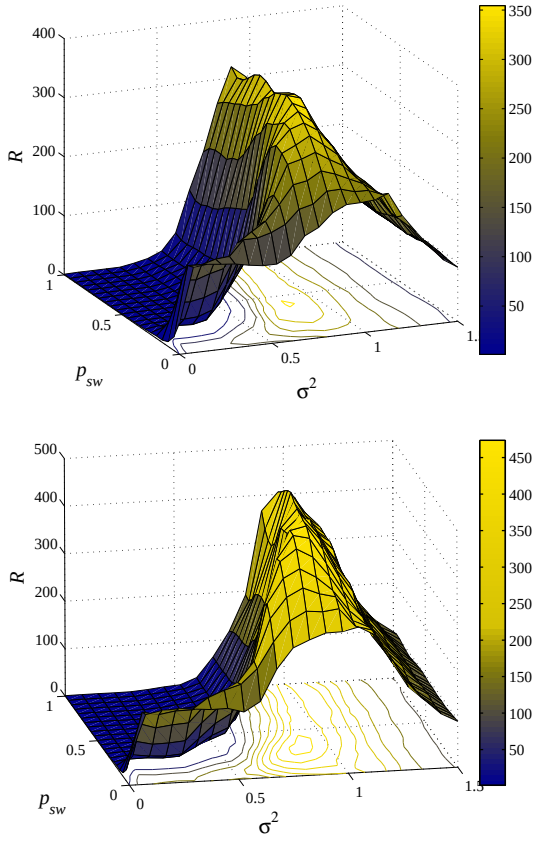

Figure 9.9: System response as a function of diversity, σ^2, and the rewiring probability p_{sw} for two different values of the parameter α: $\alpha = 0$ (upper panel), and $\alpha = 1$ (lower panel). It is apparent that, regardless the exact network topology, the effect of diversity-induced resonance appears in the system, showing the existence of an optimum synchronisation between the external signal and the global dynamics of the system. The signal applied has an intensity $A = 0.02$, its frequency is $\Omega = 2\pi/512$ and the system size is $N = 10^3$.

We have also shown that a better synchronisation with respect to the external signal can be achieved if diversity (understood as a tendency of each individual to favour one opinion over the other) is considered in the model instead of random changes. The result is another example of the *diversity-induced resonance*, introduced in chapter 8: in this model, each agent having a bias is equivalent to the asymmetric potentials for the individual units in the ϕ^4-model.

Chapter 10

Noise-induced inhibitory suppression

10.1 Introduction

Excitable systems are widespread in nature. In many cases, excitability originates from the existence of a bifurcation to an oscillatory state when a control parameter is changed. Prominent examples are some varieties of cells (such as neurons, pancreatic β-cells, nerve cells from sensitive regions of the body), cardiac tissue, chemical reactions (Belousov–Zhabotinskii), etc. (for a comprehensive review on this subject, see ref. [42]). Most excitable systems require two types of dynamical variables (called generically activator and inhibitor) with different time-scales and different influence on the overall behaviour of the system. Stochastic effects, in the form of white noise or diversity, are also an important ingredient of the dynamics. The dynamics of oscillatory and excitable systems near the bifurcation attracts large interest because in this region their sensitivity is greatest and they are suitable for a reliable signal response or information exchange. The study of coherence resonance [139, 74] (also named as stochastic coherence [125]) and stochastic resonance in nonlinear excitable units [140, 30, 141, 42] arose a strong interest on this field.

Of particular interest is the study of coupled excitable systems. Usually, only coupling through the activator variables is considered, leading to a full synchronised dynamics [76]. In this work, we focus our attention on an array of noisy excitable units coupled through the inhibitory variables. Such a kind of coupling can be realized for instance by a negative coupling constant in an activator variable or by a positive one in an inhibitory variable. Previous work has shown that coupling through the inhibitor variable between identical oscillators may induce many limit cycles of different periods and phase relations [142, 143] which are stable in large regions of the control parameter space, a behaviour usually referred to as "de-phasing"

[144, 145] or "phase-repulsive" [146] interaction and which was shown to be a source of multi-rhythmicity in different systems [147, 148, 149, 150]. With noisy elements, a de-phasing interaction of stochastic limit cycles (instead of deterministic ones) may result in the coexistence of spatiotemporal regimes selectively sensitive to external signal periods. In such systems, noise plays at least two roles: first, it stimulates firing of stable elements and, thereby, their interaction during return excursions; second, it stimulates transitions between coupling-dependent attractors if the associated lifetime is sufficiently long.

In this chapter, we extend our research on the influence of inhibitory coupling. In contrast to our previous investigation of frequency selective stochastic resonance in linear chains of identical excitable FitzHugh–Nagumo models [121, 151], we consider chains of nonidentical units and focus on the influence that the internal oscillatory units have on the dynamics of the whole chain. Under the presence of an external signal, we find the counter-intuitive result that inhibitory coupling can lead to a multi-rhythmic state in which the intermediate oscillatory units are in the rest state, while the excitable ones oscillate in synchrony with the signal. This implies that the intermediate units, while "silent", are still able to transmit the information along the chain. As discussed at the end of the chapter, inhibitory coupling is of relevance for some chemical [152, 153, 154] and biological [155] systems and our results point to a generic mechanism of oscillation supression and information transmission. For the sake of simplicity, however, we have only considered a prototype excitable model (the FitzHugh–Nagumo set of equations, also called the Bonhoeffer–van der Pol model [44]). In the next section we present the main result in the simplest case of three FitzHugh-Nagumo units coupled through the inhibitory variable. To extend the study onto another architecture, in section 10.3, we analyse an array where two coupled oscillating units are connected from both sides with excitable elements. Our study ends in section 10.4 with some general conclusions and some speculations about possible applications in biological systems.

10.2 Three non-identical inhibitory coupled units

We consider a rather simplistic model with a minimal scheme of connections that can retain the basic structure of the system we want to study: an open, linear chain where both ends have an excitable unit. The middle unit represents an oscillatory unit (fig. 10.1). We want to study whether a periodic, subthreshold signal, acting on the left element can reach the right one, in such a way that no oscillations appear in the middle unit.

The scheme in fig. 10.1 corresponds to three FitzHugh–Nagumo oscilla-

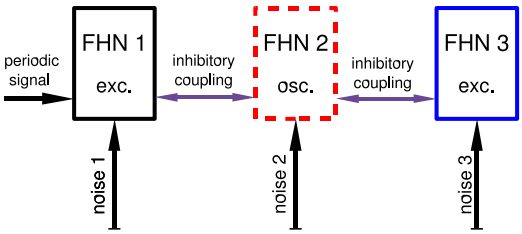

Figure 10.1: Scheme of the setup for the case $N = 3$. At both ends there are excitable units, coupled through inhibitor coupling to the middle (oscillatory) element.

tors coupled through the inhibitory variables:

$$\begin{aligned}
\epsilon \dot{x}_1 &= y_1 - \frac{x_1^3}{3} + x_1 && (10.1)\\
\dot{y}_1 &= a_1 - x_1 + \sqrt{D}\xi_1(t) + A_s \sin(\Omega t) + C_y(y_2 - y_1)\\
\epsilon \dot{x}_2 &= y_2 - \frac{x_2^3}{3} + x_2 && (10.2)\\
\dot{y}_2 &= a_2 - x_2 + \sqrt{D}\xi_2(t) + C_y(y_1 - y_2) + C_y(y_3 - y_2)\\
\epsilon \dot{x}_3 &= y_3 - \frac{x_3^3}{3} + x_3 && (10.3)\\
\dot{y}_3 &= a_3 - x_3 + \sqrt{D}\xi_3(t) + C_y(y_2 - y_3).
\end{aligned}$$

Where $\Omega = 2\pi/T_s$, is the frequency of the input signal with period T_s. The Gaussian (white) noise sources $\xi_i(t)$ satisfy $\langle \xi_i(t)\xi_j(t')\rangle = \delta(t-t')\delta_{i,j}$.

In a neural context, $x_i(t)$ represents the membrane potential of the neuron and $y_i(t)$ is related to the time-dependent conductance of the potassium channels in the membrane [68]. The dynamics of the activator variable x_i is much faster than that of the inhibitor y_i, as indicated by the small time-scale ratio parameter ϵ. It is well known that for $|a_i| > 1$ a single unit has a stable fixed point and presents excitable behaviour: small perturbations are followed by a smooth return to the fixed point, while a perturbation larger than a threshold value induces a return through a large excursion in phase space (a spike). For $|a_i| < 1$, the fixed point becomes unstable and a stable limit cycle appears. In this regime, the dynamics consists in a periodic series of spikes. Along this section, we will consider the fixed parameters: $\epsilon = 10^{-4}$, $a_1 = a_3 = 1.01$ and $a_2 = 0.99$, such that the two end units are excitable and the middle one, oscillatory. We have checked that (in the absence of external forcing and noise) the three units retain their excitable or oscillatory character despite the coupling amongst them, such

that the middle unit spikes periodically and the two end units display small subthreshold oscillations around the fixed point.

The issue now is the behaviour of these same units when noise and external forcing are present. We will show that it is possible to have a noise-induced regime in which the oscillations of the middle unit are suppressed. Most of our results come from a numerical integration of the previous equations using a stochastic Runge–Kutta-type method known as the Heun algorithm [123]. To characterise this phenomenon of oscillation suppression, we have computed $N_s^{(i)}$, the number of spikes per time unit at the $i-$th neuron, defined as the number of times the variable $y_i(t)$ surpasses a fixed threshold per time unit. $N_s^{(i)}$ represents the reciprocal of the averaged inter-spike time interval.

An important point is whether in this oscillation suppression regime, noise can help to transmit the information of the subthreshold external signal by a stochastic resonance mechanism. In order to address this issue, we compute the linear response, $\eta^{(i)}$, of the $i-$th neuron in the chain at the input frequency Ω [17, 156] (see also section 2.2.4 for a throughout definition of this measure):

$$\eta^{(i)} = \left|\langle 2y_i(t)\, \mathrm{e}^{\imath\,\Omega t}\rangle\right| / A_s^2, \tag{10.4}$$

where $\langle \ldots \rangle$ denotes a time average.

10.2.1 Oscillation suppression via a noise-induced dynamical trap

In a previous work [157] it has been shown that in a system of three FitzHugh–Nagumo units in the oscillatory regime (and in the absence of external forcing) the inhibitory coupling leads to two coexisting dynamical attractors, with different natural frequencies. These attractors correspond to an anti-phase oscillator movement and to the so-called *dynamical trap regime* where the middle oscillator is at rest and the two oscillators at the ends oscillate in anti-phase. If one now applies a weak external periodic signal to one of the end units and uncorrelated noise to every unit, one can still achieve the suppression of the self-excited oscillations of the middle unit and, at the same time, achieve a reliable transmission of the signal, provided the following two conditions hold: (i) the frequency of the external signal coincides with the natural frequency of the dynamical trap attractor, and (ii) the noise in the system is near the optimal one for the desired signal amplification (i.e. stochastic resonance phenomenon on this attractor).

A similar result appears in our system of three coupled units. For very small noise, the situation is as described at the beginning of the section with the middle unit oscillating and the end units at rest. As noise increases, one observes random switches between this state and a dynamical trap regime in which the middle unit is at rest and the two end units spike in anti-phase.

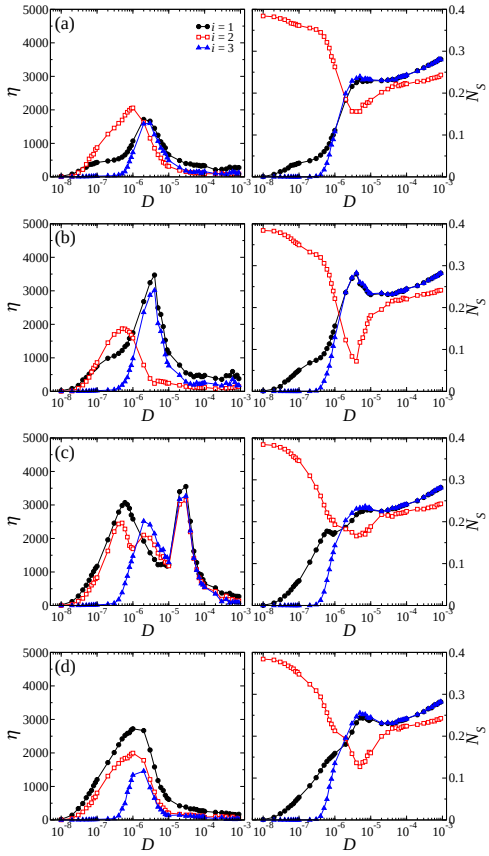

Figure 10.2: Optimal noise suppresses oscillations while letting the signal (within a certain range) to be transmitted. This effect occurs due to dynamical trap, supported by inhibitory coupling. (a) non-resonant, $T_s = 2.8$; (b) dynamic trap, $T_s = 3.1$; (c) anti-phase resonance, $T_s = 4.5$; (d) no resonance, $T_s = 6.0$. Other parameters: $\epsilon = 10^{-4}$, $a_{1,3} = 1.01$, $a_2 = 0.99$, $A_s = 0.01$, $C_y = 0.15$. The left and right columns correspond to the η and N_s measures.

This effect can be quantified by measuring the number of spikes $N_s^{(i)}$ and the responses $\eta^{(i)}$ as a function of the noise intensity. As shown in figs. 10.2, one can distinguish several behaviours depending on the period of the external forcing.

(a) This is the case where the period of the input signal equals the natural period of an isolated FitzHugh–Nagumo oscillator ($T_s = 2.8$ for $a = 0.99$). The noise-induced oscillation suppression described before is apparent in the right panel of this figure, where it is shown that the number of spikes

at the middle unit, $N_s^{(2)}$, first decreases as the noise intensity increases. This oscillation suppression is maximum at a value of the noise intensity, $D \approx 3 \cdot 10^{-6}$. At noises larger that this value, the number of spikes in the three units are very close to each other.

In the left panel we plot the response $\eta^{(i)}$ of each unit. Note that there is a range of values for the noise intensity for which the middle unit responds to the injected signal most effectively than the end units, as signalled by a higher value of the response $\eta^{(2)}$. For increasing noise intensity, beyond the value where the oscillation suppression was maximum, all units have a similar response.

(b) For an intermediate range of periods $T_s \in [3, 3.4]$, we observe that there exists a range of noise intensities ($D \in [10^{-6}, 10^{-5}]$) such that the number of spikes is strongly reduced in the middle oscillatory unit, while the response to the driving frequency is better than in the oscillatory unit, i.e. this is the manifestation of the *dynamic trap regime*. One can clearly see the effective oscillation suppression of the oscillatory middle element (see fig. 10.2(b), right panel) and –despite of this suppression in the middle of the chain– the reliable information transport from the first to the last unit by a large linear response η in these elements (fig. 10.2(b), left). The dynamic trap regime includes an anti-phase motion of the first and the last units which results in combination with the inhibitory coupling in a suppression of the oscillations of the middle element.

(c) Increasing even further the period, $T_s = 4.5$, the external signal is now in resonance with, and hence amplifies, the anti-phase motion in which the first and the last units oscillate in-phase and in anti-phase with the middle one. In this case, another interesting regime appears in the noise range $D \in [10^{-5}, 10^{-4}]$ as observed in the right panel of fig. 10.2(c), where the spike numbers of all three elements coincide nearly, as well as in the linear response plot (left panel), where all oscillators display a very similar linear response η. This anti-phase regime demonstrates a totally different behaviour than the dynamic trap regime, case (b) discussed previously. Note that the anti-phase regime appears for a much larger noise intensity than the dynamic trap regime, hence showing a double selectivity by the input frequency and the noise intensity.

(d) Finally, for much larger period, $T_s = 6.0$, there is no resonance, figs. 10.2(d). This can be observed especially at the linear response η (left panel) which is much smaller than in the resonant cases. Noteworthy, the last element in the chain exhibits a poor signal response.

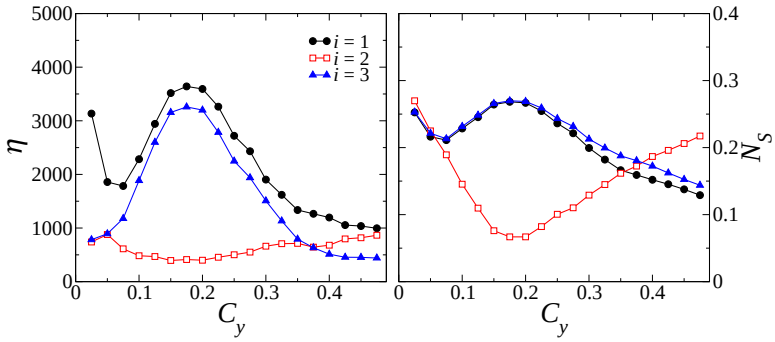

Figure 10.3: Linear response η (left), and normalised spike number N_s (right), versus inhibitory coupling strength. The other parameters are: $\epsilon = 10^{-4}$, $a_{1,3} = 1.01$, $a_2 = 0.99$, $A_s = 0.01$, $T_s = 3.1$ and $D = 3 \cdot 10^{-6}$.

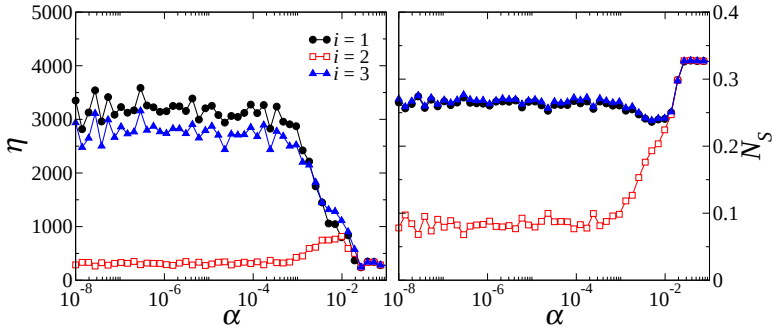

Figure 10.4: The influence of the type of coupling on the linear response η (left) and the normalised spike number N_s (right) for three coupled FitzHugh–Nagumo's. The sliding parameter α shifts the weight of the diffusion constant C_y from a pure inhibitory coupling ($\alpha = 0.0$) to a pure activator coupling ($\alpha = 1$). The other parameters are $\epsilon = 10^{-4}$, $a_{1,3} = 1.01$, $a_2 = 0.99$, $D = 4 \cdot 10^{-6}$, $A_s = 0.01$, $T_s = 3.1$ and $C_y = 0.15$.

10.2.2 Control of suppression by the coupling strength

Noise-induced dynamical trap suppression is made possible by the existence of a new attractor originated in the inhibitory nature of the coupling. Hence, the coupling intensity, C_y, controls the effectivity of the suppression, as well as the frequency of the attractor. The existence of an optimal value for C_y is shown in fig. 10.3, in which we plot the linear response η and the spike numbers N_s as a function of the coupling intensity. Setting the noise intensity D to the value of maximum of the linear response η (fig. 10.2(b), left panel), and varying the strength C_y of the inhibitory coupling, it is clear

the existence of an optimal C_y such that the middle unit is silent (fig. 10.3 right panel), while the first and last units effectively respond to the driving frequency (fig. 10.3 left panel).

Since both types of coupling, inhibitory and activator, can be immanent in neural networks, we have investigated how the suppression can be regulated if we tune the coupling from an activator to an inhibitory one. To do this, we have added activator coupling in the model by interchanging C_y by $(1-\alpha)C_y$ in the equations for the inhibitory variable y_i and inserting the terms $\alpha C_y\,(x_2 - x_1)$ in equation (10.1), $\alpha\,C_y\,(x_1 - x_2) + \alpha C_y(x_3 - x_2)$ in eq. (10.2) and $\alpha C_y(x_2 - x_3)$ in eq. (10.3). These extensions of the model are used only in this section for the calculation of fig. 10.4. With help of the new sliding parameter α we change the weight of the type coupling from $\alpha = 1$ (pure activator coupling) to $\alpha = 0$ (pure inhibitory coupling). The results are illustrated in fig. 10.4. We clearly see that increasing the weight of the inhibitory coupling (from right to left) leads to an abrupt suppression of the middle oscillator (fig. 10.4 right) and to a significant joint increase of the linear response η of the first and third oscillators, but not of the middle one (fig. 10.4 left). Note the logarithmic scaling of the parameter α at the abscissa. We clearly observe, that already a small fraction of activator coupling (in the order of 1%) destroys the dynamic trap regime in the given parameter set.

10.3 Four non-identical inhibitory coupled units

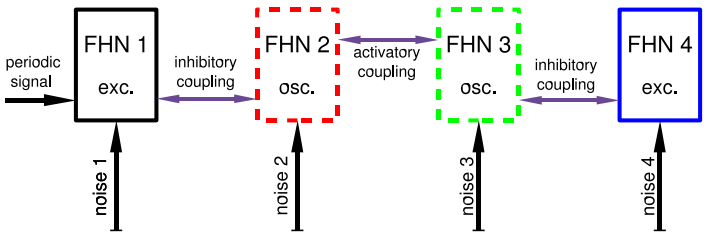

Figure 10.5: Scheme of the setup for the case $N = 4$. While at both ends there are excitable units, in the centre there are oscillatory ones. The coupling between units of different nature is inhibitory, and the coupling between the oscillatory units is through the activator variable.

Next we consider the question of whether larger chains with more coupled oscillatory units also show the same phenomenon discussed in the previous section. Although it would seem a rather trivial proposal just to enlarge it to a case in which the system size is $N = 4$, the dynamical regimes that

arise in such situation are far from being simple modifications of the results shown above.

We will not consider an enlargement of the excitable ends of the chain, because it is a well known fact that coupling them through the activator variable with a strong enough bind, will result in an entrainment of such subchain and the dynamical evolution of such units will be effectively that of one oscillator. Then, the most interesting question arises from the enlargement of the middle part, that is composed by oscillatory units. So, we add to the scheme of three elements (fig. 10.1) an oscillatory element in the middle position and couple it by an activator coupling with the other (identical) oscillatory element and with an inhibitory coupling to the adjacent excitable element (fig. 10.5).

The mathematical description of the scheme in figure 10.5 is given in eqs. (10.5) 10.8. The two oscillatory units are placed at the middle position and are both coupled to their adjacent excitable one by an inhibitory coupling as in the chain of three elements, whereas an activator coupling is set between them. As in the previous section, independent additive white noises act on the units and an external, subthreshold, periodic signal drives only the first element:

$$\begin{aligned}
\epsilon\,\dot{x}_1 &= y_1 - \frac{x_1^3}{3} + x_1 && (10.5)\\
\dot{y}_1 &= a_1 - x_1 + \xi_1(t) + A_s \sin(\Omega t) + C_y(y_2 - y_1)\\
\epsilon\,\dot{x}_2 &= y_2 - \frac{x_2^3}{3} + x_2 + C_x(x_3 - x_2) && (10.6)\\
\dot{y}_2 &= a_2 - x_2 + \xi_2(t) + C_y(y_1 - y_2)\\
\epsilon\,\dot{x}_3 &= y_3 - \frac{x_3^3}{3} + x_3 + C_x(x_2 - x_3) && (10.7)\\
\dot{y}_3 &= a_3 - x_3 + \xi_3(t) + C_y(y_4 - y_3)\\
\epsilon\,\dot{x}_4 &= y_4 - \frac{x_4^3}{3} + x_4 && (10.8)\\
\dot{y}_4 &= a_4 - x_4 + \xi_4(t) + C_y(y_3 - y_4)
\end{aligned}$$

We will fix along the following simulations the parameters: $a_{2,3} = 0.99$ (oscillatory regime), $a_{1,4} = 1.01$ (excitable regime) and the signal intensity $A_s = 0.01$ (subthreshold).

We are interested in the signal penetration along the chain from the first to the last element as a function of the signal period and the noise intensity. In order to investigate whether the same phenomenon appears in this chain, two different cases are considered: first, we take the optimal parameters from the case $N = 3$ and make the coupling between the oscillatory units strong enough such that they become entrained. In the second case, we use a weaker activator coupling.

10.3.1 Strong inter-oscillatory coupling

Let us focus first on a regime of strong coupling among the oscillatory units. We use the following set of parameters $\epsilon = 10^{-4}$, $a_{1,4} = 1.01$, $a_{2,3} = 0.99$, $C_x = 0.80$ and $C_y = 0.22$. In this case, and without an external periodic signal ($A_s = 0.0$) injected nor noise ($D = 0.0$), the analysis of the power spectrum exhibits that the natural period of the system is $T_{nat} \approx 2.67$. The oscillatory units exhibit their periodic oscillations at their natural frequency. The excitable units, at their time, show only subthreshold oscillations at the natural frequency of the oscillatory units.

In the presence of an external signal fig. 10.6 illustrates the normalised spike number and the linear response η as a function of the noise intensity D for different driving periods T_s. Figure 10.6, panel (a) depicts the results when the system is subjected both to noise and external signal and the signal period $T_s = 2.61$ is slightly below the natural period. It is observed (as in the $N = 3$ case) that now the oscillatory units respond but not the excitable one at the end of the chain.

Increasing T_s well over the natural frequency, e.g. $T_s = 2.8$ or 2.9 (figs. 10.6(b) or 10.6(c)), the dynamic trap regime appears. It is important to emphasise that the quality of the signal transmission to the last unit is enhanced with respect to the $N = 3$ case (compare figs. 10.2 and figs. 10.6).

An interesting phenomenon occurs for $T_s = 2.9$ (fig. 10.6, panel (c)) where there are two well-differenced situations of dynamics trap like regimes. First, for very low noise intensities ($D \approx 10^{-7}$) there is an almost perfect suppression of the oscillations and at the same time a perfect signal transmission which is the result of the desired dynamic trap regime. There is then a secondary oscillation suppression regime at $D \approx 2.5 \cdot 10^{-6}$, at which the signal is not transmitted with the same fidelity as compared to the case at about $D \approx 10^{-7}$. In the second regime the last unit is oscillating, neither at the driving frequency, nor at the natural one of the middle oscillators, but at another one. Figure 10.7 shows the power spectrum for such secondary regime in the interesting frequency range around driving and resonance frequency. Let us consider the particular case of the fourth oscillator. It is subject to two different signals, one of them with the natural frequency of the third unit, and one with the external driving frequency. It is not trivial how this two signals interact in order to produce this unit's response, but it has been demonstrated that in non-linear systems [158] subjected to two signals, the response may appear at neither of the driving ones. Nevertheless these facts, the important footprint of this secondary regime is the low response of the last unit to the driving frequency.

One can clearly see in fig. 10.7 three peaks in the frequency range $\Omega \in [1.8, 2.8]$ in the system output. The first and highest peak at $\Omega \approx 2.16$ is well pronounced only for the first and driven oscillator and corresponds

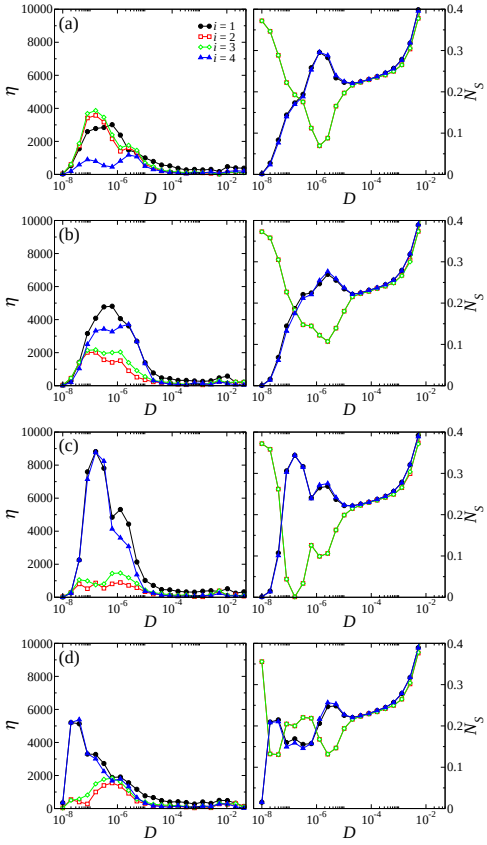

Figure 10.6: Linear response η (left column) and N_s (normalised spike number), in the right column, versus noise intensity for a chain of four oscillators. (a) $T_s = 2.61$; (b) $T_s = 2.8$; (c) $T_s = 2.9$; (d) $T_s = 3.1$; Other parameters: $\epsilon = 10^{-4}$, $a_{1,4} = 1.01$, $a_{2,3} = 0.99$, $A_s = 0.01$. The couplings are, $C_x = 0.80$ and $C_y = 0.22$ (strong inter-oscillatory coupling regime).

to a period $T \approx 2.9$, equal to the driving period T_s, i.e. only the driven oscillator exhibits a good response to the signal. The second peak, very close to the first one, at $\Omega \approx 2.245$ ($T \approx 2.8$) is displayed mainly by the last unit. The third peak at $\Omega \approx 2.49$ ($T \approx 2.52$) can be found in all elements with nearly equal hight. The third peak has a very small influence on the total responses of the system (note the logarithmic scale) and it is produced by small sub-threshold oscillations. The corresponding time series is as follows: the first (driven) oscillator shows a reliable spiking behaviour with a period equal to the driving period, while the two middle oscillators are mostly silent and the last oscillator spikes with a slightly reduced period of $T_s = 2.8$ (so leading to the difference in the linear response at the signal frequency η between the first and last FitzHugh–Nagumo in this regime).

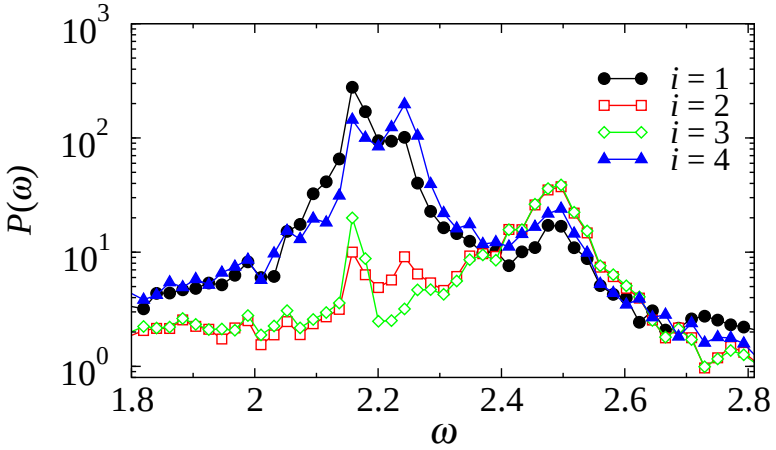

Figure 10.7: Power spectrum of a four oscillator system for the parameters: $\epsilon = 10^{-4}$, $a_{1,4} = 1.01$, $a_{2,3} = 0.99$, $A_s = 0.01$, $T_s = 2.9$, $C_x = 0.80$, $C_y = 0.22$, and $D = 2.56 \cdot 10^{-6}$.

Due to the small difference in the periodicity, there is no phase locking in this regime and a continuous phase slip between the first and last unit appears. If the phase difference is large enough, the chain switches to an anti-phase regime, i.e. the otherwise silent middle oscillators spike in anti-phase to their excitable neighbors. This transition to the anti-phase attractor induces a delay of the last unit compared to the first one. This anti-phase regime is unstable at the considered parameter set and the chain switches back to the previous attractor with the silent middle elements and the phase slip between the first and last one. The interruption of this long-life attractor by the unstable anti-phase attractor results in a nearly equal spike number of the first and last unit. Therefore, the interesting behaviour in figs. 10.6, panel (c) at a noise intensity $D \approx 2.5 \cdot 10^{-6}$ is caused by a regime which is only similar to the dynamic trap regime, but is not exactly the desired dynamic trap and hence does not provide a reliable information transport.

As a summary of this section, it could be said that the dynamic trap regime still occurs, but in a narrower region of the driving period ($T_s \in [2.8, 3.0]$, fig. 10.8) than in the case of $N = 3$ ($T_s \in [3.0, 3.4]$).

Finally, fig. 10.9 shows that there is also a range of inhibitory coupling C_y such that dynamic trap regime occurs. This resonance like behaviour with respect to the inhibitory coupling strength is caused by the influence of this parameter on the resonance frequency of the dynamic trap regime. This figure shows the existence of a maximum (located at a coupling $C_y \approx 0.25$) in the response as a function of this parameter.

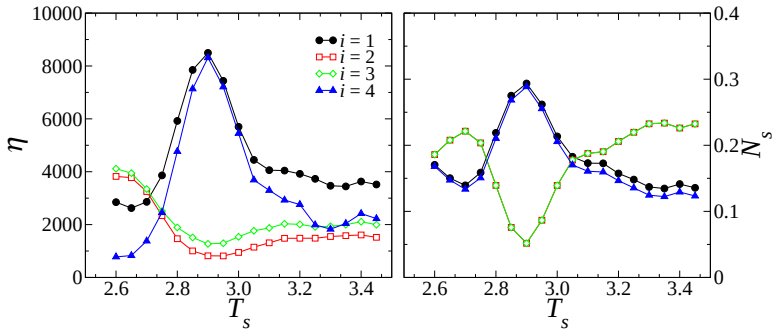

Figure 10.8: Linear response η and normalised spike number N_s versus time periodicity T_s. The system is composed by four units in the strong inter-oscillatory coupling regime and the rest of parameters, are: $\epsilon = 10^{-4}$, $a_{1,4} = 1.01$, $a_{2,3} = 0.99$, $A_s = 0.01$, $C_x = 0.80$, $C_y = 0.22$, and $D = 2 \cdot 10^{-7}$.

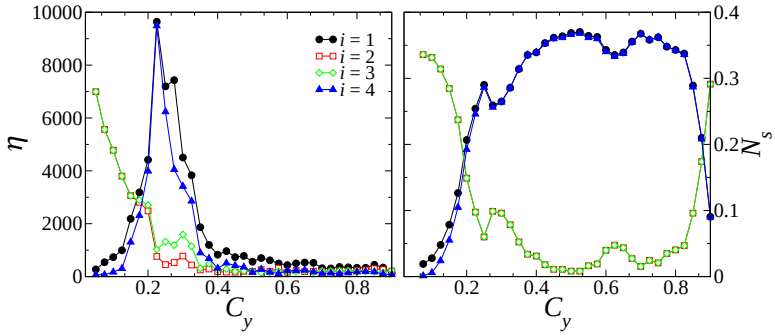

Figure 10.9: Linear response η and normalised spike number N_s as a function of the inhibitory coupling strength C_y. The system is composed by four units in the strong inter- oscillatory coupling regime and the rest of parameters, are: $\epsilon = 10^{-4}$, $a_{1,4} = 1.01$, $a_{2,3} = 0.99$, $A_s = 0.01$, $C_x = 0.80$, $D = 2 \cdot 10^{-7}$ and $T_s = 2.9$.

10.3.2 Intermediate inter-oscillatory coupling

We also found another kind of dynamic regime in this model with a smaller activator coupling. The analysis of the power spectrum in the absence of noise and external signal shows that the oscillatory units exhibit their periodic oscillations at their natural period $T_{nat} \approx 2.54$. The excitable units, at their time, generate only subthreshold oscillations at the natural frequency of the oscillatory units. Note that the natural frequency is shifted from the previous case of a strong inter-oscillatory coupling ($T_{nat} \approx 2.67$). In this case, however, the dependence with T_s of the linear response η curves and

the oscillation suppression is quite different from the previous case. Even for slightly detuned input signals $T_s = 2.55$ a strong dynamic trap arises in the system (fig. 10.10(a)). This oscillation suppression mechanism is very robust over a wide range of driving periods T_s (figs. 10.10(a)-(c)), whereas a reliable signal transmission along the chain can be observed only in a much narrower range of the driving period, $T_s \in [2.6, 2.65]$ (fig. 10.10(b)).

The oscillation suppression here is really robust, showing that the middle units do not spike for very large periods of time. The result is also robust to changes of almost four decades in the noise intensity.

Note that the curves for the number of spikes show an exact coincidence between the first and the last units (i.e. the excitable ones), although such a perfect matching does not occur for the linear response η. The first and the last units fire at the same rate (same normalised spike number N_s), but they are not phase locked, i.e. there is a random phase slip. When the difference in phase between these two excitable units is large enough, this dynamic regime destabilises and a regime in which there is an in-phase motion of excitable units, and (in anti-phase) spikes of the oscillatory units appears. But this last dynamic regime is unstable and rapidly falls to the previous one. It is interesting that the matching in the number of spikes occurs in the dynamic trap regime, i.e. that the sub-threshold dynamics of the oscillatory units is sufficient to carry information from one end of the chain to the other one.

Figures 10.11 and 10.12 demonstrate that there are optimal values of couplings for the suppression to occur. While the dependence on the activator coupling C_x is such that the suppression holds for couplings larger than a given value, we observe a much narrower range, a resonance-like behaviour, as a function of the inhibitor coupling C_y. Even further, for C_y large enough, the oscillation suppression phenomenon disappears, and most of the spikes occur at frequencies different to the driving one (i.e. η vanishes).

Figure 10.13 shows the dependence on the signal periodicity T_s. It is clear that the oscillation suppression and signal transmission are optimal at the same parameter values. Furthermore, in the same figure it can be seen that there is a very narrow peak around the natural period ($T_s = T_{nat} = 2.54$) of the oscillatory units at which they respond optimally. Note that the oscillation suppression holds for a wide range of values of the driving period T_s. But the main result shown in this figure is the fact that the suppression of oscillations in the oscillatory units is much more robust than in the previous cases, i.e. $N = 3$ and $N = 4$ with strong inter-oscillatory coupling. This result is somewhat unexpected given the fact that these couplings are not as strong as in the previous parameter sets, and then the units are allowed to move more freely.

To show the different influence of activator and inhibitory couplings, we have added an extra activator coupling in the model by interchanging C_y by $(1 - \alpha)C_y$ in the equations for the inhibitory variable y_i and inserting the

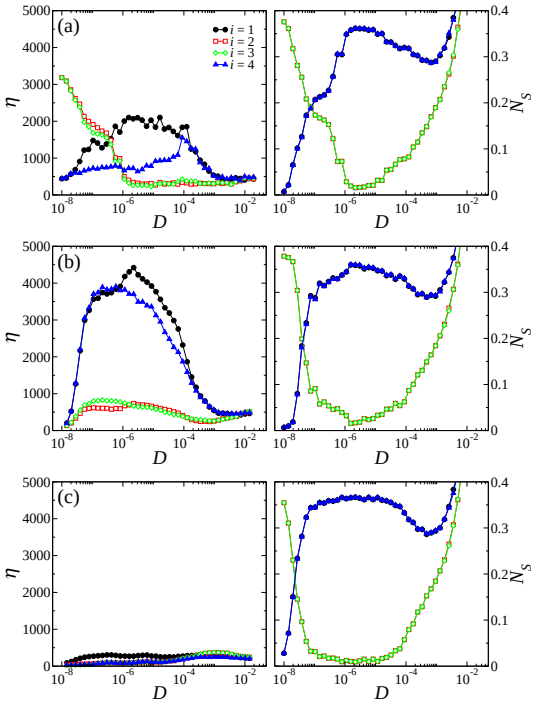

Figure 10.10: Linear response η and normalised spike number N_s (left and right columns, respectively) versus noise intensity. The time periodicities, are (a) $T_s = 2.55$; (b) $T_s = 2.61$; (c) $T_s = 5.2$. The other parameters are: $\epsilon = 10^{-4}$, $a_{1,4} = 1.01$, $a_{2,3} = 0.99$, $A_s = 0.01$, $C_x = 0.20$, and $C_y = 0.50$ (intermediate inter-oscillatory coupling).

terms $\alpha C_y(x_2 - x_1)$ in equation (10.5), $\alpha C_y(x_1 - x_2)$ in eq. (10.6), $\alpha C_y(x_4 - x_3)$ in eq. (10.7) and $\alpha C_y(x_3 - x_4)$ in equation (10.8). These extensions of the model are used only in this section for the calculation of figure 10.14. We shift the balance between the activator and inhibitory coupling between these elements continuously with the parameter α. In figure 10.14, two clearly different regimes can be observed: for $\alpha < 3 \cdot 10^{-3}$ there is a situation of dynamic trap regime with reliable information transport; while for $\alpha > 3 \cdot 10^{-3}$, there are oscillations in the middle units position and no response to the driving frequency.

As shown in figure 10.14, a very sharp transition to a situation of oscillation suppression and no response to the driving frequency in the middle units is observed when the activator coupling is strong enough, $\alpha > 3 \cdot 10^{-3}$. Figure 10.14 (as fig. 10.4 for the $N = 3$ case) shows the essential imperative of the inhibitory coupling between the excitable and oscillatory units to reach the dynamic trap regime with the desired feature of oscillation suppression and information transmission.

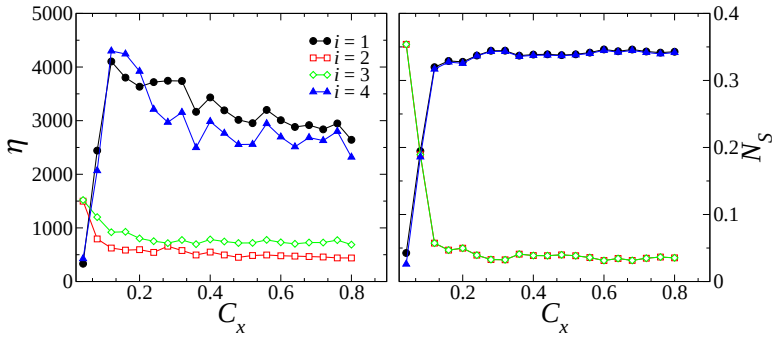

Figure 10.11: Linear response η and normalised spike number N_s versus activator coupling C_x. The system is composed by four units, and the other parameters are: $\epsilon = 10^{-4}$, $a_{1,4} = 1.01$, $a_{2,3} = 0.99$, $A_s = 0.01$, $C_y = 0.50$, $T_s = 2.61$ and $D = 2 \cdot 10^{-7}$.

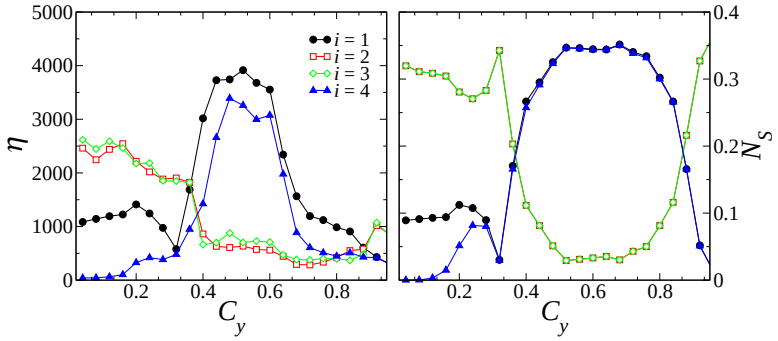

Figure 10.12: Linear response η and normalised spike number N_s versus inhibitory coupling C_y. The parameters are: $\epsilon = 10^{-4}$, $a_{1,4} = 1.01$, $a_{2,3} = 0.99$, $A_s = 0.01$, $C_x = 0.20$, $T_s = 2.61$ and $D = 2 \cdot 10^{-7}$.

10.4 Conclusions

In the present work we have studied chains of three or four coupled FitzHugh–Nagumo's units subject to noise and to an external signal. The number of units has been chosen in order to keep the number of parameters small, but our model could be exemplary also for larger systems if one regards one oscillator in the model as a representation of a cluster of many oscillators in a close area with similar properties. Conversely, due to the high signal quality at the end of the chain, if we consider replicas of this basic setup coupled linearly to others, the same phenomenon should hold along this chain.

We have found new mechanisms which, with the help of a constructive role of the noise, help to suppress self-sustained oscillations in chains of ex-

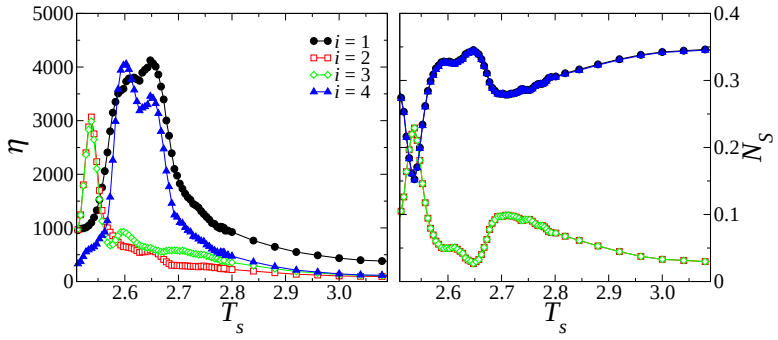

Figure 10.13: Linear response η and normalised spike number N_s versus driving period T_s. For this four units system, the parameters are: $\epsilon = 10^{-4}$, $a_{1,4} = 1.01$, $a_{2,3} = 0.99$, $A_s = 0.01$, $C_x = 0.20$, $C_y = 0.50$ and $D = 2 \cdot 10^{-7}$.

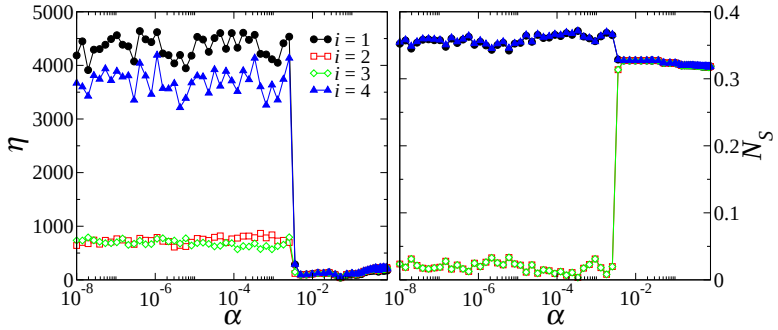

Figure 10.14: The influence of the type of coupling on the the linear response η and the normalised spike number N_s in a system composed by four coupled FitzHugh–Nagumo's. The sliding parameter α shifts the weight of the diffusion constant C_y from a pure inhibitory coupling ($\alpha = 0.0$) to a pure activator coupling ($\alpha = 1$). The other parameters are $\epsilon = 10^{-4}$, $a_{1,4} = 1.01$, $a_{2,3} = 0.99$, $D = 2 \cdot 10^{-6}$, $A_s = 0.01$, $T_s = 2.61$, $C_x = 0.20$ and $C_y = 0.50$.

citable systems while yet allowing for the propagation of external stimuli. In our scheme, an inhibitory coupling between oscillatory and excitable units is essential to reach the dynamic trap regime which is responsible for the oscillation suppression and the information transport. This dynamic trap regime is characterised by an anti-phase spiking behaviour (with the same frequency of the external signal) of the excitable units at both ends of the chain and a silent (oscillation suppressed) behaviour of the originally oscillatory units in between. The desired dynamic trap regime is sensitive with respect to the driving frequency, the noise intensity and the coupling strength. We have found other attractors which also offer a reliable oscillation suppression but,

however, do not provide a good information transport along the chain. It is interesting to note that the oscillation suppression can also be achieved (in the absence of noise) in the presence of a strong enough driving force. Further study would be needed in order to determine the main features of this suppression of oscillations by the injection of a nonperiodic external signal.

We have considered only paradigmatic models in a very general framework, but we expect that our results are also relevant to other models with inhibitory coupling, used, for example, to describe various physical [159], electronic [149], chemical [152, 153, 154, 45, 160], biological systems [155], including spatial non-uniformities [161], animal coat pattern formation [162], or artificial gene networks synchronisation with slow auto-inducer diffusion [163, 164]. An important example is that of the Calcium-signalling mechanism [165, 166] present in neurons in thalamus, pancreatic acinar cells, etc. It occurs in regions where the Ca^{2+} (often responsible for intra-cell communication) is across the cell membrane to form what is called Ca^{2+} wave. Another example is that of the neuron-glion interaction [167, 168] in which the glion acts in some circumstances as an intermediary messenger between pre- and post-synaptic neurons. Interestingly enough, most of the models of this interaction are rather simplistic circuits with three or four compartments connected diffusively at first approximation, very close to our own approach.

A similar architecture to the one studied here may be responsible, for example, for the activities of neural circuits in a nucleus found in the brain of songbirds [169]. In such circuits the connection between different functional units of the brain is mainly due to inhibitory coupling, whereas the connections within each unit are mainly through the activator variables. Since a strong activator coupling tends to synchronise the population of interacting units, one can neglect, as a first approximation, that each functional unit is composed itself of several units, and restrict oneself to a case in which only one (mean) unit is considered for each region of the brain, coupled with others through the inhibitor variable. In this architecture the oscillating element is directly surrounded by inhibitory coupled excitable elements.

The suppression of global oscillations and the prevention of undesirable neural synchronisation is an ongoing issue in medicine and neuro-science and many techniques have been proposed previously in the literature, e.g. the *permanent high-frequency stimulation* [170, 171], the *demand-controlled deep brain stimulation* techniques [172, 173], the *delay feedback control of collective synchrony* [174] or the *noise-induced excitability* [175]. The results of the present chapter can be also potentially useful for this research direction if applied not to inhibitory but negative coupling which can also lead to the appearance of multirhythmicity [102]. There, our result should imply that it is possible to suppress undesirable oscillations while still being able to propagate external stimuli.

Chapter 11

Selective coupling in extended excitable systems

11.1 Introduction

Stochastic resonance is one of the most interesting *noise-induced phenomena* that arises from the interplay between *deterministic* and *random* dynamics in a *nonlinear* system [17]. A large number of examples showing stochastic resonance occur in *extended* systems: for example, diverse experiments were carried out to explore the role of SR in sensory and other biological functions [32, 176, 177] or in chemical systems [178, 179, 180]. These, together with the possible technological applications, motivated many recent studies showing the possibility of achieving an enhancement of the system response by means of the coupling of several units in what conforms an *extended medium* [181, 182, 183, 184, 185, 186, 187].

In previous works [183, 184, 185, 186, 187] stochastic resonant has been studied in extended systems, when transitions between two different spatial patterns occur, exploiting the concept of the *non-equilibrium potential* (NEP) [188, 189, 190, 191, 192, 193, 194, 195]: a Lyapunov functional of the associated deterministic system that, for non-equilibrium systems, plays a role similar to that of a thermodynamic potential in equilibrium thermodynamics. Such NEP characterises the global properties of the dynamics: attractors, relative (or nonlinear) stability of these attractors, height of the barriers separating attraction basins and, in addition, allowing us to evaluate the transition rates among the different attractors. In another work [115] it has also been shown that, for a scalar reaction-diffusion system with a density-dependent diffusion and a known form of the NEP, the non-homogeneous spatial coupling changes the effective dynamics of the system and contributes to enhance the SR phenomenon.

In this chapter, we study SR in an extended system: an array of FitzHugh–Nagumo [44, 196, 42] units, with a density-dependent (diffusive-like) cou-

pling. The NEP for this system was found within the excitable regime and for particular values of the coupling strength [187]. In the general case, however, the form of the NEP has not been found yet. Nevertheless, the idea of the existence of such a NEP is always *underlying* our study. Hence, we have resorted to an study based on numerical simulations, analysing the influence of different parameters on the system response. The results show that the enhancement of the signal-to-noise ratio found for a scalar system [115] is robust, and that the indicated non-homogeneous coupling could clearly contribute to enhance the SR phenomenon in more general situations.

11.2 Non-equilibrium potential

The non-trivial behaviour found in models such that complex Ginzburg–Landau equations, reaction-diffusion –where FitzHugh–Nagumo model finds also an application–, and many other non-equilibrium systems, is not due to the non-variational character of the dynamics: for those systems there is no Lyapunov functional for their dynamics. However, Graham *et al.* [188, 189], showed that it is possible to write a functional that preserves some properties of a Lyapunov potential. It corresponds to an extension of the notion of the (equilibrium) thermodynamical potential to non-equilibrium problems.

Let us consider a dynamical system whose dynamics is given by

$$\dot{x}_i = F_i(\{x_i\}) + \sqrt{D\,Q_i}\,\xi_i(t) \qquad i \in 1 \ldots N. \tag{11.1}$$

We stick here to a situation in which the noises are delta-correlated, additive sources: $\langle \xi_i(t)\xi_j(t')\rangle = \delta_{ij}\,\delta(t-t')$ (in which $\delta_{ij} = 1$ if $i = j$, zero otherwise and $\delta(t-t')$ is the Dirac's delta function). Once again, $D\,Q_i$ is the noise strength of the i–th noise source. All the elements Q_i are non-negative and fulfil $Q_i \leq 1$. In particular, if the i–th term whose noise intensity is the largest, then $Q_i = 1$.

The Fokker–Planck equation for this system is given by

$$\frac{\partial}{\partial t}P = \sum_i \frac{\partial}{\partial x_i}\left(F_i(\{x_i\})\,P\right) + \frac{D}{2}\sum_i Q_i \frac{\partial^2}{\partial x_i^2}P. \tag{11.2}$$

Asymptotically, the solution to this equation tends to a stationary distribution $P_S(\{x_i\})$. In [188], the non-equilibrium potential (NEP), $\Phi(\{x_i\})$, associated to this Fokker–Planck equation, is defined by

$$\Phi(\{x_i\}) = -\lim_{D\to 0} D \ln\left(P_S(\{x_i\}, Q_i)\right). \tag{11.3}$$

This definition, also implies that

$$P_S(\{x_i\}) = \mathcal{Z}\exp\left(-\frac{\Phi(\{x_i\})}{D} + \mathcal{O}(D)\right), \tag{11.4}$$

with $\mathcal{Z}$ is a normalising constant.

The normalisation condition of the probability distribution function, and equation (11.3), ensure that the non-equilibrium potential has a finite global minimum.

It has been shown [188], that the non-equilibrium potential satisfies a Hamilton–Jacobi-like equation

$$\sum_i \frac{\partial \Phi(\{x_i\})}{\partial x_i} + \sum_i \frac{Q_i}{2} \left(\frac{\partial \Phi(\{x_i\})}{\partial x_i} \right)^2 = 0, \tag{11.5}$$

which allows to write for the time-evolution for the functional Φ,

$$\frac{d\Phi\,\{x_i\}}{dt} = \sum_i F_i(\{x_i\}) \frac{\partial \Phi(\{x_i\})}{\partial x_i} = -\sum_i \frac{Q_i}{2} \left(\frac{\partial \Phi(\{x_i\})}{\partial x_i} \right)^2 \leq 0, \tag{11.6}$$

thus showing that it is a decreasing function of time.

11.3 The model

For the sake of concreteness, we consider a simplified version of the FitzHugh–Nagumo [187, 192, 193, 194, 195, 44, 197, 196, 42] model. This model has been useful for gaining qualitative insight into the excitable and oscillatory dynamics in neural and chemical systems [42]. It consist of two variables, in one hand u, a (fast) activator field that in the case of neural systems represents the voltage variable, while in chemical systems represents a concentration of a self-catalytic species. On the other hand v, the inhibitor field, associated with the concentration of potassium ions in the medium (within a neural context), that inhibits the generation of the u species (in a chemical reaction). Instead of considering the usual cubic like nonlinear form, we use a piece-wise linear version

$$\epsilon \frac{\partial u(x,t)}{\partial t} = \frac{\partial}{\partial x} \left(D_u(u) \frac{\partial u}{\partial x} \right) + f(u) - v + \xi(x,t) \tag{11.7}$$

$$\frac{\partial v(x,t)}{\partial t} = \frac{\partial}{\partial x} \left(D_v(v) \frac{\partial u}{\partial x} \right) + \beta\, u - \alpha\, v, \tag{11.8}$$

where $f(u) = -u + \Theta(u - \phi_c)$ (with $\Theta(x)$ the Heaviside function), and $\xi(x,t)$ is a δ-correlated white Gaussian noise, that is $\langle \xi(x,t) \rangle = 0$ and $\langle \xi(x,t)\xi(x',t') \rangle = 2\gamma\delta(x-x')\delta(t-t')$. Here γ indicates the noise intensity and ϕ_c is the "discontinuity" point, at which the piece-wise linearised function $f(u)$ presents a jump. In what follows, the parameters α and β are fixed as $\alpha = 0.3$ and $\beta = 0.4$. Finally, ϵ is the parameter that indicates the time-scale ratio between activator and inhibitor variables, and is set as $\epsilon = 0.03$. We consider Dirichlet boundary conditions at $x = \pm L$: $u(0) = u(L) = 0$ and

$v(0) = v(L) = 0$. Although the results are qualitatively the same as those that could appear considering the usual FitzHugh–Nagumo equations, this simplified version allows us to compare directly with the previous analytical results for this system [187].

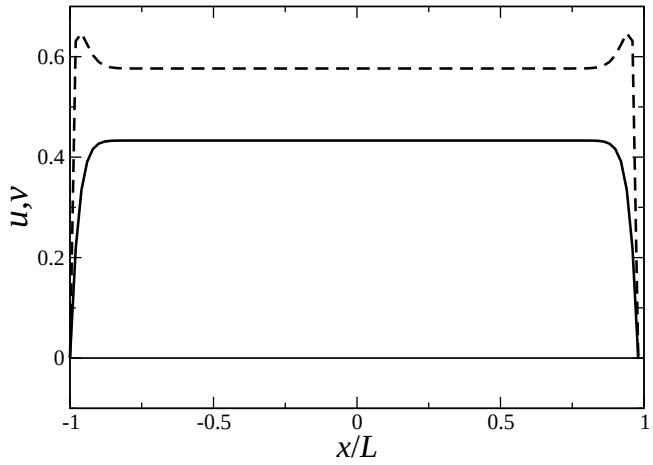

Figure 11.1: We show the stable patterns that arise in the system. There is one stable pattern that is identically zero, i.e. $P_0^u(x) = P_0^v(x) = 0$ and another which is non-zero ($P_1^u(x)$, $P_1^v(x)$). The patterns for the fields $u(x)$ and $v(x)$ are plotted in dashed and solid lines, respectively. The parameters, are $D_u = 0.3$, $D_v = 1$, $h = 2$.

As in [115], we assume that the diffusion coefficient $D_u(u)$ is not constant, but depends on the field u according to $D_u(u) = D_u\,[1 + h\,\Theta(u - \phi_c)]$. This form implies that the value of $D_u(u)$ depends "selectively" on whether the field u fulfils $u > \phi_c$ or $u < \phi_c$. D_u is the value of the diffusion constant without such "selective" term, and h indicates the size of the difference between the diffusion constants in both regions (clearly, if $h = 0$ then $D_u(u) = D_u$ constant). $D_v(v)$ is the diffusion for the inhibitor v, that here we assume to be homogeneously constant.

It is worthwhile noting that when the parameter h is negative, the coupling term might become negative. This is what is known as "inhibitory coupling" [102]. This is a very interesting kind of coupling that has attracted much attention in the last years, both in neural and chemical context, that we will not discuss here.

This system is known to exhibit two stable stationary patterns. One of them is $u(x) = 0$, $v(x) = 0$, while the other is one with non-zero values and can be seen in figure 11.2. We will denote with $P_0^{u,v}(x)$ and $P_1^{u,v}(x)$, the patterns for u and v fields. Further, we consider that an external, periodic,

signal enters into the system through the value of the threshold ϕ_c,

$$\phi_c(t) = \phi_c + \delta\phi \cos(\omega t), \tag{11.9}$$

where ω is the signal frequency, and $\delta\phi$ its intensity.

All the results shown in this chapter were obtained through numerical simulations of the system. The second order spatially discrete version of the system indicated in equations (11.7) and (11.8) reads

$$\begin{aligned} \dot{u_i} &= D_{u,i}(u_{i-1} + u_{i+1} - 2u_i) + (D_{u,i+1} - D_{u,i-1})(u_{i+1} + u_{i-1}) \\ &\quad + f(u_i) - v_i + \xi_i(t) \qquad (11.10) \\ \dot{v_i} &= D_v(v_{i-1} + v_{i+1} - 2v_i) + \beta\, u_i - \alpha\, v_i. \qquad (11.11) \end{aligned}$$

We have performed extensive numerical simulations of this set of equations exploiting the Heun's algorithm [12, 123].

11.3.1 Response's measures

Since the discovery of the stochastic resonance, several different forms of characterising it have been introduced in the literature. Some examples are: (i) output signal-to-noise ratio (SNR) [17, 29], (ii) the spectral amplification factor (SAF) [119, 39], (iii) the residence time distribution [198, 35], and, more recently, (iv) information theory based tools [199, 200, 201]. Along this chapter, we will use the output SNR at the driving frequency ω.

In this spatially-extended system, there are different ways of measuring the overall system response to the external signal. In particular, we evaluated the output SNR in two different ways (the units being given in dB)

- SNR for the element $N/4$ of the chain evaluated over the dynamical evolution of $u_{N/4}$, that we call SNR_1. Having Dirichlet boundary conditions, the local response depends on the distance to the boundaries. Although that, (and except for the units located at the ends of the chain) the results are independent on the exact position of the unit in which the response is measured.

- In order to measure the overall response of the system to the external signal, we computed the SNR as follows: We digitised the system dynamics to a dichotomic process $s(t)$: At time t the system has an associated value of $s(t) = 1\,(0)$ if the Hilbert distance to pattern $1\,(0)$ is lower than to the other pattern. Stated in mathematical terms, we computed the distance $\mathcal{D}_2[\cdot,\cdot]$ defined by

$$\mathcal{D}_2[f,g] = \left(\int_{-L}^{L} dx\ \left(f(x) - g(x)\right)^2 \right)^{1/2}$$

in the Hilbert space of the real-valued functions in the interval $[-L, L]$, i.e. $\mathcal{L}_2$. At time t, a digitised process is computed by means of

$$s(t) = \begin{cases} 1 & \text{if} \mathcal{D}_2\left[P_1^u(x), u(x,t)\right] < \mathcal{D}_2\left[P_0^u(x), u(x,t)\right] \\ 0 & \text{if} \mathcal{D}_2\left[P_1^u(x), u(x,t)\right] \geq \mathcal{D}_2\left[P_0^u(x), u(x,t)\right] \end{cases} , \quad (11.12)$$

We call this measure SNR_p.

11.4 Results

As indicated above, equations (11.10) and (11.11) have been integrated by means of the Heun method [12]. We have fixed the parameters $\epsilon = 0.03$, $\phi_c = 0.52$ and adopted an integration step of $\Delta t = 10^{-3}$. For the signal frequency we adopted $\omega = 2\pi/3.2 = 1.9634295\ldots$. The simulation was repeated 250 times for each parameter set, and the SNR was computed by recourse of the average power spectral density.

Figure 11.2 depicts the results for the different SNR's measures we have previously defined as function of the noise intensity γ. We adopted the following values: $\delta\phi = 0.4$, $D_v = 1.$ and $N = 51$. In all three cases it is apparent that there is an enhancement of the response for $h > 0$, when compared with the $h = 0$ case, while for $h < 0$ the response is smaller.

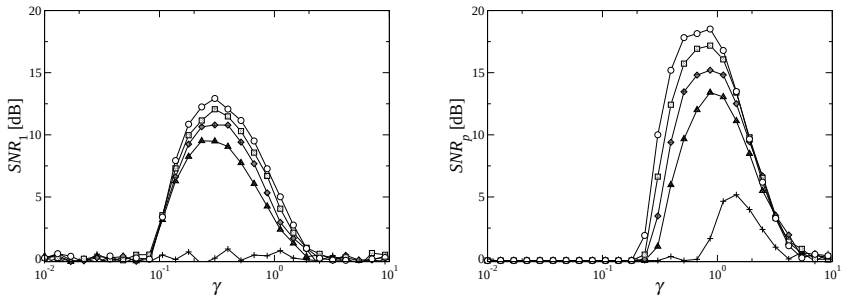

Figure 11.2: SNR vs. γ, the noise intensity, for the two different measures we use. The parameters are $\delta\phi = 0.4$, $D_v = 1.$, $\omega = 2\pi/3.2$, $N = 51$. The different curves represent different values of h, showing an enhancement of the response to the external signal for $\gamma > 0$. In particular it is shown: $h = -2$ (+), $h = -1$ ($\triangle$), $h = 0$ ($\diamond$), $h = 1$ ($\square$) and $h = 2$ ($\bigcirc$).

In figure 11.3 we show the same two response's measures, but now as a function of h. We have plotted the maximum of each SNR curve, for three different values of the noise intensity, and for $\delta\phi = 0.4$, $D_v = 1.$, $\gamma = 0.01, 0.1, 0.3$, $D_u = 0.3$, and $N = 51$. It is clear that there exists an optimal value of γ such that, for such a value, the phenomenon is stronger (that is, the response is larger). It is apparent the rapid fall in the response for $h < 0$.

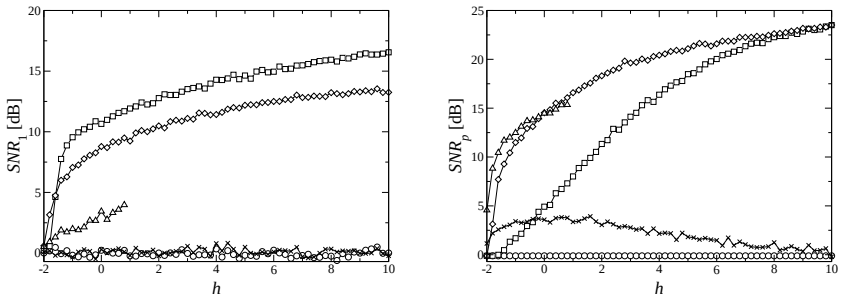

Figure 11.3: SNR vs. h, the selectiveness of coupling, for the two different measures we use. The parameters are $\delta\phi = 0.4$, $D_v = 1.$, $\gamma = 0.032\ (\bigcirc), 0.32\ (\square), 0.6\ (\diamond), 1.2\ (\square), 3.2\ (\times)$, $D_u = 0.3$, $N = 51$.

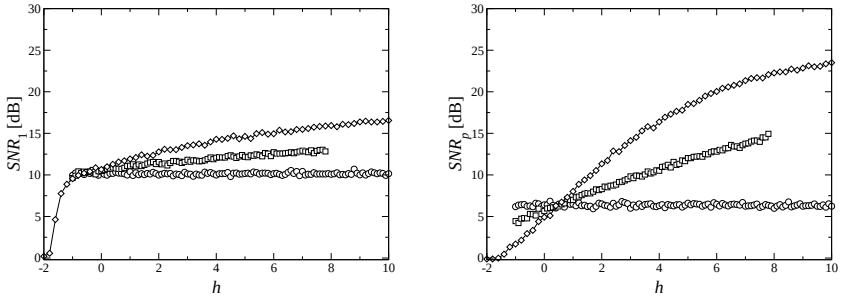

Figure 11.4: SNR vs. h, the selectiveness of coupling, for different values of D_u. The parameters are $\delta\phi = 0.4$, $D_v = 1.$ $\gamma = 0.32$, $D_u = 0.0\ (\bigcirc), 0.1\ (\square), 0.3\ (\diamond)$, $N = 51$.

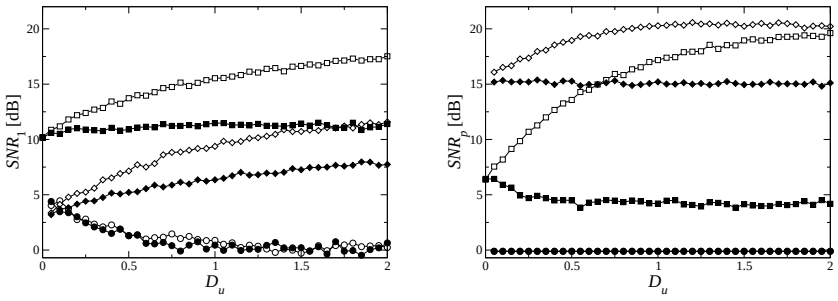

Figure 11.5: SNR vs. D_u, the diffusiveness in activator variable u, for the two different measures we use. The parameters are $\delta\phi = 0.4$, $D_v = 1.$, $\gamma = 0.1$ (◯), 0.32 (□), 1.0 (◇), while the white symbols represent $h = 2$ and the black ones, $h = 0$. The system size is $N = 51$.

In figure 11.4 we show the dependence of SNR on h, for different values of the diffusion which depends on the activator density D_u. It is apparent that the response becomes larger when the value of D_u is larger. However, as was discussed in [183, 184, 185, 186, 187], it is clear that for still larger values of D_u, the symmetry of the underlying potential (that is the relative stability between the attractors) is broken and the response finally falls-down.

Figure 11.5 shows the results of the SNR, but now as function of D_u, the activator diffusivity, for different values of γ, and for $\delta\phi = 0.4$, $D_v = 1.$ and $N = 51$. It can be seen that, independently from the coupling strength D_u, the response to the external signal grows with the selectiveness of the coupling, showing the robustness of the phenomenon.

Next, in figure 11.6, we present the results for the SNR as function of D_v, the activator diffusivity, for different values of γ, and for $\delta\phi = 0.4$, $D_u = 0.3$, and $N = 51$. We see that for $h \geq 0$ the response is more or less flat, however, it is again apparent the SNR's enhancement for $h > 0$. For $h < 0$ we see that the system's response decays very fast with increasing D_v. This effect could be associated to the fact (as found in those cases where the NEP is known [183, 184, 185, 186, 187]) that in the underlying NEP the bistability is lost as a consequence of the disappearance of some of the attractors [192, 193, 194, 195].

Finally, in figure 11.7 we depict the same two SNR's measures but as a function of N, the system size. For the two measures SNR_1 and SNR_2, we see that, for different values of h and γ, the response is very flat, and does not seem to be too much dependent on N. It is clear that there is an increase of the response when h increases. At variance, for SNR_p, the dependence to N is apparent: the SNR decays to zero, in a fast or slow way, depending of $h = 0$ or $h > 0$. Here $\delta\phi = 0.4$, $D_u = 0.3$, $D_v = 1.$, $\gamma = 0.01, 0.1, 0.3$.

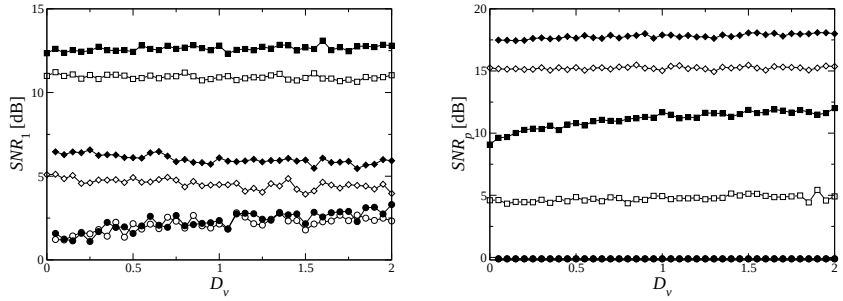

Figure 11.6: SNR vs. D_v, the diffusiveness in the inhibitor variable v. The parameters are $\delta\phi = 0.4$, $D_u = 0.3$, $\omega = 2\pi/3.2$, $N = 51$. $\gamma = 0.1\ (\bigcirc), 0.32\ (\square), 1.0\ (\diamond)$, while the white symbols represent $h = 2$ and the black ones, $h = 0$.

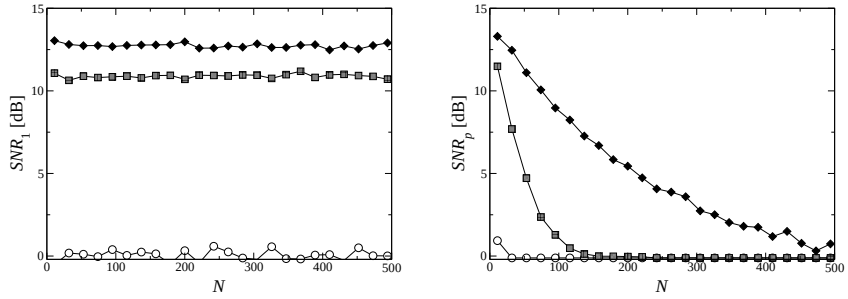

Figure 11.7: SNR vs. N, the system size, for the two different measures we use. The parameters are $\delta\phi = 0.4$, $D_u = 0.3$, $D_v = 1.$, $\gamma = 0.32$, $h = -2\ (\bigcirc), 0$ (greysquares), $2\ (\blacklozenge)$.

11.5 Conclusions

We have analysed a simplified version of the FitzHugh–Nagumo model [187, 192, 193, 194, 195, 197, 196], where the activator's diffusion is density-dependent. Such a system, when both diffusions are constant (that is: $D_u > 0$ and $D_v = 0$), has a known form of the NEP [187]. However, in the general case we have not been able to find the form of the NEP. Thus, we restricted ourselves to study numerically the system in presence of selective coupling in the activator variable inspired on those results.

Through the numerical approach we have studied the influence of the different parameters on the system response. From the results it is apparent the enhancement of the output SNR as h, the selectivity parameter, is increased. This is seen through two different ways of characterising the system's response. We can conclude that the enhancement of the SNR, due to a selectivity in the coupling, initially found for a scalar system [115] is robust, and that the indicated nonhomogeneous coupling could clearly contribute to enhance stochastic resonance in very general systems. This is also robust to variations of the parameter that controls the selectiveness of the coupling, up to a point that even in the case of inhibitory coupling the phenomenon holds.

An aspect worth to be studied in detail is the dependence of the SNR on N, the number of coupled units. In this way we could analyse the dependence of the so called *system size stochastic resonance* [129, 134, 97] on the *selective coupling*. The thorough study of this problem will be the subject of further work.

Part III

Conclusions and Prospectives

In this work, we have explored different coupled systems, focusing on the *improving* role that disordering ingredients can have on them. Most of the results concern excitable systems, which are of predominant interest not only in Physics, but also in Biology, Chemistry, and other sciences.

We will now summarise our main results divided by chapters, in the same order in which they appeared during the exposition. The results of this thesis open many possible extensions, and in the last section of this chapter we discuss some of the possible prospectives that could be explored in the future.

Results

5. Collective firing in excitable media

Large variety of physical, chemical and biological systems show excitable behaviour, characterised by a nonlinear response under external perturbations: only perturbations exceeding a threshold induce a full system response (firing). It has been reported that in coupled excitable identical systems noise may induce the simultaneous firing of a macroscopic fraction of units. A complete understanding of the role of noise and that of natural diversity present in realistic systems is still lacking.

We have developed a theory for the emergence of collective firings in non-identical excitable systems subject to noise. In particular, we have focused on the study of a system composed by *active-rotator* units. Excitable systems can be classified in two different types, according to the bifurcation they undergo to the oscillatory regime. Active-rotators are a prototypical system for type I excitability. Our treatment allows us to find analytical expressions for the relevant order parameters. We show that three different dynamical regimes arise in this system: sub-threshold motion, where all elements remain confined near the fixed point; coherent pulsations, where a macroscopic fraction fire simultaneously; and incoherent pulsations, where units fire in a disordered fashion.

We also show that the mechanism for collective firing is generic: it arises from degradation of entrainment originated either by increasing noise or diversity or also by reducing coupling strength.

6. Synchronisation of coupled FitzHugh–Nagumo systems

We extended the previous results to a system of coupled FitzHugh–Nagumo systems is considered. This system is prototypical of Type II excitability.

We show, by means of extensive numerical simulations, that the main results described in the previous chapter also hold for this kind of excitable systems. We show that diversity and noise can produce a collective firing phenomenon, which disappears whenever the disorder in the position they produce is too large. The main problem here concerns the proper definition

of a phase in this system, a non-trivial issue. We have opted to define it through the use of the Hilbert transform, although similar results are found for simpler phase definitions.

In these two chapters, we have shown that synchronisation phenomena must be studied in a different way in autonomous (or oscillatory) and excitable systems. In the latter, some degree of disorder in the position of the units must be present in order to observe a collective, synchronous state. The typical scenario of oscillatory systems, where noise or diversity degrades the quality of the response, is only reproduced for excitable systems in the limit of very large noise intensity (or very large diversity). For a small degree of disorder, these disordering elements, have instead a positive role regarding the coherence of the output.

7. Global firing induced by network disorder

We have studied the effect of adding some repulsive links as the only source of disorder in a set of otherwise identical active-rotator units: neither noise nor diversity is added onto the system. We first isolate the effect of repulsive links, showing that it can be rewritten separating the contributions of attractive and repulsive links. In such a system, the only possible fully synchronised state is a non-dynamic one, with all the units resting at the fixed point of the dynamics.

For a fully random network of repulsive links, we show that there is an intermediate amount of repulsive links such that collective firing appears. Similar theoretical arguments than those developed in previous chapters allow us to predict the transition point to collective firing. For this kind of network, however, the size of the region of coherent pulses decreases for increasing system size. We also show that the instability of the fully synchronised state is the origin of the emergence of this coherent behaviour.

We finally demonstrate that for network realizations with defined degree distributions, the size of the region of collective firings can remain even in the thermodynamic limit. We show that the only relevant parameter is the proportion of units that are coupled mainly through repulsive links to the rest of the system.

8. Diversity-induced resonance

We present conclusive evidence showing that different sources of diversity, such as those represented by quenched noise or disorder, can induce a resonant collective behaviour in an ensemble of coupled bistable or excitable systems.

We first consider a bistable ϕ^4 model composed by many coupled units and show that the global response to an external periodic forcing is enhanced under the presence of the right amount of diversity (measured as the

dispersion in one of the parameters defining the model).

We first present a theoretical treatment that allows us to qualitatively explain the phenomenon. The origin lays in the increase in the dispersion of the position of the units as diversity increases. This increase in the dispersion causes that the effective potential governing the dynamics of the macroscopic (global) position of the units experience a decrease in the height of the inter-well unstable maximum. Then, a weak signal suffices to cause a motion between both minima.

We extend our analytical study, obtaining analytical expressions for the global response of the system. These results are in good agreement with numerical results, showing that the response is indeed optimised for an intermediate value of the diversity. These findings show that intrinsic diversity might have a constructive role and suggest that natural systems might profit from their diversity in order to optimise the response to an external stimulus.

We also show that the same results appear in excitable systems, although the explanation is more involved. Here, the diversity changes the relative position of the fixed point of the macroscopic variables, in such a way that the excitability threshold is lowered.

9. System size and diversity in an opinion formation model

We study a model for opinion formation which incorporates three basic ingredients for the evolution of the opinion held by an individual: imitation, influence of fashion and randomness. We show that in the absence of fashion, the model behaves as a bistable system with random jumps between the two stable states with a distribution of times following Kramers' law. We also demonstrate the existence of system size stochastic resonance, by which there is an optimal value for the number of individuals N for which the average opinion follows better the fashion.

As an extension of the results in the previous chapter, we propose an extension to the model considering that the individuals are not equal when deciding their opinion: we consider that each agent has a *bias* that favours one of the states. We show that this ingredient suffices in order to obtain larger response to the external influence (in this case *fashion*). This confirms, the generality of the results obtained in previous chapters.

10. Noise-induced inhibitory suppression

For small chains of excitable and oscillatory FitzHugh–Nagumo units we study the effect of *inhibitory* coupling. An important example is that of the calcium-signalling mechanism present in neurons in thalamus, pancreatic acinar cells, neuron-glion interaction, etc.

We have studied the control of oscillations in a system of inhibitory coupled noisy excitable and oscillatory units where one of the end units is

subjected to a periodic signal.

Using dynamical properties of inhibition, we have found regimes where the oscillations in the internal units can be suppressed. However, the information signal (of a certain frequency) can be transmitted through the system. The mechanism is a resonant interplay between noise and the transmission signal provided by certain value of inhibitory coupling. Analysing a system of three or four oscillators representing neural clusters, we show that this suppression can be effectively controlled by coupling and noise amplitudes.

11. Selective coupling in extended excitable systems

Here we present a study of *stochastic resonance* in an extended FitzHugh–Nagumo system with a field dependent activator diffusion. We show that the system response (here measured through the output signal-to-noise ratio) is enhanced due to the particular form of the non-homogeneous coupling.

Such a result supports previous ones obtained in a simpler scalar reaction-diffusion system and shows that such an enhancement, induced by the field dependent diffusion –or selective coupling–, is a robust phenomenon.

Open questions and future work

The results presented in this thesis, indicate that in heterogeneous interacting systems (i.e. those whose composing units are not identical) can exhibit a coherent behaviour both: in presence or in absence of an external signal. One can hypothesise that evolution could have adjusted the naturally present diversity to values that allow (for example) sensory systems to optimal values.

The finding of the diversity-induced resonance and the mechanism behind collective firing in excitable systems, was done in systems with minimal ingredients. We thus expect them to be of broad application and be of relevance for varied research fields. We also demonstrated that the exact source of disorder is not important at all, leading also to many possible extensions.

One of these possibilities is that of considering excitable chaotic systems. There, it is their dynamics who naturally induce disorder in the positions. We then envision that in them, a similar ordering role could be played directly by their chaotic dynamics. This study should be done in systems not strongly coupled –in such a way that the units do not become entrained-,- and the disorder of the positions is preserved along one excursion.

Another possible scenario that must be considered is that of time-delayed interactions. They emerge naturally in biological systems, where some signals take some time to reach the interacting neighbors. Time-delay causes the units to evolve chaotically, as the effective dimension of the new system is infinite. It would be of interest to investigate if the collective firing

mechanism applies to this situation.

We have developed very simple analytical arguments that have allowed us to understand how natural diversity can play a constructive role in dynamical systems. However, a full theoretical framework to study this kind of systems is lacking, and its development would be of fundamental interest. This is, however, a non-trivial task. A first attempt would be to develop Liouville equations in presence of diversity, although this appears to be a very involved task that, anyway, could only be solved for particular cases of the force terms.

Of course, an experimental verification, for example by recourse of analogous electronic circuits, of our theoretical predictions would be most welcome. If there is an optimum degree of diversity in the internal parameters of natural systems, for example, neurons, is a more interesting question with no clear answer.

It would be also of interest to analyse the role of diversity in extended media. For example, non-linear optical media with impurities, or chemical reactions occurring in non-homogeneous gels would be candidates to investigate on them if self-sustained waves or spirals can exist and propagate. The question is intriguing, and similar analytical arguments to those found regarding the transition to global firings in excitable systems show that some oscillatory patterns can appear. Under which conditions these patterns can become self-sustained would be also of great relevance.

With regards to discrete systems, the same applies. Heterogeneous systems apply naturally in Physics, for example, when one considers mesoscopic representations of magnetic materials with impurities. The analytical description of the ϕ^4-model we introduced when presenting the Disorder-induced resonance phenomenon, is a direct representation of this Physical problem. But similar considerations would lead to a similar model if one introduces heterogeneity in the model for opinion formation introduced in the last chapter.

We also studied spatially extended excitable systems. And specially the role of inhibitory coupling on them. This kind of coupling is very interesting by itself. And is present not only in inter-neuron or neuron-glion interactions, but even in a system that is gaining much attention in the last years: *the genetic oscillators*. This dynamical system is a mathematical representation of the protein synthesis within the cells. On them, this kind of coupling also arises naturally.

We studied non-trivial dynamical regimes that appear in systems coupled through inhibitor variables. However, a complete understanding (even only through numerical simulations) of the synchronisation phenomenon in presence of this coupling is still lacking. We observed that multi-cluster solutions appear in the mean-field case. But a detailed study should be done in order to understand it.

For short, we expect that the work exposed in this pages will trigger interest and will be a useful starting point for new research.

List of publications

This section lists the references where the results described in this thesis were published, and the corresponding chapters. As of today, there are some accepted papers whose references are not completely determined.

- "Disorder-induced resonance"
  C.J. Tessone, C. Mirasso, R. Toral and J. Gunton
  Physical Review Letters, **97** 194101 (2006).
  - 8. Diversity-induced resonance

- "Noise-induced inhibitory suppression by frequency selective stochastic resonance"
  C.J. Tessone, E. Ullner, A.A. Zaikin, J. Kurths and R. Toral
  Physical Review E **74**, 046220 (2006).
  - 10. Noise-induced inhibitory suppression

- "Global firing induced by noise or diversity in excitable media"
  C.J. Tessone and A. Scirè and P. Colet and R. Toral
  Accepted in *Physical Review E*. Pending reference.
  - 5. Collective firing in excitable media

- "Collective effects induced by diversity in extended systems"
  R. Toral, C.J. Tessone, J. Viana Lopes
  Accepted in *European Physical Journal - Special Topics"* . Pending reference.
  - 8. Diversity-induced resonance
  - 5. Collective firing in excitable media

- "Finite size effects in the dynamics of opinion formation"
  R. Toral and C.J. Tessone
  Communications in Computational Physics **2** , 177 (2007).

  - 9. System size and diversity in an opinion formation model

- "Stochastic Resonance in an Extended FitzHugh-Nagumo System: the Role of Selective Coupling"
  C.J. Tessone and H.S. Wio
  Physica A **374**, 46 (2006).

  - 11. Selective coupling in extended excitable systems

- "Synchronization Properties of Coupled FitzHugh-Nagumo Systems"
  C.J. Tessone, R. Toral, C. Mirasso, D. Gunton
  Il Nuovo Cimento, Proceedings of the International Enrico Fermi School on Physics: **L** 461, (2005).

  - 6. Synchronisation of coupled FitzHugh–Nagumo systems

- "System size stochastic resonance in a model for opinion formation"
  C.J. Tessone and R. Toral
  Physica A, **351** (2005) 106.

  - 9. System size and diversity in an opinion formation model

The results of chapter 7, Global firing induced by network disorder are still unpublished.

Bibliography

[1] E. Ott. *Chaos in dynamical systems*. Cambridge University Press, Cambridge, 1993.

[2] H. Goldstein, C. Poole, and J. Safko. *Classical Mechanics*. Addison–Wesley, San Francisco, 3rd edition, 2000.

[3] J.D. Murray. *Mathematical Biology*. Springer–Verlag, Berlin, 1993.

[4] T. Kapitaniak and S.R. Bishop. *The illustrated dictionary of nonlinear dynamics and chaos*. John Wiley & Sons, New York, 1999.

[5] S.H. Strogatz. *Nonlinear dynamics and chaos*. Addison–Wesley, 2nd edition, 1994.

[6] E.M. Izhikevich. *Dynamical Systems in Neuroscience: The Geometry of Excitability and Bursting*. MIT Press, Cambridge, 2006.

[7] Y. Kuramoto. *Chemical Oscillations, Waves, and Turbulence*. Springer–Verlag, New York, 1984.

[8] R. Adler. A study of locking phenomena in oscillators. *Proc. IRE*, 34:351, 1946.

[9] N.G. van Kampen. *Stochastic Processes in Physics and Chemistry*. NorthHolland, Amsterdam, 1st edition, 1981.

[10] C.W. Gardiner. *Handbook of Stochastic Methods for Physics, Chemistry and the Natural Sciences*. Springer–Verlag, Berlin, 1983.

[11] H. Risken. *The Fokker–Planck equation*. Springer–Verlag, Berlin, 2nd edition, 1989.

[12] M. San Miguel and R. Toral. *Instabilities and Nonequilibrium Structures VI*, volume VI, chapter Stochastic Effects in Physical Systems. Kluwer Ac. Press, 1999.

[13] A. Einstein. Über von der molekular-kinetischen Theorie der Wärme geforderte Bewenung von in ruhenden Flüssigkeiten suspendierten Teilchen. *Ann. Phys. (Leipzig)*, 17:549, 1905.

[14] M. von Smoluchowski. Zur kinetischen Theorie der Brownschen Molekularbewegung und der Suspensionen. *Ann. Phys. (Leipzig)*, 21:756, 1906.

[15] P. Langevin. Sur la théorie du movement brownien. *Comptes. Rendues*, 146:530, 1908.

[16] S.O. Rice. *Bell Syst. Tech. J.*, 23:282, 1944.

[17] L. Gammaitoni, P. Hänggi, P. Jung, and F. Marchesoni. Stochastic resonance. *Rev. Mod. Phys.*, 70:223, 1997.

[18] K. Falconer. *Fractal Geometry.* John Wiley and Sons, London, 1990.

[19] J.M. Sancho and San Miguel. Langevin equations with colored noise. In P. McClintock and F. Moss, editors, *Noise in Nonlinear Dynamical Systems*, volume 1, page 72. Cambridge University Press, 1989.

[20] T.C. Gard. *Introduction to Stochastic Differential Equations*, volume 114 of *Monographs and Textbooks in Pure and Applied Mathematics.* Marcel Dekker, 1987.

[21] A.D. Fokker. *Ann. Phys. (Leipzig)*, 43:310, 1915.

[22] M. Planck. *Preuss. Akad. Wiss. Phys. Math.*, 325, 1917.

[23] R. Benzi, A. Sutera, and A. Vulpiani. *Journal of Physics A*, 14:L453, 1981.

[24] R. Benzi, G. Parisi, A. Sutera, and A. Vulpiani. Stochastic resonance in climatic change. *Tellus*, 34:10, 1982.

[25] C. Nicolis. Solar variability and stochastic effects on climate. *Sol. Phys.*, 74:473, 1981.

[26] C. Nicolis. Stochastic aspects of climatic transitions-response to a periodic forcing. *Tellus*, 34:1, 1982.

[27] S. Fauve and F. Heslot. Stochastic resonance in a bistable system. *Phys. Lett.*, 97A:5, 1983.

[28] B. Mc Namara, K. Wiesenfeld, and R. Roy. Observation of stochastic resonance in a ring laser. *Phys. Rev. Lett.*, 60:2626, 1988.

[29] B. Mc Namara and K. Wiesenfeld. Theory of stochastic resonance. *Phys. Rev. A*, 39:4854, 1989.

[30] K. Wiesenfeld, D. Pierson, E. Pantazelou, C. Dames, and F. Moss. Stochastic Resonance in a circle. *Phys. Rev. Lett.*, 72:2125, 1994.

[31] B.J. Gluckman, T.I. Netoff, E.J. Nee, W.L. Ditto, M.L. Spano, and S.J. Schiff. Stochastic resonance in a neuronal network from mammalian brain. *Phys. Rev. Lett.*, 77:4098, 1996.

[32] J.K. Douglas, L. Wilkens, E. Pantazelou, and F. Moss. Noise enhancement of information transfer in crayfish mechanoreceptors by stochastic resonance. *Nature*, 365:337, 1993.

[33] K. Kitajo, D. Nozaki, L.M. Ward, and Y. Yamamoto. Behavioral stochastic resonance within the human brain. *Phys. Rev. Lett.*, 90:218103, 2003.

[34] Z. Neda. Stochastic resonance in Ising systems. *Phys. Rev. E*, 51:5315, 1995.

[35] L. Gammaitoni, E. Menichella-Saetta, S. Santucci, F. Marchesoni, and C. Presilla. Periodically time-modulated bistable systems: Stochastic resonance. *Phis. Rev. A*, 40:2114, 1989.

[36] P. Hänggi and P. Jung. Colored noise in dynamical systems. *Adv. Chem. Phys*, 89:239, 1995.

[37] L. Gammaitoni, E. Menichella-Saetta, S. Santucci, and F. Marchesoni. Multiplicative stochastic resonance. *Phys. Rev. E*, 49:4878, 1994.

[38] H. Kramers. Brownian motion in a field of force and the diffusion model of chemical reactions. *Physica (Ultrecht)*, 7:284, 1940.

[39] P. Jung and P. Hänggi. Amplification of small signals via stochastic resonance. *Phys. Rev. A*, 44:8032, 1991.

[40] B. Caroli, C. Caroli, B. Roulet, and D. Saint-James. On fluctuations and relaxation in systems described by a one-dimensional fokker-planck equation with a time-dependent potential. *Physica A*, 108:233, 1981.

[41] E. Meron. Pattern formation in excitable media. *Phys. Rep.*, 218:1, 1992.

[42] B. Lindner, J. García-Ojalvo, A. Neiman, and L. Schimansky-Geier. Effects of noise in excitable systems. *Physics Reports*, 392:321, 2004.

[43] A.L. Hodgkin and A.F. Huxley. The dual effect of membrane potential on sodium conductance in the giant axon of loligo. *J. Physiol. (London)*, 116:497, 1952.

[44] R.A. FitzHugh. Impulses and physiological states in theoretical models of nerve membrane. *Biophys. J.*, 1:445, 1961.

[45] V.K. Vanag, L.F. Yang, M. Dolnik, A.M. Zhabotinskii, and I.R. Epstein. Oscillatory cluster patterns in a homogeneous chemical system with global feedback. *Nature*, 406:389, 2000.

[46] W.O. Kermack and A.G. McKendrick. *Proc. R. Soc. Lond. A*, 94, 1927.

[47] A. Mikhailov. *Foundations of Synergetics*, volume I. Springer–Verlag, Berlin, 2nd edition, 1994.

[48] E.M. Izhikevich. Neural excitability, spiking and bursting. *Int. J. of Bif. and Chaos*, 10(1171), 2000.

[49] A.L. Hodgkin. The local electric changes associated with repetitive action in a non-medulated axon. *J. Physiol.*, 107(165), 1948.

[50] J. Rinzel and G.B. Ermentrout. *Analysis of neural excitability and oscillations*. Methods in Neuronal Modeling. MIT Press, Cambridge, 1989.

[51] R.A. FitzHugh. Mathematical models of threshold phenomena in the nerve membrane. *Bull. Math. Biophys.*, 17:257–278, 1955.

[52] C. Morris and H. Lecar. Voltage oscillations in the barnacle giant muscle fiber. *Biophys. J.*, 35:193–213, 1981.

[53] B.R. Belousov. Oscillation reaction and its mechanism. *Sbornik Referatov po Radiacioni Medicine*, page 145, 1959.

[54] A.N. Zaikin and A.M. Zhabotinskii. *Nature*, 225:535, 1970.

[55] Y. Kuramoto. In H. Araki, editor, *International Symposium on Mathematical Problems in Theoretical Physics*, volume 39, New York, 1975. Springer–Verlag.

[56] S. Shinomoto and Y. Kuramoto. Phase transitions in active rotator systems. *Prog. Theor. Phys.*, 75:1105, 1986.

[57] G.B. Ermentrout. Type i membranes, phase resetting curves, and synchrony. *Neural Comput.*, 8:979, 1996.

[58] B.S. Gutkin and G.B. Ermentrout. Dynamics of membrane excitability determine inter-spike interval variability: A link between spike generation mechanisms and cortical spike train statistics. *Neural Comput.*, 10:1047, 1998.

[59] R.E. Mirollo and S.H. Strogatz. Synchronization of pulse-coupled biological oscillators. *SIAM J. Appl. Math.*, 50:1645, 1990.

[60] G.B. Ermentrout and J. Rinzel. Beyond a pacemaker's entrainment limit: phase walk-through. *Am. J. Physiol.*, 426:R102, 1984.

[61] C. Liu, D.R. Weaver, S.H. Strogatz, and S.M. Reppert. Cellular construction of a circadian clock: Period determination in the suprachiasmatic nuclei. *Cell*, 91:855, 1997.

[62] T. Van Duzer and C.W. Turner. *Principles of superconductive devices and circuits.* Elsevier, New York, 1981.

[63] P. Reimann. Brownian motors: noisy transport far from equilibrium. *Phys. Rep.*, 361:57, 2002.

[64] P. Reimann, C. Van den Broeck, H. Linke, P. Hänggi, M. Rubi, and A. Perez-Madrid. Giant acceleration of free diffusion by use of tilted periodic potentials. *Phys. Rev. Lett*, 87:010602, 2001.

[65] M. van der Pol. On relaxation oscillations. *Phil. Mag.*, 2, 1926.

[66] K.F. Bonhoeffer. Über die Aktivierung von passiven Eisen in Salpetersäure. *Z. Elektrochem.*, 47:147, 1941.

[67] K.F. Bonhoeffer. Activation of passive iron as a model for the excitation nerve. *J. Gen. Physiol.*, 32:69, 1948.

[68] J.P. Keener and J. Sneyd. *Mathematical Physiology.* Springer–Verlag, New York, 1998.

[69] J. Nagumo, S. Arimoto, and S. Yoshitzawa. Active pulse transmission line simulating nerve axon. *Proc. IRE*, 50:2061, 1962.

[70] B. Lindner and L. Schimansky-Geier. Coherence and stochastic resonance in a two-state system. *Phys. Rev. E*, 61:6103, 2000.

[71] J.L. Callot, F. Diener, M. Diener, and C.R. Seances. *Acad. Sci. Ser. A*, 286:1059.

[72] B. Lindner, M. Kostur, and L. Schimansky-Geier. Optimal diffusive transport in a tilted periodic potential. *Fluct. Noise Lett.*, 1:R25, 2001.

[73] H.E. Plesser and T. Geisel. Markov analysis of stochastic resonance in a periodically driven integrate-and-fire neuron. *Phys. Rev. E*, 59:7008, 1999.

[74] A. Pikovsky and J. Kurths. Coherence resonance in a noise-driven excitable system. *Phys. Rev. Lett.*, 78:775, 1997.

[75] K. Pakdaman, S. Tanabe, and T. Shimokawa. Coherence resonance and discharge time reliability in neurons and neuronal models. *Neural Networks*, 14:895, 2001.

[76] A. Pikovsky, M. Rosenblum, and J. Kurths. *Synchronization: A universal concept in nonlinear sciences*. Cambridge University Press, 1st edition, 2001.

[77] S.H. Strogatz. *Sync: the emerging science of spontaneous order*. Hyperion, New York, 1st edition, 2003.

[78] A.T. Winfree. Biological rhythms and the behavior of populations of coupled oscillators. *J. Theoret. Biol.*, 16:15, 1967.

[79] A.T. Winfree. *The Geometry of Biological Time*. Springer–Verlag, New York, 1st edition, 1980.

[80] L.M. Pecora and T.L. Carroll. Synchronization in chaotic systems. *Phys. Rev. Lett.*, 64:821, 1990.

[81] K. Kaneko. Oscillation and doubling of torus. *Prog. Theor. Phys.*, 72:202, 1984.

[82] M.C. Cross and P.H. Hohenberg. Pattern formation outside of equilibrium. *Rev. Mod. Phys.*, 65:851, 1993.

[83] S.H. Strogatz. From Kuramoto to Crawford: exploring the onset of synchronization in populations of coupled oscillators . *Physica D*, 143:1, 2000.

[84] J.A. Acebrón, L.L. Bonilla, C.J. Pérez-Vicente, F. Ritort, and R. Spigler. The kuramoto model: A simple paradigm for synchronization phenomena. *Rev. Mod. Phys.*, 77:137, 2005.

[85] S. Kadar, J. Wang, and K. Showalter. Noise-Supported Traveling Waves in Subexcitable Media. *Nature*, 391:770, 1998.

[86] S. Alonso, I. Serdi, V. Pez-Mu, and F. Sagu. Regular wave propagation out of noise in chemical active media. *Phys. Rev. Lett.*, 87:078302–1–4, 2001.

[87] S. Tanabe and K. Pakdaman. Noise-induced transition in excitable neuron models. *Biol. Cybern.*, 85:269, 2001.

[88] D.E. Potsnov, S.K. Han, T.G. Yim, and O.V. Sosnovtseva. Experimental observation of coherence resonance in cascaded excitable systems. *Phys. Rev. E*, 59:R3791–R3795, 1999.

[89] C. Kurrer and K. Schulten. Noise-induced synchronous neuronal oscillations. *Phys. Rev. E*, 51:6213, 1995.

[90] M.A. Zaks, A.B. Neiman, S. Feistel, and L. Schimansky-Geier. Noise-controlled oscillations and their bifurcations in coupled phase oscillators. *Phys. Rev. E*, 68:066206–1–8, 2003.

[91] S.H. Park and S. Kim. Noise-induced phase transitions in globally coupled active rotators. *Phys. Rev. E*, 53:3425–3430, 1996.

[92] C. van den Broeck, J.M.R. Parrondo, and R. Toral. Noise-induced nonequilibrium phase transition. *Phys. Rev. Lett.*, 73:3395, 1994.

[93] J.A. Acebrón and L.L. Bonilla. Asymptotic description of transients and synchronized states of globally coupled oscillators. *Physica D*, 114:296, 1998.

[94] J.H.E. Cartwright. Emergent global oscillations in heterogeneous excitable media: The example of pancreatic beta cells. *Phys. Rev. E*, 62:1149–1154, 2000.

[95] M. Abramowitz and I.A. Stegun. *Handbook of mathematical functions*. Dover Publisher, New York, 1964.

[96] N. Niedemeyer and F.H. Lopes da Silva. *Electroencephalography, Basic Principles, Clinical Applications and Related Fields*. Urban & Schwarzenberg, Baltimore, 2001.

[97] R. Toral, C. Mirasso, and J. Gunton. System size coherence resonance in coupled FitzHugh–Nagumo models. *Europhys. Lett.*, 61:162, 2003.

[98] B. Lindner and L. Schimansky-Geier. Analytical approach to the stochastic FitzHugh–Nagumo system and coherence resonance . *Phys. Rev. E*, 60:7270, 1999.

[99] C. Zhou and J. Kurths. Noise-induced synchronization and coherence resonance of a hodgkin–huxley model of thermally sensitive neurons. *Chaos*, 13:401, 2003.

[100] C. Koch. *Biophysics of Computation*. Oxford University Press, New York, 1999.

[101] L. Glass, P. Hunter, and A. McCulloch. *Theory of Heart*. Springer–Verlag, Berlin, 1991.

[102] Peter Dayan and Laurence F. Abbott. *Theoretical neuroscience: computational and mathematical modeling of neural systems*. Computational neuroscience. MIT Press, Cambridge, 2001.

[103] H. Daido. Population Dynamics of Randomly Interacting Self-Oscillators I. *Prog. Theor. Phys.*, 77:622, 1987.

[104] H. Daido. Quasientrainment and slow relaxation in a population of oscillators with random and frustrated interactions. *Phys. Rev. Lett.*, 68:1073, 1992.

[105] H. Daido. Algebraic relaxation of an order parameter in randomly coupled limit-cycle oscillators. *Phys. Rev. E*, 61:2145, 2000.

[106] D.H. Zanette. Synchronization and frustration in oscillator networks with attractive and repulsive interactions. *Europhys. Lett.*, 72:190, 2005.

[107] P. Erdős and A. Rényi. *Publ. Math. Inst. Hung. Acad. Sci.*, 5:17, 1960.

[108] P. Erdős and A. Rényi. *Publ. Math. (Debrecen)*, 6:290, 1959.

[109] R. Albert and L. Barabási. Statistichal mechanics of complex networks. *Rev. Mod. Phys.*, 74:47, 2002.

[110] D.J. Watts and S.H. Strogatz. Collective dynamics of small-world networks. *Nature*, 393:440, 1998.

[111] F. Juhász. *Algebraic Methods in Graph Theory.* North Holland, Amsterdam, 1981.

[112] M.L. Mehta. *Random Matrices.* Academic Press, New York, 2 edition, 1991.

[113] F. Moss, A. Bulsara, and M.F. Shlesinger, editors. *Stochastic resonance: noise-enhanced order*, volume 70 of *Proceedings of the NATO Advanced Research Workshop.* J. Stat. Phys., 1993.

[114] T. Wellens, V. Shatokhin, and A. Buchleitner. Stochastic resonance. *Rep. Prog. Phys.*, 67:45, 2004.

[115] B. von Haeften, R. Deza, and H.S. Wio. Enhancement of stochastic resonance in distributed systems due to a selective coupling. *Phys. Rev. Lett.*, 84:404, 2000.

[116] H. Hong. Enhancement of coherent response by quenched disorder. *Phys. Rev. E.*, 71:021102, 2005.

[117] R.Toral and A. Chakrabarti. Numerical determination of the phase diagram of the f4 model in two dimensions. *Phys. Rev. B*, 42:2445, 1990.

[118] R. Desai and R. Zwanzig. Statistical mechanics of a nonlinear stochastic model. *J. Stat. Phys.*, 19:1, 1978.

[119] P. Jung and P. Hänggi. Stochastic nonlinear dynamics modulated by external periodic forces. *Europhys. Lett.*, 8:505, 1989.

[120] C. Zhou, J. Kurths, and B. Hu. Array-enhanced coherence resonance: Nontrivial effects of heterogeneity and spatial independence of noise. *Phys. Rev. Lett*, 87:098101, 2001.

[121] E.I. Volkov, E. Ullner, A.A. Zaikin, and J. Kurths. Frequency-dependent stochastic resonance in inhibitory coupled excitable systems. *Phys. Rev. E*, 68:061112–1, 2003.

[122] M. Ibañes, J. Garcia-Ojalvo, R. Toral, and J.M. Sancho. Noise-induced scenario for inverted phase diagrams. *Phys. Rev. Lett.*, 87:20601, 2001.

[123] J. García-Ojalvo and J. M. Sancho. *Noise in Spatially Extended Systems*. Springer–Verlag, New York, 1999.

[124] C. Palenzuela, R. Toral, C. Mirasso, O. Calvo, and J. Gunton. Coherence resonance in chaotic systems. *Europhys. Lett.*, 56:347, 2001.

[125] A.A. Zaikin, J. García-Ojalvo, R. Báscones, E. Ullner, and J. Kurths. Doubly stochastic coherence via noise-induced symmetry in bistable neural models. *Phys. Rev. Lett.*, 90:030601, 2003.

[126] H. Gang, T. Ditzinger, C.Z. Ning, and H. Haken. Stochastic resonance without external periodic force. *Phys. Rev. Lett.*, 71:807, 1993.

[127] W. Rappel and S.H. Strogatz. Stochastic resonance in an autonomous system with a nonuniform limit cycle. *Phys. Rev. E*, 50, 1994.

[128] C. van den Broeck, J.M.R. Parrondo, R. Toral, and K. Kawai. Nonequilibrium phase transitions induced by multiplicative noise. *Phys. Rev. E*, 55:4084, 1997.

[129] G. Schmid, I. Goychuk, and P. Hänggi. Stochastic resonance as a collective property of ion channel assemblies. *Europhys. Lett.*, 56:22, 2001.

[130] G. Schmid, I. Goychuk, and P. Hänggi. Effect of channel block on the spiking activity of excitable membranes in a stochastic hodgkin–huxley model. *Phys. Biol.*, 1:61, 2004.

[131] P. Jung and J.W. Shuai. Optimal sizes of ion channel clusters. *Europhys. Lett.*, 56:29, 2001.

[132] J.W. Shuai and P. Jung. Optimal intracellular calcium signaling. *Phys. Rev. Lett.*, 88:068102, 2002.

[133] C.J. Tessone, R. Toral, P. Amengual, H.S. Wio, and M. San Miguel. Neighborhood models of minority opinion spreading. *Eur. Phys. J. B*, 39:535, 2004.

[134] A. Pikovsky, A.A. Zaikin, and M.A. de la Casa. System size resonance in coupled noisy systems and in the ising model. *Phys. Rev. Lett.*, 88:050601, 2002.

[135] M. Kuperman and D.H. Zanette. Stochastic resonance in a model of opinion formation on small world networks. *Eur. Phys. J. B*, 26:387, 2002.

[136] W. Weidlich. Physics and social science - the approach of synergetics. *Phys. Rep.*, 204:1, 1991.

[137] A.L. Barabási and R. Albert. Emergence of scaling in random networks. *Science*, 286:509, 1999.

[138] P. Babinec. Stochastic resonance in the weidlich model of public opinion formation. *Phys. Lett. A*, 225:179, 1997.

[139] H. Gang, H. Haken, and X. Fagen. Stochastic resonance with sensitive frequency dependence in globally coupled continuous systems. *Phys. Rev. Lett.*, 77:1925, 1996.

[140] F. Moss, J.K. Douglass, L. Wilkens, D. Pierson, and E. Pantazelou. Stochastic resonance in an electronic fitzhugh–nagumo model. *Ann. N. Y. Acad. Sci.*, 706:26, 1993.

[141] V.S. Anishchenko, A.B. Neiman, F. Moss, and L. Schimansky-Geier. Stochastic resonance: noise-enhanced order. *Sov. Phys. Usp.*, 42:7, 1999.

[142] E.I. Volkov and M.N. Stolyarov. Birhythmicity in a system of two coupled identical oscillators. *Phys. Lett. A*, 159:61, 1991.

[143] E.I. Volkov and M.N. Stolyarov. Temporal variability in a system of coupled mitotic timers. *Biol. Cybern.*, 71:451, 1994.

[144] S.K. Han, C. Kurrer, and Y. Kuramoto. Dephasing and bursting in coupled neural oscillators. *Phys. Rev. Lett.*, 75:3190, 1995.

[145] D. Postnov, S.K. Han, and H. Kook. Synchronization of diffusively coupled oscillators near the homoclinic bifurcation. *Phys. Rev. E*, 60:2799, 1999.

[146] Gábor Balázsi, A. Cornell-Bell, A.B. Neiman, and Frank Moss. Synchronization of hyperexcitable systems with phase-repulsive coupling. *Phys. Rev. E*, 64:041912, 2001.

[147] A. Sherman and J. Rinzel. Rhythmogenic effects of weak electrotonic coupling in neuronal models. *Proc. Natl. Acad. Sci.*, 89:2471, 1992. Proceedings of the National Academy of Sciences, Vol 89, 2471-2474, Copyright 1992 by National Academy of Sciences.

[148] G.S. Cymbalyuk, E.V. Nikolaev, and R.M. Borisyuk. In-phase and antiphase self-oscillations in a model of two electrically coupled pacemakers. *Biol. Cybern*, 71(2):153, 1994.

[149] D. Ruwisch, M. Bode, D.V. Volkov, and E.I. Volkov. Collective modes of three coupled relaxation oscillators: the influence of detuning. *Int. J. Bifurcation and Chaos*, 9(10):1969, 1999.

[150] E.I. Volkov and D.V. Volkov. Multirhythmicity generated by slow variable diffusion in a ring of relaxation oscillators noise induced abnormal interspike variability. *Phys. Rev. E*, 65:046232–1, 2002.

[151] E.I. Volkov, E. Ullner, and J. Kurths. Stochastic multiresonance in the coupled relaxation oscillators. *Chaos*, 15(2):023105, 2005.

[152] V.K. Vanag, A.M. Zhabotinskii, and I.R. Epstein. Role of dibromomalonic acid in the photosensitivity of the ru(bpy)$_3^{2+}$-catalyzed belousov-zhabotinskii reaction. *J. Phys. Chem. A*, 104:8207, 2000.

[153] W. Wang, I.Z. Kiss, and J.L. Hudson. Clustering of arrays of chaotic chemical oscillators by feedback and forcing. *Phys. Rev. Lett.*, 86:4954, 2001.

[154] S. Nakata, T. Miyata, N. Ojima, and K. Yoshikawa. Self-synchronization in coupled salt-water oscillators. *Physica D*, 115:313, 1998.

[155] D.T.W. Chik, S. Coombes, and Z.D. Wang. Clustering through postinhibitory rebound in synaptically coupled neurons. *Phys. Rev. E*, 70:011908, 2004.

[156] P.S. Landa and P.V.E. McClintock. Vibrational resonance. *J. Phys. A: Math. Gen*, 33:L433, 2000.

[157] E.I. Volkov and D.V. Volkov. Multirhythmicity generated by slow variable diffusion in a ring of relaxation oscillators noise induced abnormal interspike variability. *Phys. Rev. E*, 65:046232, 2002.

[158] D.R. Chialvo, O. Calvo, D.L. González, O. Piro, and G.V. Savino. Subharmonic stochastic synchronization and resonance in neuronal systems. *Phys. Rev. E*, 65:050902, 2002.

[159] B. Kerner and V. Osipov. *Sov. Phys. Usp.*, 33:679, 1990.

[160] V. Castets, E. Dulos, J. Boissonade, and P. De Kepper. Experimental evidence of a sustained standing turing-type nonequilibrium chemical pattern. *Phys. Rev. Lett.*, 64(24):2953, 1990.

[161] G. Balázsi, A.H. Cornell-Bell, and F. Moss. Increased phase synchronization of spontaneous calcium oscillations in epileptic human versus normal rat astrocyte cultures. *Chaos*, 13(2):515, 2003.

[162] H. Meinhardt. *Models of Biological Pattern Formation*. Academic Press, New York, 1982.

[163] D. McMillen, N. Kopell, J. Hasty, and J.J. Collins. Synchronizing genetic relaxation oscillators by intercell signaling. *Proc. Natl. Acad. Sci.*, 99:679, 2002.

[164] A. Kuznetsov, M. Kærn, and N. Kopell. Frequency-dependent stochastic resonance in inhibitory coupled excitable systems. *SIAM J. Appl. Math.*, 65:392, 2004.

[165] X.J. Wang, J. Rinzel, and M.A. Rogawski. A model of the t-type calcium current and the low-threshold spike in thalamic neurons. *J. Neurophysiol.*, 66:839, 1991.

[166] G. Ullah, P. Jung, and A.H. Cornell-Bell. Antiphase calcium oscillations in astrocytes via inositol (1,4,5)-triphosphate regeneration. *Cell Calcium*, 39:197, 2006.

[167] D. Postnov, L. Ryazanova, E. Mosekilde, and O. Sosnovtseva. *Int. J. Neural Syst.*, 16:99, 2006.

[168] D. Postnov, L. Ryazanova, and O. Sosnovtseva.

[169] R. Laje and G.B. Mindlin. Diversity within a birdsong. *Phys. Rev. Lett.*, 89(28):288102, 2002.

[170] A.L. Benabid, P. Pollack, and C. Gervason. Long-term suppression of tremor by chronic stimulation of the ventral intermediate thalamic nucleus. *Lancet*, 337:403, 1991.

[171] S. Blond, D. Caparros Lefebvre, F. Parker, and et al. Control of tremor and involuntary movement disorders by chronic stereotactic stimulation of the ventral intermediate thalamic nucleus. *J. Neurosurg*, 77:62, 1992.

[172] P.A. Tass. *Phase Resetting in Medicine and Biology - Stochastic Modelling and Data Analysis*. Springer–Verlag, Berlin, 1999.

[173] P.A. Tass. Effective desynchronization by means of double-pulse phase resetting. *Europhys. Lett.*, 53:15–21, 2001.

[174] M.G. Rosenblum and A.S. Pikovsky. Controlling synchrony in ensemble of globally coupled oscillators. *Phys. Rev. Lett.*, 92:114102, 2004.

[175] E. Ullner, A. Zaikin, J. García-Ojalvo, and J. Kurths. Noise-induced excitability in oscillatory media. *Phys. Rev. Lett*, 91:180601, 2003.

[176] J.J. Collins, C.C. Chow, and T. Imhoff. Stochastic resonance without tuning. *Nature*, 376:236, 1995.

[177] S.M. Bezrukov and I. Vodyanoy. Noise-induced enhancement of signal transduction across voltage-dependent ion channels. *Nature*, 378:362, 1995.

[178] A. Guderian, G. Dechert, K.P. Zeyer, and F. W. Schneider. Stochastic resonance in chemistry. 1 the belousov–zhabotinskii reaction. *J. Phys. Chem.*, 100:4437, 1996.

[179] A. Förster, M. Merget, and F.W. Schneider. Stochastic resonance in chemistry. 2. the peroxidase-oxidase reaction. *J. Phys. Chem.*, 100:4442, 1996.

[180] W. Hohmann, J. Mller, and F.W. Schneider. Stochastic resonance in chemistry. 3. the minimal-bromate reaction. *J. Phys. Chem.*, 100:5388, 1996.

[181] J.F. Lindner, B.K. Meadows, W.L. Ditto, M.E. Inchiosa, and A.R. Bulsara. Array enhanced stochastic resonance and spatiotemporal synchronization. *Phys. Rev. Lett.*, 75:3, 1995.

[182] J.F. Lindner, B.K. Meadows, W.L. Ditto, M.E. Inchiosa, and A.R. Bulsara. Scaling laws for spatiotemporal synchronization and array enhanced stochastic resonance. *Phys. Rev. E*, 53:2081, 1996.

[183] H.S. Wio. Stochastic resonance in a spatially extended system. *Phys. Rev. E*, 54:R3075, 1996.

[184] F. Castelpoggi and H.S. Wio. Stochastic resonance in extended systems: enhancement due to coupling in a reaction-diffusion model. *Europhys. Lett.*, 38:91, 1997.

[185] F. Castelpoggi and H.S. Wio. Stochastic resonant media: Effect of local and nonlocal coupling in reaction-diffusion models. *Phys. Rev. E*, 57:5112, 1998.

[186] S. Bouzat and H.S. Wio. Stochastic resonance in extended bistable systems: The role of potential symmetry. *Phys. Rev. E*, 59:5142, 1999.

[187] H.S. Wio, S. Bouzat, and B. von Haeften. In A. Robledo and M. Barbosa, editors, *IUPAP International Conference on Statistical Physics, STATPHYS21*, volume 306C, page 140. Physica A, 2002.

[188] R. Graham. *Instabilities and Nonequilibrium Structures*. D. Reidel, Dordrecht, 1987.

[189] R. Graham and T. Tél . Steady-state ensemble for the complex ginzburg-landau equation with weak noise. *Phys. Rev. A*, 42(8):4661, Oct 1990.

[190] R. Graham and T. Tél. *Instabilities and Non-equilibrium Structures III*. Kluwert, 1991.

[191] H.S. Wio. 4th Granada Seminar in Computational Physics. page 135, Berlin, 1997. Springer–Verlag.

[192] G. Izús, R. Deza, O. Ramírez, H.S. Wio, D. H. Zanette, and C. Borzi. Global stability of stationary patterns in bistable reaction-diffusion systems. *Phys. Rev. E*, 52:129, 2000.

[193] D.H. Zanette, H.S. Wio, and R. Deza. Nonequilibrium potential for a reaction-diffusion model: Critical behavior and decay of extended metastable states. *Phys. Rev. E*, 53:353, 1996.

[194] F. Castelpoggi, H.S. Wio, and D.H. Zanette. Critical slowing down of spatially nonhomogeneous patterns in a reaction-diffusion model. *Int. J. Mod. Phys. B*, 11:1717, 1997.

[195] G. Drazer and H.S. Wio. Nonequilibrium potential approach: Local and global stability of stationary patterns in an activator-inhibitor system with fast inhibition. *Physica A*, 240:571, 1997.

[196] H.S. Wio. *An Introduction to Stochastic Processes and Nonequilibrium Statistical Physics*. World Scientific, Singapore, 1994.

[197] A.S. Mikhailov. *Foundations of Synergetics I*. Springer–Verlag, Berlin, 1990.

[198] I. Goychuk and P. Hänggi. Stochastic resonance in ion channels characterized by information theory. *Phys. Rev. E*, 61:4272, 2000.

[199] A. Bulsara and A. Zador. Threshold detection of wideband signals: A noise-induced maximum in the mutual information. *Phys. Rev. E*, 54:R2185, 1996.

[200] L. Schimansky-Geier, J.A. Freund, A.B. Neiman, and B. Shulgin. Noise induced order: Stochastic resonance. *Int. J. of Bif. & Chaos*, 8:869, 1997.

[201] C.J. Tessone, A. Plastino, and H.S. Wio. Stochastic resonance and generalized information measures. *Physica A*, 326:37, 2003.